IMPROVED REPRESENTATION OF CROSS-SHORE SEDIMENT TRANSPORT CHARACTERISTICS

By

ZHANXIAN WANG

A DISSERTATION PRESENTED TO THE GRADUATE SCHOOL
OF THE UNIVERSITY OF FLORIDA IN PARTIAL FULFILLMENT
OF THE REQUIREMENTS FOR THE DEGREE OF
DOCTOR OF PHILOSOPHY

UNIVERSITY OF FLORIDA

2004

This document is dedicated to my graduate advisor, Dr. Robert G. Dean,
to my wife, my parents and parents-in-law

ACKNOWLEDGMENTS

First of all, I would like to express my sincere appreciation and utmost respect from the bottom of my heart to my advisor and the chair of my supervisory committee, Dr. Robert G. Dean, for his financial and academic support and for the many valuable lessons gained from his work ethic, his character, and his tireless enthusiasm for coastal engineering. Under his constructive direction and advice, my life in the University of Florida was an important, challenging, and unforgettable experience. I am grateful to the other members of my committee (Dr. Daniel M. Hanes, Dr. Robert J. Thieke, Dr. Ulrich H. Kurzweg, and Dr. Ashish J. Mehta) for their instruction, valuable advice, and involvement during the course of my studies.

I also thank other faculty members and staff in the department (Dr. Michel K. Ochi, Dr. William G. McDougal, Dr. Donald N. Slinn, Dr. Andrew Kennedy, and Dr. Peter Y. Sheng for contributing their knowledge; Becky Hudsen, Helen Twedell, Kim Hunt, and Subarna B. Malaker for their kindly assistance in my daily life; Sidney Schofield and Jim Joiner for their help in the lab). Special thanks go to Dr. William R. Dally, Dr. Magnus Larson, Dr. Juergen Newe, Dr. Rajesh Srinivas, Dr. Albert E. Browder, and Dr. Jie Zheng, for providing valuable assistance during my dissertation preparation.

I have made a lot of friends during my life in Gainesville: Chenxia Qiu, Detong Sun, Jon Miller, Chris Bender, and so on. I cannot name all of them here. A special long-time friend, Yanfeng Zhang, I was fortunate to meet him again here in American in the same department and had some fun together.

Finally, I wish to thank my lovely, beautiful wife for her support, encouragement, and endless love. she has made my life easier than the lives of other foreign students. Both my parents and parents-in-law provided financial and mental support, whish I always appreciate

TABLE OF CONTENTS

Page

ACKNOWLEDGMENTS iii

LIST OF TABLES viii

LIST OF FIGURES ix

ABSTRACT xvi

CHAPTER

1 INTRODUCTION AND OBJECTIVE 1

1.1 Introduction 1
1.2 Characteristics of Beach Systems 3
1.2.1 Approach to Equilibrium 3
1.2.2 Equilibrium Beach Profiles 4
1.2.3 Forces Acting in the Nearshore 14
1.2.4 Parameters Affecting Profile Evolution 15
1.3 Objectives and Scope of Study 19

2 LITERATURE REVIEW 21

2.1 Laboratory Studies 21
2.2 Numerical Modeling Studies 26
2.2.1 Closed Loop Models 26
2.2.2 Open Loop Models 38
2.3 Summary 44

3 CROSS SHORE PROFILE EVOLUTION MODEL DEVELOPMENT 47

3.1 Wave Energy Transformation Models 48
3.1.1 Wave Breaker Type 48
3.1.2 Wave Transformation Models 51
3.1.3 Roller Models 57
3.2 Equilibrium Beach Profiles 61
3.2.1 EBP under Spilling Breaker Assumption 62
3.2.2 EBP Using D^3 Model 62
3.2.3 EBP Using Roller Model 63
3.2.4 Reevaluation of the Profile Scale Factor 66

3.3 Cross-Shore Profile Evolution Model 70
3.3.1 Global Consideration of Transport Rate Exponents 71
3.3.2 Transport Rates 73
3.3.3 Numerical Modeling Process 74

4 MODEL CALIBRATION WITH LABORATORY EXPERIMENTS 82

4.1 Introduction 82
4.2 LWT Experiments 83
4.2.1 Description of Experiments 83
4.2.2 Modeling Results 85
4.3 CRIEPI Wave Flume Experiments 86
4.4 German Large Wave Flume 92
4.4.1 1986/1987 Experiments 92
4.4.2 1996/1997 Experiments 95
4.5 Summary of Laboratory Calibration 102

5 MODEL EVALUATION AND SENSITIVITY ANALYSIS 111

5.1 Evaluation of K value with Laboratory Experiments 111
5.2 Sensitivity Analysis of Modal Parameters 124
5.2.1 Influence of Breaking Index 124
5.2.2 Influence of D^3 Breaking Wave Model Parameters 124
5.2.3 Influence of Roller Model Coefficient 126
5.2.4 Influence of Equilibrium Energy Dissipation 126
5.2.5 Influence of Wave Height and Period 127
5.2.6 Influence of Limiting Onshore and Offshore Slopes 128
5.3 Effect of Varying Water Level 128
5.4 Initial Beach Slope Effect 130
5.5 Summary of Model Evaluation 131

6 MODEL APPLICATION 133

6.1 Laboratory Experiments Studies 133
6.1.1 SUPERTANK Project 134
6.1.2 LIP 11D Delta Flume Experiments 140
6.2 Field Studies 146
6.2.1 Ocean City, Maryland 147
6.2.2 Panhandle Coast of Florida 159
6.3 Summary 168

7 SUMMARY, CONCLUSIONS AND RECOMMENDATIONS 170

7.1 Summary 170
7.2 Conclusions 171
7.3 Recommendations for Future Study 173

APPENDIX

A FORTRAN PROGRAM CODE LISTING 175

B SIMULATION RESULTS FOR OCEAN CITY, MARYLAND 186

REFERENCES 199

BIOGRAPHICAL SKETCH 208

LIST OF TABLES

Table		page
3-1	Summary of breaker type classification criteria.	48
3-2	Conditions and test cases in LWT and CRIEPI Flume experiments	50
3-3	Recommended A values ($m^{1/3}$).	66
4-1	Summary of the LWT experiment tests used for model calibration.	85
4-2.	Best-fit K values for LWT experiments	85
4-3.	Best-fit K values for CRIEPI experiment.	92
4-4	Best-fit K values for German wave flume 1986/1987 experiment.	95
4-5.	Best-fit K values for German flume 1996/1997 experiments.	96
4-6	Summary of laboratory calibration.	103
4-7	Best-fit RMS errors of eroded volume (unit: m^2)	108
5-1	Root-mean-square errors of profile depths predicted by the model with best-fit and average K values, and the corresponding deviations	124
6-1.	Summary of the tests conditions in the SUPERTANK project	135
6-2.	Summary of test conditions in LIP 11D project	142
6-3	Measured volume changes during the Halloween storm and adjustment.	152
6-4	Measured volume changes during the NJ storm and adjustment	158

LIST OF FIGURES

Figure page

1-1 Calculated transport rate distributions with time for Test CE300 with measured profiles (H = 1.68 m, T = 11.33 s, D_{50} = 0.22 mm). 4

1-2. Calculated transport rate distributions with time for Test CE201 with measured profiles (H = 0.55 m T = 11.33 s, D_{50} = 0.4 mm) 4

1-3 Definition sketch of bar-berm and shoreface profile 6

1-4 Comparison between measured and theoretical EBP 9

1-5 Comparison of sediment size effects on profile evolution 15

1-6. Comparison of profile evolution under different wave heights. 16

1-7. Comparison of profile evolution under different wave periods 17

1-8. Profile Changes under random and monochromatic waves for case ST-10 in SUPERTANK (H_{mo} = 0.8 m, T_p = 3 s) 18

1-9 Transport rates under random and monochromatic waves for case ST-10 in SUPERTANK (H_{mo} = 0.8 m, T_p = 3 s). 18

2-1 Stable points on storm and normal profiles. 22

2-2 Three types of beach profiles 23

2-3 Relationship between net transport rate and Shields parameter 23

2-4. Types of net transport rate distributions 24

2-5 Comparison of EDUNE model results with large wave tank data by Saville 28

2-6 Comparison of EDUNE model results with a field profile affected by Hurricane Elonse 28

2-7 Principal zones of cross-shore transport 31

2-8 Definition of dune, shoreline and offshore slope 33

2 9 Comparison of linear (n=1) and nonlinear (n=3) transport rates with measured data in German large wave flume 34

2-10 Comparison of the averaged net sediment transport rates computed from the single-bar and multi-bar numerical models with CE Case 300 experimental data after 5 hours (measured profile had two bars) 36

2-11 Comparison of the single-bar and multi-bar numerical results with SBEACH and CE Case 400 data after 40 hours 36

2 12 Example output to illustrate characteristics of the Dally and Dean model 39

2 13 Computed bed profiles by UNIBEST-TC, COSMOS, CROSMOR2000, BEACH1/3D, and CIRC with comparison to measured results. 43

2 14 Computed significant wave heights, longshore current velocities, cross-shore current velocities and peak orbital velocities by UNIBEST TC, COSMOS, CROSMOR2000, BEACH1/3D and CIRC with comparison to measured results 44

3 1 Surf similarity parameter and fall velocity parameter versus beach erosion/accretion. 51

3 2. Comparison of D^3 model and "0 78" criterion to laboratory data for 1/20, 1/30, 1/65 and 1/80 beach slope 53

3 3 Test of D^3 model at prototype scale on large wave tank profile (H = 1 68 m T = 3 75 s) Wave breaks, reforms, shoals and breaks again. 53

3-4 The pdf of wave height R compared with the Rayleigh distribution 56

3 5 Comparison of the numerical results with the density function Eq 3 37 of Longuet-Higgins 58

3-6 Roller area prediction. 61

3-7. Comparison of EBP under different wave transformation models 64

3-8 Initial and predicted profile for the hypothesis example. 65

3-9 Predicted H/h ratio and calculated EBP from Eq 3 31 65

3-10 Best-fit equilibrium beach profile for CE300 The A value based on Table 3-2 is 0 106$m^{1/3}$ 68

3 11 Relationship between the fall velocity parameter and the ratio of the best fit A values to the recommended A values. 68

3-12 Modified relationship between the fall velocity parameter and the ratio of the best-fit A values to the recommended A values. 69

3-13 Modified best-fit equilibrium profile for CE500. The A value based on Table 3-2 is 0.106 $m^{1/3}$ 69

3-14 Best-fit equation for modification function, LWT data only 70

3-15 Investigation of transport relationship. Eq 3.1, for n = 1 72

3-16 Transport rates versus energy dissipation, n = 1, D^3 model 72

3-17 Transport rates versus energy dissipation, n = 3, D^3 model 72

3-18 Two types of grids employed in numerical modeling of cross-shore sediment transport and profile evolution 74

4-1 Test 300 from LWT experiments. Comparison of predicted to observed profiles at different times for the best-fit K values for n = 1, 2 and 3 87

4-2 Test 400 from LWT experiments. Comparison of predicted to observed profiles at different times for the best-fit K values for n = 1, 2 and 3 88

4-3 Test 500 from LWT experiments. Comparison of predicted to observed profiles at different times for the best-fit K values for n = 1, 2 and 3 89

4-4 Test 401 from LWT experiments. Comparison of predicted to observed profiles at different times for the best-fit K values for n = 1, 2 and 3 90

4-5 Test 501 from LWT experiments. Comparison of predicted to observed profiles at different times for the best-fit K values for n = 1, 2 and 3 91

4-6 Test 6-2 from CRIEPI experiments (initial slope 1:10). Comparison of predicted to observed profiles at different times for the best-fit K values for n = 1, 2 and 3 93

4-7 Case "dune without foreshore" under regular wave conditions in German wave flume experiments (initial slope 1:4). Comparison of predicted to observed profiles at different times for the best-fit K values for n = 1, 2 and 3 94

4-8 Profile geometries for beach stability experiments in Test Phase I of German 1996/1997 experiments 96

4-9 The initial and final observed profiles in Test Phase I of German wave flume 1996/1997 experiments 97

4-10 Test A9 from German wave flume 1996/1997 experiments (initial slope 1:20). Comparison of predicted to observed profiles at different times for the best-fit K values for n = 1, 2 and 3 98

4-11 Test B2 from German wave flume 1996/1997 experiments (initial slope 1:10). Comparison of predicted to observed profiles at different times for the best-fit K values for n = 1, 2 and 3 99

4-12 Test C2 from German wave flume1996/1997 experiments (initial slope 1:5) Comparison of predicted to observed profiles at different times for the best-fit K values for n = 1, 2 and 3 100

4-13 Test H2 from German wave flume1996/1997 experiments (initial slope 1:15). Comparison of predicted to observed profiles at different times for the best-fit K values for n = 1, 2 and 3 101

4-14 Best fit K values with time for LWT Test 300 with n = 1, 2 and 3 104

4-15 Best-fit K values with time for LWT Test 400 with n = 1, 2 and 3 105

4-16 Best-fit K values with time for LWT Test 500 with n = 1, 2 and 3 106

4-17 Best fit K values with time for CRIEPI Test 6-2 with n = 1, 2 and 3 107

4-18 Comparison of best-fit to observed eroded volumes 109

5-1 Test 300 from LWT experiments Comparison of measured and predicted profiles by the model with the best fit and average K values 113

5-2 Test 400 from LWT experiments Comparison of measured and predicted profiles by the model with the best fit and average K values 114

5-3 Test 500 from LWT experiments Comparison of measured and predicted profiles by the model with the best-fit and average K values 115

5-4 Test 401 from LWT experiments Comparison of measured and predicted profiles by the model with the best fit and average K values 116

5-5 Test 501 from LWT experiments Comparison of measured and predicted profiles by the model with the best fit and average K values 117

5-6 Test 6-2 from CRIEPI experiments Comparison of measured and predicted profiles by the model with the best fit and average K values 118

5-7 Case "dune without foreshore" under regular wave conditions in German wave flume experiments Comparison of measured and predicted profiles by the model with the best-fit and average K values 119

5-8 Test A9 from German wave flume 1996/1997 experiments. Comparison of measured and predicted profiles by the model with the best-fit and average K values. 120

5-9 Test B2 from German wave flume 1996/1997 experiments. Comparison of measured and predicted profiles by the model with the best fit and average K values. 121

5-10 Test C2 from German wave flume 1996/1997 experiments. Comparison of measured and predicted profiles by the model with the best-fit and average K values ... 122

5-11 Test H2 from German wave flume 1996/1997 experiments. Comparison of measured and predicted profiles by the model with the best-fit and average K values ... 123

5-12 Effect of breaking index on eroded volume ... 125

5-13 Effect of wave decay coefficient on eroded volume. ... 125

5-14 Effect of on stable wave height coefficient eroded volume. ... 126

5-15 Effect of roller model coefficient on eroded volume ... 126

5-16 Effect of profile scale factor on eroded volume ... 127

5-17 Effect of wave period on eroded volume. ... 128

5-18 Effect of on shore limiting slope on eroded volume ... 129

5-19 Effect of offshore limiting slope on eroded volume ... 129

5-20 Comparison of observed and predicted profile evolution for variable water level 130

5-21 Comparisons of equilibrium beach profile for different initial beach slopes ... 131

6-1 Result of model simulation, SUPERTANK P1A ... 136

6-2 Result of model simulation, SUPERTANK PGA. ... 136

6-3 Result of model simulation, SUPERTANK PJA ... 137

6-4 Result of model simulation, SUPERTANK PJC ... 138

6-5 Result of model simulation, SUPERTANK PKA. ... 139

6-6 Result of model simulation, SUPERTANK PKC ... 139

6-7 Residuals for SBEACH and current model, SUPERTANK experiments ... 140

6-8 Initial beach geometry of LIP 11D experiments. ... 142

6-9 Result of model simulation: LIP 11D Test 1a. ... 143

6-10 Result of model simulation, LIP 11D Test 1b ... 143

6-11 Result of model simulation, LIP 11D Test 1c. ... 143

6-12 Result of model simulation, LIP 11D Test 2a 144

6-13 Result of model simulation, LIP 11D Test 2b 145

6-14 Result of model simulation, LIP 11D Test 2c 145

6-15 Result of model simulation LIP 11D Test 2c 145

6-16 Residuals for SBEACH and current model, LIP 11D experiments 146

6-17 The Ocean City beach nourishment project layout 148

6-18 Significant wave height, peak wave period and water level time history for the Halloween 1991 storm Ocean City, MD 151

6-19 Comparison of calculated and original measured profile of the Halloween storm for the profile at 63rd street, Ocean City, MD 152

6-20 Comparison of calculated and shifted measured profile of the Halloween storm for the profile at 63rd street Ocean City, MD 152

6-21 Comparison of measured and simulated volume change above NGVD for the Halloween storm, Ocean City, MD 154

6-22 Comparison of measured and simulated recession of the +1.5m contour for the Halloween storm, Ocean City, MD 154

6-23 Residuals for SBEACH and current model for the Halloween storm, Ocean City MD 154

6-24 Significant wave height, peak wave period and water level time history for the November 1991 storm, Ocean City, MD 155

6-25 Significant wave height, peak wave period and water level time history for the January 1992 storm, Ocean City MD 156

6-26 Comparison of calculated and original measured profile of the NJ storm for the profile at 63rd street, Ocean City MD 158

6-27 Comparison of calculated and shifted measured profile of the NJ storm for the profile at 63rd street, Ocean City, MD 158

6-28 Comparison of measured and simulated volume change above NGVD for the NJ storm, Ocean City, MD 160

6-29 Comparison of measured and simulated recession of the +1.5m contour for the NJ storm, Ocean City, MD 160

6-30 Residuals for SBEACH and current model for the NJ storm, Ocean City, MD 160

6-31 Panhandle Coast of Florida ... 161

6-32 Estimated storm surge hydrograph near the western end of Walton County for Hurricane Eloise ... 161

6-33 Comparison of calculated and measured profile of the Hurricane Eloise for the profile at R-41 Walton County FL ... 163

6-34 NOAA data collection stations which recorded Opal data ... 164

6-35 Wave data at NDBC buoy 42036 during passage of Opal ... 165

6-36 Storm surge hydrograph for Hurricane Opal at Panama City Beach ... 165

6-37 Beach and dune erosion and offshore sand deposition in Bay County after Hurricane Opal 1995 ... 167

6-38 Wave conditions of Hurricane Opal for model application in Bay County ... 167

6-39 Comparison of calculated and measured profiles for Hurricane Opal, profile at R-21T, Bay County, FL ... 168

6-40 Comparison of calculated and measured profiles for Hurricane Opal, profile at R-41, Bay County FL ... 168

B-1 Results of simulation of the Halloween storm for profile at 37th street ... 187

B-2 Results of simulation of the Halloween storm for profile at 45th street ... 188

B-3 Results of simulation of the Halloween storm for profile at 56th street ... 189

B-4 Results of simulation of the Halloween storm for profile at 63rd street ... 190

B-5 Results of simulation of the Halloween storm for profile at 74th street ... 191

B-6 Results of simulation of the Halloween storm for profile at 103rd street ... 192

B-7 Results of simulation of the Nov-Jan storm for profile at 37th street ... 193

B-8 Results of simulation of the Nov Jan storm for profile at 45th street ... 194

B-9 Results of simulation of the Nov Jan storm for profile at 56th street ... 195

B-10 Results of simulation of the Nov-Jan storm for profile at 63rd street ... 196

B-11 Results of simulation of the Nov-Jan storm for profile at 74th street ... 197

B-12 Results of simulation of the Nov-Jan storm for profile at 103rd street ... 198

Abstract of Dissertation Presented to the Graduate School
of the University of Florida in Partial Fulfillment of the
Requirements for the Degree of Doctor of Philosophy

IMPROVED REPRESENTATION OF
CROSS-SHORE SEDIMENT TRANSPORT CHARACTERISTICS

By

Zhanxian Wang

May 2004

Chair: Robert G. Dean
Major Department: Civil and Coastal Engineering

An improved cross-shore beach profile evolution model was developed based on equilibrium beach profile and surface roller concepts. A more physically sound wave transformation model and roller model were adopted to improve the calculation of wave height transformation and energy dissipation inside the surf zone. Including the surface roller model produced a new equilibrium beach profile shape which can represent bar profiles to a limited degree. The profile scale factor in the equilibrium beach profile formulae was modified through the fall velocity parameter based on best fits of measured profiles from large-scale laboratory experiments. To predict beach profile response under wave action, a finite difference method was applied to solve the sediment transport and continuity equations numerically through an implicit, double sweep schema. After model calibration with eleven large-scale wave flume experimental data, it was found that a nonlinear transport relationship with n = 2 provided better overall predictions than n values of 1 and 3. This nonlinear relationship provided a reasonable explanation for

different time scales of beach profile evolution under different wave and initial profile conditions

The model was applied to additional large-scale wave flume experimental data from SUPERTANK and LIP 11D and field data after major storms at Ocean City, Maryland and the Panhandle Coast of Florida, along with comparisons with two other closed loop models (SBEACH and CROSS). Results showed that all three models had different degrees of underprediction of volume changes and contour recessions after storms. The model can generate bar profiles under both regular and random wave conditions, which is similar to the SBEACH model but no empirical assumption is made in the wave transition region.

CHAPTER 1
INTRODUCTION AND OBJECTIVE

1.1 Introduction

Sand beaches are valuable resources. They not only provide protection from severe storms and hurricanes, but also generate substantial revenue as a recreational amenity. Under the continuous seasonal action of waves, currents and winds, beaches often erode during winter and accrete during summer. The sediment transport at a point in the nearshore zone includes cross-shore and longshore components. Cross-shore sediment transport includes both offshore transport such as occurs during storms and onshore transport during mild wave climates. Transport in these two directions occurs in significantly distinct modes (suspended load dominates offshore transport, while bedload dominates onshore transport) and with remarkably disparate time scales. The offshore transport moves sand from the upper profile to offshore in hours to days during a storm whereas the onshore transport may take months to years to move sand to the dry beach in which a "ridge and runnel" system often develops. Difficulties in predicting transport in the two directions also differ substantially. Offshore transport is the more predictable of the two. This is fortunate for coastal engineers, since there is considerably greater engineering concern and interest in offshore transport because of its potential damage to structures and loss of land.

Cross-shore sediment transport is relevant to a number of coastal engineering problems including the following:

- Beach and dune response to storms

- Cross-shore equilibration of a beach nourishment project
- Profile nourishment in which the sand is placed in the nearshore with the expectation that it will move landward nourishing the beach
- Shoreline response to sea level rise
- Seasonal shoreline changes
- Overwash, the process of landward transport due to overtopping of the normal land mass due to high tides and waves
- Scour immediately seaward of shore parallel structures, such as seawalls
- Cross-shore and longshore coupled transport around shore-normal structures in which the steeper and milder slopes on the updrift and downdrift sides induce seaward and landward transport components, respectively.

One successful and commonly adopted method to protect storm damage and attract more people to the beach is beach nourishment, especially in Florida. Beach nourishment projects restore the eroded beach with additions of large quantities of good quality sand to the natural system. Beach nourishment profiles are usually constructed with slopes steeper than equilibrium. The time scale for profile equilibration is very significant to design and interpretation of beach nourishment project evolution, because wider beaches during equilibration provide more area for recreation and a greater degree of storm protection to upland structures. Additionally, profile equilibration can be misinterpreted as a loss of material and consequently a poor and unanticipated performance.

A clear understanding of the time scales of profile equilibration provides guidance in the beach nourishment project design process. Examples include the volume of sand to be placed in order to attain the desired beach width during the life span of the project, and the best design slope of the placement to ensure that less sand is carried offshore. This understanding is also helpful for analysis of beach nourishment project performance and for regulatory purposes such as establishing coastal construction control lines.

Forces governing beach profile equilibration processes include natural and artificial forces. The natural forces include tides, waves and sea level rise. The most significant artificial force is due to profiles placed at slopes steeper than equilibrium that induces seaward sediment transport and associated shoreline retreat. Due to the complexities of surf zone hydrodynamics, sediment characteristics and wave conditions, an analytical treatment of beach profile change is very difficult. Thus, numerical modeling (which allows flexibility in the specification of initial and boundary conditions and the representation of arbitrary forcing) is a powerful and appropriate tool.

1.2 Characteristics of Beach Systems

1.2.1 Approach to Equilibrium

Beach profiles can attain equilibrium states under constant environment conditions. An equilibrium profile, by definition, is approached when the cross-shore transport rates at all points become zero, as are the longshore gradients in longshore transport. So the decay of cross-shore transport rate with time is one direct measure of profile equilibration. Figures 1-1 and 1-2 show two cases of transport rate distribution with time calculated from profile measurements, one for an erosional case and one for an accretionary case from LWT experiments (Kraus and Larson, 1988). Other quantities that can be used to represent the profile equilibration process include eroded volume (or bar volume) for erosional profiles and berm volume for accretionary profiles, shoreline position changes, bar positions, and so on. These confirm that the equilibrium concept is valid and that a numerical model developed for simulating realistic beach profile change needs to include this property.

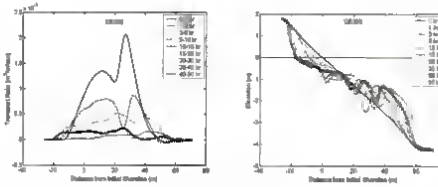

A B

Figure 1-1 Calculated transport rate distributions with time for Test CE300 with measured profiles (H = 1 68 m, T = 11 33 s, D_{50} = 0.22 mm). A) Transport rates B) Measured profiles.

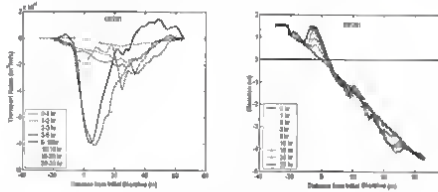

A B

Figure 1-2. Calculated transport rate distributions with time for Test CE201 with measured profiles (H = 0 55 m, T = 11 33 s, D_{50} = 0 4 mm) A) Transport rates. B) Measured profiles

1.2 2 Equilibrium Beach Profiles

A quantitative understanding of the characteristics of equilibrium beach profiles is central to rational design of many coastal engineering projects and to the interpretation of nearshore processes. Several features of equilibrium profiles are well known

- They tend to be concave upward
- Smaller and larger sand diameters are associated with milder and steeper slopes, respectively

- The beach face is approximately planar
- Steep waves and finer sands result in milder slopes and a tendency for bar formation

1.2.2.1 Statistical approach to equilibrium beach profiles

Through analysis of beach profiles from the Danish North Sea coast and Mission Bay, California, Bruun (1954) found that profiles tended to follow the simple relationship

$$h = Ay^{2/3} \tag{1.1}$$

where A is a dimensional scale parameter with units of length $^{2/3}$ and depends primarily on sediment characteristics

Using 502 beach profiles from the Atlantic and Gulf Mexico shorelines and a least-square procedure, Dean (1977) fitted an equation of the form $h = Ay^m$. A central value of m = 2/3 was found, which, according to linear wave theory, is consistent with uniform wave energy dissipation per unit volume within the surf zone as the dominant destructive force

Bodge (1992) proposed an exponential expression for equilibrium profile as

$$h = B(1 - e^{-ky}) \tag{1.2}$$

where B and k are constant parameters. This expression along with the 2/3 power equilibrium profile were fit to a set of data from 504 beach profiles from the U.S. east coast and Gulf of Mexico which Dean (1977) originally used to investigate the $h = Ay^m$ shape. Bodge found that most (80% to 86%) were better fit by the exponential form relative to the 2/3-power shape. He concluded that the improved fit of the exponential expression was likely to be most notable for beaches with decreasing grain size in the offshore direction. The leading coefficient B may yield insight to the depth of closure and the coefficient k may describe sediment type or its gradation in the offshore

direction However, no attempt was made to correlate the parameters with beach or wave characteristics

Komar and McDougal (1994) considered an alternative form of the exponential beach profiles (Eq 1 3)

$$h = \frac{S_b}{k}(1 - e^{-kr}) \tag{1.3}$$

where S_B is the beach face slope They noted that because there have been many past studies that relate S_b to beach sediment grain sizes and wave conditions, this exponential beach profile form only contains one adjustable coefficient, k, whose evaluation can be based on the coordinates of the closure depth of profile change or equally on some arbitrary chosen offshore depth coordinate

By reasoning that the forcing mechanism landward and seaward of the breakpoint bar (by shoaling waves and breaking waves respectively) can be significantly different, Inman et al. (1993) divided the beach profile into two independent portions separated by the bar crest. The two portions were termed as bar berm, from the berm crest to the breakpoint bar; and shorerise, seaward of the breakpoint bar (Figure 1-3)

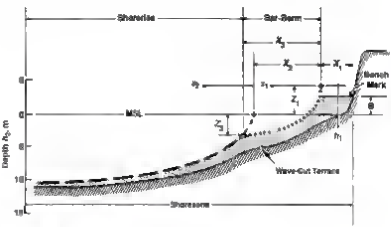

Figure 1-3 Definition sketch of bar berm and shorerise profile (Inman et al , 1993).

Two power functions similar to $h = Ay^m$ were used independently to reconstruct the two segments. It was demonstrated that the barred profiles were reproduced better, especially in the vicinity of the bar and the offshore portion, than the one segment model by $h = Ay^m$. This profile model has 8 parameters requiring quantification.

Wang and Davis (1998) developed a three-segment beach profile model based on the Inman et al. (1993) approach for reproducing the commonly observed bar and trough features. The model was developed under the general form of

$$h = F(Ay^m) \tag{1.4}$$

where the function F is determined empirically based on regional boundary condition. The three segments used are

- Inner surf zone, from the lowest elevation of the trough to the shoreline, dominated by secondary wave shoaling and breaking.

$$h = A_1 y^{m_1}, \quad 0<y<y_{tr} \tag{1.5}$$

- Landward of the bar crest, characterized by a landward dip and a landward increasing depth. The dominant hydrodynamic process is rapid energy dissipation at the bar top due to breaking and wave reformation caused by increasing water depth.

$$h = h_{tr} + \frac{h_{bt} - h_{tr}}{y_{bt} - y_{tr}}(y - y_{tr}), \quad y_{tr}<y<y_{bt} \tag{1.6}$$

- Nearshore, from the bar crest to the closure depth, this portion is dominated by wave shoaling and breaking on the bar top.

$$h = A_2 (y - y_2)^{m_2}, \quad y_{bt}<y<y_{cd} \tag{1.7}$$

where A_1 and A_2 are dimensional scale parameters related to grain size for inner surf and nearshore, respectively; m_1 and m_2 are empirical shape parameters controlling the beach slopes; h_{tr} and y_{tr} are water depth at trough and its distance to the shoreline, h_{bt} and y_{bt} are water depth at bar top and its distance to the shoreline, y_{cd} is the distance from shoreline

to the closure depth of the profile and y_2 is the intercept of the nearshore portion with zero water level The quantity m_1 was found to be well approximated by 2/3, while m_2 was larger than 2/3 with an averaged best-fit value of 0.82 Application of this model requires knowledge of 10 parameters, none of which can be determined without availability of the profile. Thus, this model can be applied in a diagnostic, but not a predictive manner

1.2.2.2 Based on equilibrium mechanisms

Bowen (1980) established an equilibrium beach profile model using an energetic model of suspended sediment transport based on wave orbital motions and a perturbation or drift velocity within the nearshore The first-order solution, assuming symmetrical wave-orbital motions yielded a beach profile having a 2/3-power depth variation However, when the higher harmonic terms were included to simulate the more realistic asymmetrical wave-orbital motions as found in Stokes-type waves, the analysis then yielded a profile having a 2/5 power depth variation

Based on Bagnold's energetic approach for bed load and suspended load under steady flows, Leont'ev (1985) developed an equilibrium profile model based on the following considerations: (1) Bottom sediment grains are homogeneous in density and size; (2) Bedload sediment transport is onshore due to the wave orbital velocity asymmetry; (3) Suspended-load transport is offshore and its rate is equal to the product of the suspended sediment concentration and the undertow velocity The model results in Eq 1 8

$$\frac{dh}{dy} + \frac{8}{\gamma^3}\frac{w}{C_0}\left(\frac{h_b}{h}\right)^{1/2} - B = 0 \qquad (1\ 8)$$

where y is positive onshore with origin at the breaking point, h is water depth, h_b is the water depth at wave-breaking point $\gamma = H/h$, H is wave height, w is the particle fall velocity, C_b is the wave phase speed at the break point and B is a constant of the order of 10^{-3}. Using two different γ forms at the offshore (Green's law) and onshore region (constant) from the breaking point, an equilibrium profile was obtained which was convex in the offshore region (where wave energy grows) and concave in the surf zone (where wave energy dissipation occurs). This model was applied to both monochromatic and random waves. Figure 1-4 compares measured and theoretical results.

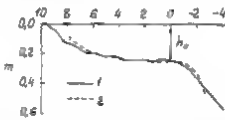

Figure 1-4 Comparison between measured and theoretical EBP (Leont'ev, 1985). Solid line 1 and dashed line 2 refer to measured and calculated profile, respectively.

Larson (1988) modified the concept of Dean's energy dissipation per unit volume by replacing the spilling breaker assumption with the breaking model by Dally et al. (1984), which considers the dissipation due to breaking in the surf zone to be given by

$$\frac{dF}{dy} = -\frac{K}{h}(F - F_s) \tag{1.9}$$

where the energy flux $F = EC_g$, F_s is the stable energy flux based on a stable breaking wave height $H_s = \Gamma h$. Equating this energy flux relationship to Dean's uniform energy dissipation per unit volume leads to the resulting equilibrium profile

$$y = 2\frac{h}{K} + \frac{5}{24}\rho g^{3/2}\left(\frac{\Gamma^2 h^{3/2}}{D_*}\right) \tag{1.10}$$

which includes a linear term that removes the infinite slope at the shoreline that occurs in Eq.1.1. Dean (1991) obtained a similar form by including the effect of gravity

$$y = \frac{h}{m} + \left(\frac{h}{A}\right)^{3/2} \tag{1.11}$$

Following the Larson (1988) model, Creed et al. (1992) developed an EBP model under random waves by using the random wave dissipation model from Thornton and Guza (1983). They obtained the following simple EBP model

$$h(y) = \beta y^{4/7} \tag{1.12}$$

where

$$\beta = \left(\frac{136 D_*}{31 \rho g^{3/2}} \left\{\frac{A}{\gamma^3 D_*}\right\}^{2/7}\right)^{4/7} \tag{1.13}$$

Larson et al. (1999) presented simple theoretical models to determine the equilibrium profile shape under breaking and nonbreaking waves. For the case of breaking waves, they assumed that the seaward transport in the undertow is locally balanced by a net vertical sedimentation, so that no bottom changes occur at equilibrium. Three different models were developed to derive the profile shape under nonbreaking waves: (1) A variational formulation where the wave energy dissipation in the bottom boundary layer is minimized over the part of the profile affected by nonbreaking waves; (2) An integration of a small-scale sediment transport formula over a wave period where the slope conditions that yield zero net transport determine equilibrium, (3) A conceptual formulation of mechanisms for onshore and offshore sediment transport where a balance between the mechanisms defines equilibrium conditions. The purpose was to investigate the sensitivity in the resulting EBP shape given different assumptions regarding the

conditions of equilibrium and the governing mechanisms The resulting EBP shapes under breaking and nonbreaking waves are given by

$$h = Ay^m,\ 0 < y < y_b \tag{1.14}$$

$$h = [h_b^{1/A} + B(y - y_b)]^A,\ y > y_b \tag{1.15}$$

where A and B are dimensional shape parameters A is related to grain size (or fall speed), whereas B is a function of offshore wave conditions and sediment characteristics. The values of the powers were determined to be m = 2/3 and n = 0.15 to 0.30 Note that the theoretical EBP models were essentially based on monochromatic (or representative) wave conditions and the effects of wave randomness were not addressed explicitly

Medina et al (2000) proposed a new equilibrium beach profile formulation that treats the shoaling portion of the profile independently from that of the breaking portion. The formulation considers wave reflection from the beach and the variation of sea level due to tide The theoretical basis of the model is the time averaged wave energy flux equation for straight and parallel bottom contours

$$\frac{dF}{dy} = -\varepsilon \tag{1.16}$$

where F is the net shoreward energy flux per unit width and ε is the energy dissipation rate per unit surface area. The equation involves three variables wave height, water depth and wave energy dissipation. Two different wave energy dissipation models and wave height variations across the profile are proposed for breaking and non-breaking waves, respectively

- EBPs under breaking waves

$$\varepsilon = D_b^* h \tag{1.17}$$

$$H = \gamma h \tag{1.18}$$

$$y = \left(\frac{h}{A}\right)^{3/2} + \frac{B}{A^{3/2}} h^3,\ 0 < y < y_b \tag{1.19}$$

$$A = \left[\frac{24 D_f^*}{5 \rho g^{3/2} \gamma^3}\right] \tag{1.20}$$

where D_b^* is the wave energy dissipation per unit water depth caused by wave breaking, γ is the breaker to-depth ratio, B is a constant which depends on wave period, and is related to the reflected energy flux and is zero if reflection is negligible.

- EBPs under nonbreaking waves

$$\varepsilon = D_f^* \tag{1.21}$$

$$H = \beta \sqrt{h} \tag{1.22}$$

$$Y = y - y_a = \left(\frac{h}{C}\right)^{3/2} + \frac{D}{C^{3/2}} h^3,\ y_a < y < y_a \tag{1.23}$$

$$C^{3/2} = \frac{8 D_f^*}{\rho g^{3/2} H_a^3 h_a} \tag{1.24}$$

$$y_a = y_b \left(1 - \frac{A^{3/2}}{C^{3/2}}\right) + \frac{B - D}{C^{3/2}} h_a^3 \tag{1.25}$$

where D_f^* is the constant wave energy dissipation per unit area caused by friction, β and D are constants. Similar to B in the breaking zone, D is also related to reflected energy flux and is zero if no reflection. The subscript "a" refers to the offshore limit of the shoaling profile.

An increase in wave height will have two effects on the equilibrium shape. First, the shoaling profile will become steeper as the shape parameter C increases. Second, the offshore limit of the surf profile will also increase due to the greater breaking depth

Besides these, wave reflection adds a new link between both portions of the profile. A variation in the wave period will change the shape parameters B and D and consequently, the overall shape of the profile. Best-fit tests using the above EBP shape against over 50 profiles from 13 beaches along the Spanish coast were conducted to determine relationships among the shape parameters (A, B, C, D) and the wave or the sediment characteristics of a beach profile. The best fit was obtained using the dimensionless fall velocity, $\Omega = H_b / wT$. For the range of $1.5 < \Omega < 5$, the following expressions were obtained

$$A = 0.21 - 0.02\Omega \tag{1.26}$$

$$B = 0.89\exp(-1.24\Omega) \tag{1.27}$$

$$C = 0.66 + 0.04\Omega \tag{1.28}$$

$$D = 0.22\exp(-0.83\Omega) \tag{1.29}$$

1.2.2.3 Non-uniform grain size effects

On most beaches the median grain size decreases with distance offshore, producing a profile that is steeper inshore and more gently sloping offshore. Based on the same assumption as Dean's equilibrium profile concept, a modified equilibrium profile model was proposed for varying sediment size along the beach by Larson (1991). A simple description of the variation in equilibrium energy dissipation, D_{eq}, with distance from the shoreline is assumed as

$$D_{eq} = D_\infty + (D_0 - D_\infty)\exp(-\lambda y) \tag{1.30}$$

where D_0 and D_∞ are the equilibrium energy dissipation for the material at the shoreline and far offshore respectively ($D_0 > D_\infty$), and λ is an empirical coefficient describing the rate at which D_{eq} approaches D_∞. The equilibrium profile shape is given by

$$h = A[y + \frac{1}{\lambda}(\frac{D_b}{D_w} - 1)(1 - e^{-\lambda y})]^{2/3} \quad (1.31)$$

in which A is defined based on D_w. Three different beach profile data sets were used to compare the modified equilibrium profile shape with the classical 2/3-power equilibrium profile, and a better fit with the measured profile was found by the modified equilibrium profile form.

1.2.3 Forces Acting in the Nearshore

An equilibrium beach profile represents a balance of "destructive" and "constructive" forces acting on the beach. At present, neither the complete identification nor the quantification of these forces is well understood. Dean (1995) and Dean and Dalrymple (2002) described these forces in detail.

Destructive forces are those that cause offshore transport and beach erosion. Gravity is the most obvious destructive force. It acts downslope reducing the profile slope. Gravity also tends to smooth any irregularities that occur in the profile. Another significant destructive force is the turbulence generated by wave breaking within the surf zone. The turbulent fluctuations dislodge sediment particles and suspend them into the water column. The seaward return flow, undertow, then transports these suspended sediment offshore. The undertow also causes seaward-directed shear stresses that contribute to an offshore bedload transport.

Constructive forces, on the other hand, cause onshore transport and beach accretion. Three individual constructive forces are identified. The first is due to the net onshore shear stresses at the bottom resulting from the nonlinear shallow-water wave forms. The wave crests are higher and of less duration than the troughs for the nonlinear waves. The second constructive force is that due to the streaming velocities in the

direction of propagating waves within the bottom boundary layer. An additional constructive force is due to the intermittent suspension and selective transport of the particles by the wave induced crest velocities. This force could be constructive or destructive depending on the transport direction caused.

1.2.4 Parameters Affecting Profile Evolution

1.2.4.1 Sand grain size

The transportability of a sand grain is affected by its characteristics (such as size, shape, porosity, specific gravity, etc.). A hydraulically relevant sand particle parameter is its fall velocity. Coarse sand grains (which fall rapidly) are less likely than finer sand grains to be suspended in the water column. Coarse sand also can sustain larger shear stresses without moving than fine sand. Thus, coarse sediments can withstand the destructive forces more easily than fine sands, and usually form a steeper beach slope. Figure 1-5 compares different sediment size effects on profile shape for the same wave conditions.

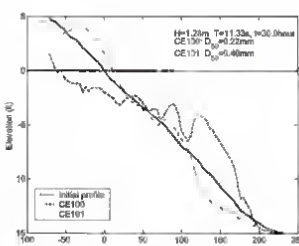

Figure 1-5. Comparison of sediment size effects on profile evolution (Data from Kraus and Larson, 1988)

1 2.4 2 Wave height

For the same profile, increasing wave height results in a wider surf zone and more wave energy dissipated thus causing more erosion Under higher waves such as storm conditions, a so-called "storm" or "winter" profile will be developed, single or multiple bars usually will appear on this kind of profile. By contrast, under lower waves, a "normal" or "summer" profile will be formed. Transport in these two conditions appears to occur in significantly distinct modes and with markedly disparate time scales, as a result, the difficulties in predictive capabilities differ substantially Figure 1-6 compares different wave height effects on the profile evolution

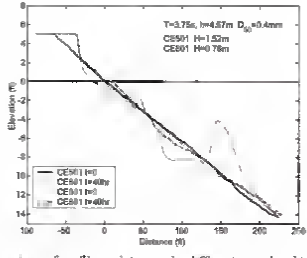

Figure 1-6 Comparison of profile evolution under different wave heights (Data from Kraus and Larson, 1988)

1.2 4.3 Wave period

According to the fall time model of Dean (1973), if the fall time of a suspended sand particle is less than half the wave period, the sand grain should move onshore Alternatively, if the fall time is greater than half the wave period, the sand particle would be carried offshore Thus longer wave periods tend to cause sediment to be transported

shoreward and the mean shoreline to advance seaward such that the average beach slope is steeper than for shorter period waves. Figure 1-7 shows different profile development under different wave periods. In both tests, grain sizes are the same, and the incident wave heights are almost the same. The test with longer wave period has an accretionary profile, on the other hand, the test with shorter wave period has an erosional profile.

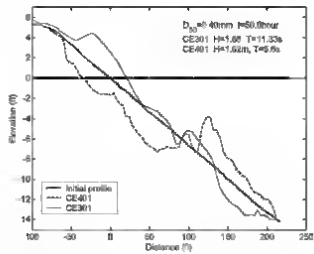

Figure 1-7. Comparison of profile evolution under different wave periods (Data from Kraus and Larson, 1988)

1.2.4 4 Regular and irregular waves

Random waves typically break across a much wider portion of the beach profile than monochromatic waves with the same average energy, producing a more evenly distributed energy dissipation across shore. Thus, the net cross-shore transport rate distribution is expected to be more uniform under random waves, causing a more gradual evolution. Figures 1-8 and 1 9 show profile changes and transport rates of two runs in SUPERTANK (Kraus and Smith 1994) under monochromatic and random waves. The beach profile was first exposed to random waves until near equilibrium. Then a

monochromatic wave was used, with a wave height the same as the significant wave height of the random wave and a wave period the same as the peak spectral period. The shape of the bar clearly changed after it was exposed to monochromatic waves. Bar size increased simultaneously as a pronounced trough developed

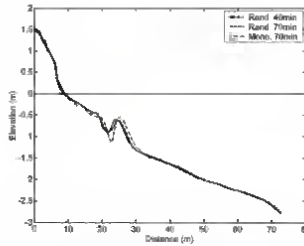

Figure 1-8 Profile Changes under random and monochromatic waves for case ST-10 in SUPERTANK (H_{mo} = 0.8 m T_p = 3 s)

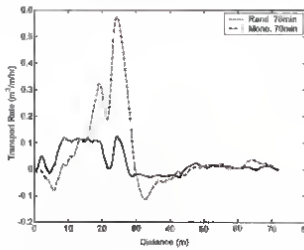

Figure 1-9 Transport rates under random and monochromatic waves for case ST-10 in SUPERTANK (H_{mo} = 0.8 m, T_p = 3 s)

1.3 Objectives and Scope of Study

At present, although progress has been made in cross-shore sediment transport modeling, there are no known models which have been demonstrated to predict adequately the time scales for nourishment profile equilibration for practical purposes The main objective of this study is to provide a better understanding of cross-shore sediment transport relationships and develop a numerical model to represent the beach profile equilibration process and determine the time scale of profile evolution, which can be applied by practicing engineers

Chapter 2 provides a detailed literature review on the subject, which includes previous valuable findings in laboratory experiments, and some analytical and numerical models developed previously

Chapter 3 is the main part of the dissertation and presents detailed descriptions of the model developed herein Three different wave energy dissipation models under monochromatic waves are examined (1) $H = \gamma h$, the spilling breaker assumption which indicates a saturated surf zone, (2) the wave transformation model of Dally Dean and Dalrymple (1985), and (3) Dally et al model coupled with the roller model of Dally and Brown (1995) The relationship between the transport rates and the deviation of the actual wave energy dissipation per unit volume from equilibration is adopted. An empirical relationship is developed which incorporates wave effects in the profile scale parameter, A (see Eq 1 1), of the equilibrium beach profile An implicit finite difference scheme with a uniformly spaced grid in the offshore direction is applied to solve the model governing equations The transport and profile evolution under random waves are determined using a wave-by-wave approach.

The model calibrations evaluations and sensitivity analyses are given in Chapters 4 and 5 The data from four large wave flume experiments are utilized for the model calibration and evaluation, these data include both regular waves and random waves. Sensitivity analyses investigate the influences of several model parameters on the model performance. In Chapter 6, both additional laboratory data and field data are applied to further investigate the model performance The model comparisons with SBEACH (Larson and Kraus, 1989) and CROSS (Zheng, 1996, Zheng and Dean, 1997) are also provided in Chapter 6

Chapter 7 presents the summary and conclusions from the study and proposes some recommendations for future model development. The program code in FORTRAN90 is presented in the appendix, where more case studies are also provided.

CHAPTER 2
LITERATURE REVIEW

2.1 Laboratory Studies

Due to the complexity of forcing and beach change processes in nature, laboratory examination under controlled conditions remains a powerful tool. Many laboratory research studies have been conducted during past decades, including small-scale and large-scale wave flume experiments. These experiments provide useful information and guidance for our understanding and modeling of beach profile evolution processes.

Reetor (1954) conducted laboratory experiments of equilibrium beach profile characteristics. He suggested that the wave steepness and the ratio of median grain size to wave length (d_{50}/L_0) played an important role in beach profile formation.

Watts (1954) investigated the influence of varying wave periods on beach profiles. It was found that the final foreshore and offshore slopes produced were essentially identical under constant period wave and varying period waves (with the mean value equal to the constant period wave), and the variable period tests created less actual material movement and less apparent bed features (bar and trough) than the constant period tests.

Raman and Earattupuzha (1972) examined the stable points on beach profiles commencing with a planar profile. A stable point is the point on a beach profile that does not undergo any considerable change during the process of profile modification due to incident waves of essentially constant characteristics. Figure 2-1 shows examples of stable points on storm and normal profiles. For a storm profile, there exists a stable point

near the breaker zone and a second stable point may exist in the offshore zone depending on the steepness of the incident waves. In the case of a normal profile, the stable point does not exist in the strict sense but there is one point on the modified profile which seems to serve the same function as a stable point in the storm profile case. They found that the depth at the stable point was proportional to the dimensionless parameter H_0gT/ν, where ν is the kinematical viscosity of water.

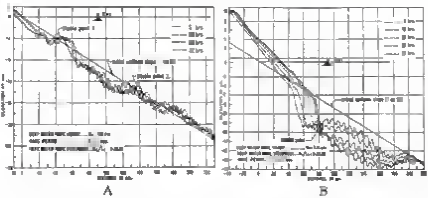

Figure 2-1 Stable points on storm and normal profiles (Raman and Easanthupuzha, 1972) A) Two stable points on a storm profile. B) Stable point on a normal profile.

Based on laboratory experiments, Sunamura and Horikawa (1974) proposed a beach classification criterion for cases in which the initial profile was planar and which included the effects of wave steepness, initial beach slope and the ratio of sand size to wave length. The three beach profile types (shown in Figure 2-2) were classified by

$$\frac{H_0}{L_0} = C(\tan\beta)^{-0.27}\left(d/L_0\right)^{0.67} \tag{2.1}$$

where β is the initial slope. For Type I profile, $C \geq 4$, Type II profile: $4 \leq C \leq 8$, Type III profile: $C \leq 8$.

Watanabe et al. (1980) conducted a series of small-scale experiments using two different sand diameters (0.2 mm and 0.7 mm). Each experiment began with a uniform

initial slope of 1/10 or 1/20 and was conducted under different wave conditions for one-hour. They confirmed the beach profile classification criterion of Sunamura and Horikawa (1974) and related the net sediment transport rates to the Shields parameter by

$$\Phi = A(\Psi - \Psi_{cr}) \qquad (2.2)$$

where $\Phi = Q/wd$ is the dimensionless transport rate, w the fall velocity, d the grain diameter, $\Psi = \frac{\tau_b}{\rho(s-1)gd}$ is the Shields parameter and Ψ_{cr} is the critical value for the initial sediment movement. Figure 2-3 shows the results of their relationship between net transport rate and Shields parameter.

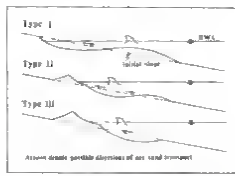

Figure 2-2, Three types of beach profiles (Sunamura and Horikawa, 1974)

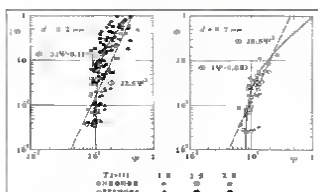

Figure 2-3 Relationship between net transport rate and Shields parameter (Watanabe et al., 1980)

Kajima et al. (1982) classified the net transport rate into five types (Figure 2-4) based on their large wave flume data. They also proposed a model of beach profile change by assuming that the total on-offshore transport rate Q could be represented as the sum of three independent components of net sand transport rate

$$Q = Q_1 - Q_2 + Q_3 \tag{2.3}$$

where Q_1 = net onshore transport outside the surf zone caused by nonlinearity of the fluid motion under waves, Q_2 = net offshore transport inside the surf zone caused by time-averaged seaward-directed currents, and Q_3 = net onshore transport in the swash zone caused by wave run-up. The three components were each assumed to be Gaussian distributed.

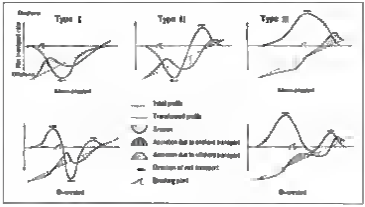

Figure 2-4 Types of net transport rate distributions (Kajima et al., 1982)

Sunamura and Maruyama (1987) used large wave flume experimental data to examine eroding beach characteristics. They found the bar migration directions could be classified by dimensionless parameter K defined as

$$K = H_b^2 / g T^2 A \tag{2.4}$$

If K > 10, bars move offshore; whereas they move onshore if K < 10

The time required for the attainment of steady state, t_s, in the height of seaward migrating bars, t_s was found to be described by

$$t_s/T = 1.2\times10^5\left(H_b/gT^2\tan\beta\right) \tag{2.5}$$

where the parameter in the bracket is the square of the Iribarren number and indicates the breaker type. With increasing values of this parameter, the breaker type changes from plunging to spilling. The time variation of the bar crest location, X, was expressed by an exponential form as

$$X - X_e\{1-\exp(-t/\tau)\} \tag{2.6}$$

where X_e is the equilibrium value of X, τ is a so-called equilibrium time scale. At $t=\tau$, X reaches 63% of the total change X_e. τ was found to be

$$\tau = 2.87\times10^7 H_b^{1.5}/g^{1.5}T^2 \tag{2.7}$$

Other experiments include the large wave tank (LWT) experiment in 1956-1957 and 1962 by Saville in Dalecarlia, Washington, D.C. (Kraus and Larson, 1988), Large Wave Flume in Hannover, Germany (Dette and Uliczka, 1987, Dette et al., 1998), experiments at the Central Research Institute of Electric Power Industry in Japan (Sunamura and Maruyama, 1987). SUPERTANK project in the large wave tank at the Ottc Hinsdale Wave Research Laboratory, Oregon State University (Kraus and Smith, 1994), and LIP 1-D Delta Flume experiments (Roevink and Reniers, 1995), etc. Some of the tests include regular waves, whereas others include both regular and irregular waves. They provide many useful data for later studies on the profile evolution process.

2.2 Numerical Modeling Studies

Some recent interesting reviews of cross shore sediment transport models have been reported from different methods and viewpoints by Broker Hedegaard et al (1992), Steetzel (1993), and Schoonees and Theron (1995) Broker Hedegaard et al made an intercomparison of six different coastal profile models against measured profile evolutions from a large wave flume (under dune erosion conditions) Steetzel classified transport formulae as empirical transport shear stress related transport, energy dissipation related transport, energy dissipation related suspension and velocity related transport Schoonees and Theron summarized ten internationally developed transport models according to their theoretical basis and morphological verification data.

Generally, numerical models of profile evolution can be termed as "open loop" and "closed loop" (Dean, 1995, Dean and Dalrymple, 2002) An open loop model is not constrained to a final profile and the sediment transport is determined by sediment fluid properties Open loop models required detailed or idealized representation of the hydrodynamics and sediment transport processes. Closed loop models are characterized by the specification of a particular "target profile," to which the computed profile will converge if the forcing mechanisms are held constant indefinitely Cross-shore transport is modeled by deviations of a beach profile from equilibrium Open loop models are microscale related approaches, whereas closed loop models are more macroscale and use empirical equations based on laboratory and/or field data to provide reasonable solutions

2.2.1 Closed Loop Models

2.2.1 1 EDUNE model

One of the first closed loop models developed was that of Kriebel (1982) and Kriebel and Dean (1985) (originally called EBEACH and later called EDUNE) based on

the energy dissipation concept The basic concept was that, for a uniform sand size across the profile, a uniform energy dissipation rate per unit volume resulted in the $Ay^{2/3}$ profile as an equilibrium beach If the beach profile differed from this equilibrium form, the dissipation rates across the surf zone would differ from the equilibrium value. The cross-shore sediment transport rate at any point in the surf zone, Q, was related to the difference between the actual and equilibrium levels of wave energy dissipation in the surf zone (D and D_*, respectively)

$$Q = K(D - D_*) \tag{2.8}$$

where K is a transport rate parameter found during calibration tests first based on the LWT data of Saville and later Hurricane Eloise profile data (Kriebel 1986), resulting in a value of 8.75×10^{-6} m^4/N Using shallow water wave theory and assuming spilling breakers, D was determined as

$$D = \frac{5}{16}\rho g^{1.5}\gamma^2 h^{2.5}\frac{dh}{dy} \tag{2.9}$$

where $\gamma = 0.78$ is the breaker index, ρ is density of sea water and g is gravity To obtain time-dependent profile evolution, an implicit double-sweep method was employed to solve the transport equation and the conservation of sand equation

$$\frac{dy}{dt} = -\frac{\partial Q}{\partial h} \tag{2.10}$$

Both Q and y are defined as positive in the offshore direction and h is positive below the still water level. Offshore, sediment transport was assumed to be effectively limited at the break-point of the incoming waves Later developments included the effects of wave run-up, dune steepening, and dune overwash in the onshore boundary region (Kriebel,

1990) Figures 2-5 and 2 6 show examples of application of the model for large wave tank and field data, respectively

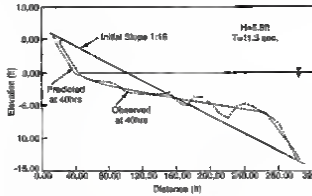

Figure 2-5 Comparison of EDUNE model results with large wave tank data by Saville (Kriebel, 1986)

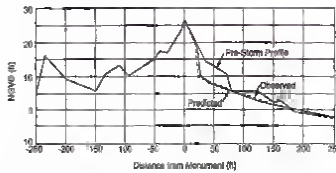

Figure 2-6 Comparison of EDUNE model results with a field profile affected by Hurricane Eloise (Kriebel, 1986)

2.2.1 2 SBEACH model

Based on observations from large wave tank data (mainly from Kraus and Larson, 1988 and Kajima et al., 1982), Larson (1988) and Larson and Kraus (1989) developed a model called SBEACH to predict beach profile change resulting from cross-shore sand transport, focusing on the main morphologic features of bars and berms Changes in the beach profile were assumed to be produced by breaking waves; therefore, the cross-shore transport rate was determined from the local wave, water level, and beach profile

properties and the conservation equation of sand in the cross-shore direction was solved to compute profile changes as a function of time

This model included a wave module to calculate the wave height and other wave-related properties at grid points on a profile line The wave height was determined by linear wave theory in regions of nonbreaking by assuming locally plane and parallel depth contours and using the Dally, Dean and Dalrymple (1984) model in the surf zone Based on the wave dissipation model of Dally et al an equilibrium profile (Eq.2 11) was determined,

$$y = \frac{h}{m} + \left(\frac{h}{A_*}\right)^{3/2} \tag{2 11}$$

where m is shoreline slope, the A_* value is different from the A value used in the usual equilibrium profile equation due to the additional linear slope dependence.

The distribution of transport rate across the nearshore zone was calculated using different relationships in four distinct zones (Figure 2-7)

- Zone 1 Pre-breaking zone, extending offshore from the breaking point.

The sediment transport rate was expressed as

$$Q = Q_{BP} \exp[-\lambda_1 (y - y_{BP})] \tag{2 12}$$

where Q_{BP} is the sediment transport at the break point, y_{BP} is the break point location, λ_1 is the spatial decay coefficient given by

$$\lambda_1 = \begin{cases} 0\,11 & \text{For Accretionary Conditions} \\ 0\,4\left(\frac{d_{50}}{H_b}\right)^{0.67} & \text{For Erosion Conditions} \end{cases}$$

where d_{50} is the median grain size in mm, H_b is the breaking wave height in m, and the unit of λ_1 is m^{-1}

- Zone II Transition zone from the break point to the plunge point.

The sediment transport was given by

$$Q = Q_{PP} \exp[-\lambda_2 (y - y_{PP})] \tag{2.13}$$

where Q_{PP} is the transport rate at the plunge point located at y_{PP}, the decay coefficient λ_2 is approximately 0.20-0.25 of the value of λ_1

- Zone III Broken wave zone from the plunge point to the seaward limit of swash zone.

The sediment transport rate was determined by

$$Q = \begin{cases} K(D - D_c + \dfrac{\varepsilon}{K}\dfrac{\partial h}{\partial y}) & D > D_c - \dfrac{\varepsilon}{K}\dfrac{\partial h}{\partial y} \\ 0 & D \le D_c - \dfrac{\varepsilon}{K}\dfrac{\partial h}{\partial y} \end{cases} \tag{2.14}$$

where ε is transport rate coefficient for the slope-dependent term, and K is an empirical transport rate coefficient This relationship was similar to that of EDUNE model except for the last term which incorporates the effect of local slope

- Zone IV Swash zone from the seaward swash zone limit to the run-up limit

The transport equation was a linear function of offshore distance

$$Q = Q_{WR} \frac{y - y_{RU}}{y_{WR} - y_{RU}} \tag{2.15}$$

where the subscripts WR and RU denote landward end of surf zone and run-up limit, respectively Eq 2.15 resulted in a plane slope above the shoreline The direction of transport rate in all four zones was determined according to Eq 2.16

$$\begin{aligned} &\frac{H_b}{L_0} < 0.0007 \left(\frac{H_b}{wT}\right)^3 && \text{Offshore transport} \\ &\frac{H_b}{L_0} \ge 0.0007 \left(\frac{H_b}{wT}\right)^3 && \text{Onshore transport} \end{aligned} \tag{2.16}$$

where H_0 and L_0 are the deep water wave height and length respectively, w is the sediment fall velocity and T is the wave period

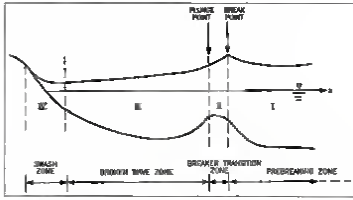

Figure 2-7. Principal zones of cross-shore transport (Larson and Kraus, 1989)

Later, Wise et al (1996) modified the model to simulate cross-shore profile changes under random waves A semi analytic random wave model based on Dally et al (1984) model was developed to predict the wave height, the fraction of broken, unbroken and reformed waves, and the wave energy dissipation across shore. Then the original transport equations were modified to represent transport under broken and unbroken waves An algorithm for dune erosion produced by overwash was also developed in this version. Later, Larson and Kraus (1998) included hard bottom effects into the model

2.2.1.3 CROSS model

Zheng (1996) and Zheng and Dean (1997) developed a non-linear cross-shore model (CROSS), which was a modification of the EDUNE model and based on scale analysis.

From Eq 2 8, the scaling relationship in Eq 2 17 can be established,

$$Q_* = \frac{(D - D_*)_{model}}{(D - D_*)_{prototype}} = (D - D_*)_r \qquad (2\ 17)$$

in which the subscript r indicates a ratio of model to prototype values. For an undistorted model, according to the definition of D (Eq 2.9), the disequilibrium scale ratio can be expressed in terms of the length scale ratio, L_r, as

$$(D-D_*)_r = \sqrt{L_r} \tag{2.18}$$

On the other hand, the Froude relationship yields the time scale ratio, T_r, as

$$T_r = \sqrt{L_r} \tag{2.19}$$

From the relationships presented, the cross-shore sediment transport, Q, should be scaled as

$$Q_r = \frac{L_r^2}{T_r} = L_r^{3/2} \tag{2.20}$$

If K is considered to be a constant, the scaling ratio of the Kriebel and Dean formulation can be shown to be

$$Q_r = L_r^{1/2} \tag{2.21}$$

which does not provide a valid scaling of the transport unless K varies with scale. A transport rate equation was then proposed

$$Q = K(D-D_*)\left|D-D_*\right|^{n-1} \tag{2.22}$$

which results in the following scale relationship

$$Q_r = K_r(D-D_*)_r\left|D-D_*\right|_r^{n-1} = K_r L_r^{n/2} \tag{2.23}$$

n = 3 was determined by assuming K_r independent of the length scale and equal unity such that both the scaling relationship and convergence to the equilibrium profile are satisfied. They argued that this relationship could provide a reasonable explanation for

the significantly different time scales of beach evolution evident in various laboratory experiments.

The model boundary conditions were from the breaking point to run-up limit. To overcome unrealistic slopes in the predicted profiles, three characteristic profile slopes (dune, shoreline and offshore slopes) were specified in the model (Figure 2-8). The dune slope, which is defined as the averaged dune scarp slope after erosion, is the maximum slope that the profile is allowed to achieve. The shoreline slope is the anticipated profile slope between the shoreline and the run-up limit. The offshore slope is introduced to control the slope at the seaward end of the deposited volume. After each time step, if the profile is steeper than the limiting slopes, avalanching occurs and the profile is smoothed to the prescribed slopes.

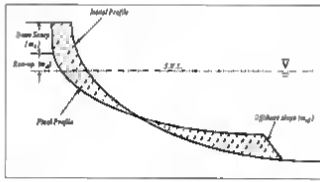

Figure 2-8 Definition of dune, shoreline and offshore slope (Zheng, 1996)

CROSS provides much better agreement for some experiments, an example of which is shown in Figure 2-9, which presents a comparison with the data in the German large wave flume experiments from Dette and Uliczka (1987). The comment from Dean (1999) about this model is

> The new transport relationship may represent profile recovery better than previous relationships employed. This is consistent with the slower transport associated with a profile only slightly out of equilibrium as occurs with n=3

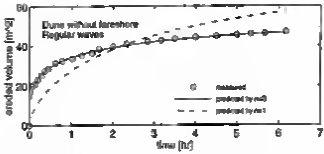

Figure 2-9 Comparison of linear (n=1) and nonlinear (n=3) transport rates with measured data in German large wave flume (Zheng 1996)

2.2 1.4 Kobayashi model

Kobayashi (1987) suggested a two-parameter sediment transport rate equation as following

$$Q = D(h)\frac{dh}{dx} \quad K \ , \ 0 \le h \le h_b \tag{2.24}$$

where D and K are empirical functions and related to the wave condition and sediment characteristics inside the surf zone The suggested form of D and K by Kobayashi (1987) are

$$D(h) = \alpha h^{(1-n)/2} \ , K - n\alpha A^{1/2} \tag{2.25}$$

which generate a steady stable solution, $h = A(x+R)^n$, similar to the equilibrium beach profile by Dean (1977) A and α are parameters related to the sediment size and fall velocity When n = 2/3, Eq 2.24 becomes identical to that of Kriebel and Dean (1985)

Lee et al (1996) used this formulation and developed a numerical model to simulate the cross-shore profile evolution with moving boundaries Further, Lee et al. (1999) extended this model to a multi domain hybrid numerical model including the generation and movement of nearshore bars by breaking waves Similar to the SBEACH model by Larson and Kraus (1989), the computation domain is divided into three

subdomains, including post-breaking zone, breaking zone and pre-breaking zone In each region, different sediment transport rate equations were used

In the post-breaking zone,

$$Q_1 = D\frac{\partial h}{\partial x} - K\,, \quad -R(t) \le x \le x_p(t) \tag{2.26}$$

$$D = \alpha\sqrt{h_p}\,, K = \frac{2}{3}\alpha A^{3/2} \tag{2.27}$$

where h_p and x_p are the water depth and distance from the origin to the plunge point, R(t) is the distance from the origin to the point h(x,t) = 0 In the breaking zone and pre-breaking zone, the sediment transport rates were assumed to have the following explicit expressions,

$$Q_2 = q_s(t)\exp(-\lambda_1(x-x_s)^2),\ x_p \le x \le x_b \tag{2.28}$$

$$Q_3 = q_b(t)\exp(-\lambda_2(x-x_b)),\ x_b \le x \le \infty \tag{2.29}$$

where $q_s(t)$ and $q_b(t)$ are time dependent amplitude functions for the respective sediment transport rates in breaking zone and pre-breaking zone. Eq 2.28 is different from the exponential function used in SBEACH. This equation means that the sediment transport rate in breaking zone has a Gaussian distribution (Kajima et al. 1982) which has a maximum value at a point x_s positioned between plunging and breaking points. The relationship between λ_1 and λ_2 was found to be

$$\lambda_1 = \lambda_2^2 \tag{2.30}$$

The empirical formula for λ_2 in the model was

$$\lambda_2 = 2.70\left(\frac{d_{50}}{H_b T}\right)^{0.75} \tag{2.31}$$

The model was formed by the combination of numerical solutions (post breaking zone I) and empirically based analytic solutions (breaking zone II and pre-breaking zone III) This model can straightforwardly be extended to multi bar problems by systematically adding more subdomains. Figures 2-10 and 2-11 show comparisons of single-bar and multi-bar results with LWT experimental data (Kraus and Larson, 1988)

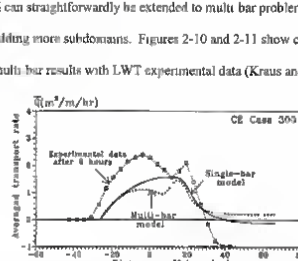

Figure 2-10. Comparison of the averaged net sediment transport rates computed from the single-bar and multi-bar numerical models with CE Case 300 experimental data after 5 hours (measured profile had two bars) (Lee et al., 1999)

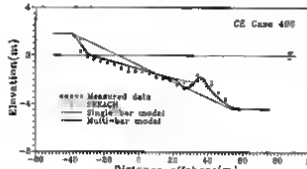

Figure 2-11 Comparison of the single-bar and multi-bar numerical results with SBEACH and CE Case 400 data after 40 hours (Lee et al., 1999)

2.2.1.5 Analytical models

Two analytical or semi analytical closed loop models have been documented in the literature Kobayashi (1987) combined the conservation equation and the transport relationship in Eq 2 24 into one equation representing the profile response,

$$\frac{\partial h}{\partial t} = \frac{\partial}{\partial y}\left(D\frac{\partial h}{\partial y} - K\right) + \frac{\partial S}{\partial t} \qquad (2.32)$$

where D and K are defined in Eq 2 25. The landward and seaward limits of the domain were treated as moving boundaries and the eroding dune face was represented as a vertical face. An analytical solution was determined for a particular initial condition. It was found that the problem is mathematically similar to a diffusion problem in which the convergence to the steady state problem first occurs rapidly and later approaches the steady state solution asymptotically. The model results were found to approximate the numerical solutions of the EDUNE model.

Kriebel et al. (1991) and Kriebel and Dean (1993) developed and illustrated a convolution method of representing beach profile evolution. The method is based on the observation from numerical solutions that for a constant forcing function, i.e., water level, a particular contour y(t) tends to approach the equilibrium value y_∞ asymptotically in approximate accordance with the following relationship

$$y(t) = y_\infty(1 - e^{-t/T_s}) \qquad (2.33)$$

in which T_s is the characteristic time scale of the exponential response. The solution is obtained in the form of a convolution integral of the response function and the water level history, f(t),

$$y(t) = \frac{y_\infty}{T_s}\int_0^t f(\tau)\exp[-(t-\tau)/T_s]d\tau \qquad (2.34)$$

The method was found to yield very similar results to those obtained through numerical modeling.

2 2 2 Open Loop Models

Open loop models usually relate cross-shore sediment transport to the detailed physics of the flow field such as sediment concentration, fluid velocity, and bottom shear stress, etc Some of these models will be reviewed briefly here.

2.2.2 1 Dally and Dean model

The Dally and Dean model (Dally, 1980 Dally and Dean, 1985) was based on net time averaged flux of suspended sediment past a section in the nearshore zone given by

$$Q = \int_{depth} u(z)C(z)dz \tag{2.36}$$

where u(z) = average horizontal velocity at level z, and C(z) = suspended sediment concentration at level z.

The flow regime was divided into an upper layer where only mean flow was considered and a lower layer where both mean flow and orbital velocity were taken into account The interface between layers was determined by the elevation at which the assumed uniform sediment would fall back to the bottom in one wave period Linear wave theory was used to predict orbital velocities and stream function wave theory had been applied to obtain second-order mean flow velocities The cross-shore wave heights were obtained from the breaker decay model of Dally et al (1984)

The suspended sediment concentration was considered to be exponential as given by

$$C(z) = C_a \exp\left[\frac{-1.5w(z - z_a)}{h\sqrt{\tau/\rho}}\right] \tag{2.37}$$

where C_a is the concentration at an arbitrary reference elevation, z_a. The ratio of the sediment fall velocity, w, to the bottom shear velocity, $\sqrt{\tau/\rho}$, governed the exponential

nature of the profile The shear velocity was assumed to be the sum of the shear velocities due to wave-induced bottom shear and breaking-induced turbulence.

The continuity equation was then solved in an explicit finite difference scheme However, to prevent numerical instability just outside the surf zone empirical transport spreading was applied. The model could produce both normal and storm profiles (Figure 2-12), however, the beach profile shapes were not very favorable quantitatively

Steetzel (1993) also presented his cross-shore transport model as the integral of the product of concentration and velocity over time and depth. The sediment concentration was found from a one-dimensional, non-stationary convection-diffusion equation. The reference concentration at the bed was assumed to be related to the breaking type and the dissipation of the turbulent kinetic energy The cross-shore transport rate was calculated in two parts, that is, below and above the mean trough level Above the trough level, concentration was a constant and given by that at the mean water level

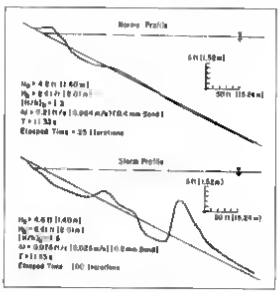

Figure 2-12 Example output to illustrate characteristics of the Dally and Dean model (Dally and Dean, 1985)

2 2.2 2 Nairn and Southgate model

A second widely used transport relationship in open loop models is based on the energetic approach (originally due to Bagnold) The energetic approach is a sediment transport prediction method based on the idea that a proportion of fluid energy is expended in maintaining a sediment transport load This method was originally developed for riverine flows and has been adapted for coastal purposes by Bailard and Inman (1981), Bailard (1981,1982) and Bowen (1980) The Bailard energetic transport relationship has been applied and adjusted by a number of investigators and incorporated into several profile evolution models

The Nairn and Southgate model (Southgate and Nairn, 1993, Nairn and Southgate, 1993) is an energetics type An expanded version of Bailard s formula by Shve (1986) was adopted

$$Q = \rho c_f \frac{\varepsilon_b}{\tan\phi}\left[< |u|^2 \tilde{u} > + \frac{3}{2} \bar{u} u_m^2 - \frac{\tan\beta}{\tan\phi} < |u|^2 > \right]$$

$$+ \rho c_f \frac{\varepsilon_s}{w}\left[< |u|^3 \tilde{u} > + 4\bar{u} < |u|^3 > - \frac{\varepsilon_s}{w} \tan\beta < |u|^5 > \right] \qquad (2\ 38)$$

where ε_b and ε_s are bed and suspended load efficiency factors c_f is a drag coefficient of the bed, ϕ is the internal angle of friction or the sediment, $\tan\beta$ is the bottom slope, u, $\bar{u}$, and $\tilde{u}$ are the horizontal instantaneous velocity mean velocity component, and time varying velocity, respectively, u_m and w are the peak bed orbital velocity and the sediment fall velocity, respectively and <> means time average over a wave period Sediment is advected as either bed or suspended load by (1) asymmetric orbital velocities, (2) mean flows, and (3) the downslope component of gravity

The model included a special treatment of the wave transition zone. The transition zone length, l_t, was calculated by a "length method"

$$l_t = 0.556 m_b L_b \xi^{1.465} \tag{2.39}$$

where $\xi = \frac{m_b}{(H_b / L_b)^{1/2}}$ and m_b, L_b, H_b are respectively the bed slope, wave length and wave height at breaking.

After the transition zone length was given, an expression for the fraction of waves, Q_t, in the breaking induced turbulence region was determined as

$$Q_t(y) = Q_b(y - l_t) \tag{2.40}$$

where Q_b is the fraction of wave breaking in the surf zone predicted by a wave transformation model, y is the cross-shore coordinate. In the Nairn and Southgate model, fixed surface and erodible surface problems were also addressed. The model has been compared with both small scale and prototype laboratory data, and the rate and type (i.e. erosion, deposition and bar migration) of beach response can be well estimated.

Plant et al. (2001) developed a simple parametric model for the cross-shore transport based on Bagnold's model

$$Q = \left(cH^3 h^{-3/2}\right)\left\{\frac{\partial h}{\partial y} - \left(r_1 \frac{H}{h}\right) + \left(r_2 \frac{H}{h}\right)^2\right\} \tag{2.41}$$

where c, r_1, and r_2 are free parameters to be calibrated, H is the local wave height. The first term in parentheses is a wave stirring term, and the terms in braces form a rectification function representing the influences of downslope transport, onshore transport due to weak wave nonlinearity (e.g. wave steepness), and offshore transport due to strong nonlinearity (e.g. undertow).

2.2.2.3 Watanabe model

Watanabe (1988) presented a sediment transport rate equation related to local wave-current conditions and bottom shear stress. The total transport rate was the sum of contributions from mean current, Q_c, and waves, Q_w, which are expressed, respectively, by

$$Q_c = A_c(\tau - \tau_c)U / \rho g \tag{2.42}$$

$$Q_w = A_w F_D(\tau - \tau_c)u_m / \rho g \tag{2.43}$$

where A_c and A_w are non-dimensional coefficients, U the current velocity vector, u_m the maximum near bottom orbital velocity vector, F_D a direction function for wave-induced net transport, τ the maximum bottom shear stress in a wave-current coexisting system, and τ_c the critical shear stress for the onset of the general movement.

These formulas are based on the wave power concept and assume that the sediments set in motion by the excess shear stress under combined wave-current action, are transported by both mean currents and wave motion into the respective directions. The coastal profile model WATAN3 developed by University of Liverpool (reviewed in Broker Hedegaard et al., 1992) is based on the Watanabe transport equations.

There are some other transport relationships such as the one developed by Nishimura and Sunamura (1986), in which the transport rate was related empirically to the Ursell number and the Hallermeier parameter, which represent the skewness of water particle velocity profile and the intensity of sediment movement, respectively. Camenen and Larroude (2003) compared four process-related sediment transport formulas with field and experimental data and gave some recommendations on the use of these different formulas.

Most open loop profile change models include modeling of hydrodynamic processes to different degrees The sediment transport calculations are related to the properties of sediment and flow field Van Rijn et al (2003) compared five major coastal profile change models developed in Europe The five models are UNIBEST-TC of Delft Hydraulics, COSMOS of HR Wallingford, CROSMOR2000 of University of Utrecht, BEACH1/3D of University of Liverpool, and CIRC of University of Catalunya The computed results from these models have been compared with large wave flume data and field data. Figures 2-13 and 2-14 show the calculated profile evolution and hydrodynamic results, respectively, with comparison to the measurements in one case from COAST3D-Storm Experiment at 3D field site of Egmond, Netherlands It is noted that the all five models present good fits for the profile although the calculated hydrodynamics are quite different It seems that considerable uncertainty in the understanding of surf zone hydrodynamics and sediment transport processes still exists

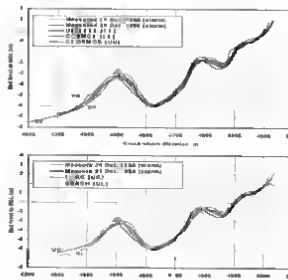

Figure 2-13 Computed bed profiles by UNIBEST-TC, COSMOS, CROSMOR2000, BEACH1/3D, and CIRC with comparison to measured results (Van Rijn et al , 2003)

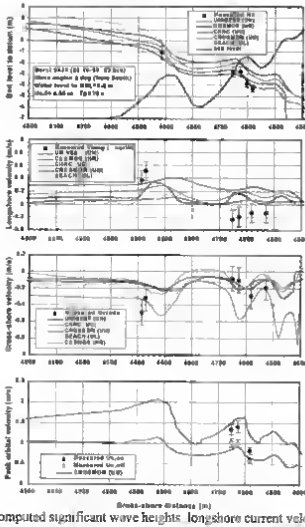

Figure 2-14. Computed significant wave heights, longshore current velocities, cross-shore current velocities and peak orbital velocities by UNIBEST TC, COSMOS, CROSMOR2000, BEACH1/3D, and CIIRC with comparison to measured results (Van Rijn et al , 2003)

2.3 Summary

Various representations have been proposed for open loop models. Both normal and storm profiles can be generated by most of the open loop models. However, open loop models do not incorporate a strong feedback mechanism that will assure equilibrium under wide ranges of conditions. Thus, it is not known whether or not these models are

stable for long run times. Due to the considerable complexities and uncertainties of hydrodynamics and related sediment transport processes in the nearshore region, and the uncertainties in convergence, it appears that the open loop models should be considered in the research rather than applications arena.

The transport equation for the closed loop models is chosen to ensure equilibration for fixed forcing conditions. These closed-loop models provide limited successful and encouraging results and easy application to practical engineering problems. These models are relatively simple and do not require detailed calculation of hydrodynamics and sediment transport processes as in open-loop models. They are all based on equilibrium beach profile concepts and capture one of the dominant causes of sediment transport inside the surf zone, namely wave energy dissipation.

However, there are some limitations to these closed loop models. (1) The grid system used is different. EDUNE and CROSS use a grid with h and t as the independent variables, while the SBEACH and Lee et al. models use a grid with y and t as the independent variables. The disadvantage of the first type of grid system is that it has difficulties in representing bar profiles. (2) The transport direction in EDUNE and CROSS is determined on the relative magnitude of wave energy dissipation per unit volume to its equilibrium value; SBEACH uses an empirical relationship to determine the transport direction along the whole profile, which can not produce an intermediate profile between fully erosion and accretion (type II profile in both Figures 2-2 and 2-4). The other severe shortcoming of SBEACH, as Dean (1995) pointed out, is that the transport direction empirical relationship used does not include any of the profile characteristics and thus even if the profile is very steep, such as after beach nourishment and the wave

and sediment characteristics indicate offshore transport, the transport direction predicted by the model is onshore (3) The equilibrium profile used in these models depends only on sediment size through the profile scale factor, which cannot explain the seasonal profile slope changes in nature (4) The wave energy dissipation in EDUNE and CROSS is based on the spilling breaker assumption and thus cannot produce bar profiles. SBEACH adopts a more robust wave model to generate bars, but deals with the transition zone on an empirical basis. (5) The transport in the swash zone, during overwash and in front of seawalls are either not included or not well described in previous models (6) Another limitation is the transport and profile changes under random waves To the author's knowledge, a representative wave height (usually root square-mean wave height or significant wave height) is used in these models except CROSS to simulate random waves.

The motivation of this study is to address the limitations present in existing models and develop a more physically robust cross-shore profile change model to better represent the cross-shore sediment transport processes inside the surf zone (such as bar formation, profile changes under random waves, etc.) which can be used in practical field applications.

CHAPTER 3
CROSS SHORE PROFILE EVOLUTION MODEL DEVELOPMENT

This chapter presents the cross-shore profile evolution model developed in conjunction with this dissertation. The proposed model extends the previous closed loop models reviewed in Chapter 2 and incorporates new findings to improve the model capability to better represent natural conditions. The following states the questions to be addressed in this effort:

- What is the best representation of sediment transport rate in
$$Q - K(D - D_*)|D - D_*|^{n-1} \tag{3.1}$$
n = 1 (as in EDUNE, SBEACH) or n = 3 (as in CROSS) or other values?
- Different breaking waves (spilling/plunging) dissipate their energy in different ways thus cause different current patterns and different sediment transport. How should these effects be represented in large-scale numerical models?
- What is the best representation of the bar-type profile generation mechanism? One promising and realistic approach is to lag (in the landward direction) the wave energy dissipation per unit volume D.
- What is the best representation of different time scales of beach profile evolution depending on initial profile and wave conditions?
- What is the best representation of sediment transport under irregular waves?

In this chapter, the wave transformation models are introduced first to determine the wave energy dissipation under both regular and random waves. This is followed by investigation of resulting different equilibrium beach profile forms. A new empirical relationship based on large-scale experimental data is then presented to incorporate the wave effects on the profile scale parameter in the equilibrium beach profile. Finally, the detailed development of the model and the numerical solution are described.

3 1 Wave Energy Transformation Models

Wave energy transformation is different for monochromatic and random waves Random waves typically break across a much wider portion of the beach profile than monochromatic waves with the same average energy, producing a more evenly distributed cross-shore energy dissipation Thus they should be treated differently in the model

3 1.1 Wave Breaker Type

Four different types of breaking waves have been identified, namely spilling, plunging, surging and collapsing In general, spilling breakers tend to occur on beaches of very low slope with waves of high steepness values plunging breakers are associated with steeper beaches and waves of intermediate steepness, surging occurs on high gradient beaches with waves of low steepness and collapsing breaker is intermediate between the plunging and surging Galvin (1968) found fairly good breaker-type correlations with the well known Iribarren number (also called surf similarity parameter)

$$\xi_0 = \frac{m}{\sqrt{H_0 / L_0}} \tag{3 2}$$

where m is the beach slope, H_0 and L_0 are the deepwater wave height and wavelength, respectively Battjes (1974), Okazaki and Sunamura (1991), and Smith and Kraus (1991) recommended adjustments on the limits to classify different breaker types. Table 3 1 summarizes the breaker type classifications from different resources

Table 3-1 Summary of breaker type classification criteria.

Breaker type	Galvin (1968)	Battjes (1974)	Okazaki and Sunamura (1991)	Smith and Kraus (1991)
Spilling	$\xi_0 < 0.46$	$\xi_0 < 0.5$	$\xi_0 < 0.5$	$\xi_0 < 0.4$
Plunging	$0.46 < \xi_0 < 3.3$	$0.5 < \xi_0 < 3.3$	$0.5 < \xi_0 < 2.5$	$0.5 < \xi_0 < 1.2$
Surging	$\xi_0 > 3.3$	$\xi_0 > 3.3$	$\xi_0 > 3.7$	$\xi_0 > 1.2$

Different breaker types decay in different manners inside the surf zone On steeply sloping reflective beaches, once waves break they immediately surge up the beach face as runup, with little intervening surf In contrast, on lower sloping dissipative to intermediate beaches, there can be an extensive surf zone, at times being crossed by several broken wave lines while a few small waves have not yet broken Plunging breakers characteristically dissipate their energy in a concentrated manner in the region just shoreward of the breaker line while spilling breakers dissipate their energy at a slower, more uniform rate over a greater surf zone width Through laboratory experiments, Ting and Kirby (1994, 1995, 1996) found that turbulent kinetic energy was transported seaward under the spilling breaker and landward under the plunging breaker by the mean flow Ting and Kirby (1994) stated that

> Nevertheless, in most situations there is a net offshore movement of sediment in spilling breakers and a net onshore movement in plunging breakers

In order to test the plausibility of their argument, 14 cases of Large Wave Tank (LWT) (Kraus and Larson, 1988) and 10 cases of CRIEPI Flume (Kajima et al , 1982) experiment data (all periodic waves) are investigated Table 3-2 lists the test conditions for these experiments and Figure 3-1 shows the results The criteria of accretive and erosive profile based on the fall velocity parameter H_b/wT and spilling/plunging breaker based on surf similarity parameter are also shown in the plot.

These results show that the surf similarity parameter alone cannot give a clear and correct classification of profile types although the model is correct in 19 of 25 cases, whereas the fall velocity parameter discriminates correctly in 22 of 25 cases. The data in Figure 3-1 also demonstrate that an approximate inverse correlation exists between the surf similarity parameter and the fall velocity parameter (as discussed by Dean, 1987)

Table 3-2 Conditions and test cases in LWT and CRIEPI Flume experiments

Case	Median diameter of sand (mm)	Initial beach slope	Wave height H (m)	Wave period T(s)	Deepwater Wave steepness
CE100	0 22	1/15	1.28	11 33	0 0054
CE200			0 55	11 33	0 0023
CE300			1 68	11 33	0 0070
CE400			1 62	5 6	0 0351
CE500			1 52	3 75	0 0750
CE600			0 61	16 0	0 0011
CE700			1 62	16 0	0 0028
CE101	0 40		1 28	11.33	0 0054
CE201			0 55	11 33	0 0023
CE301			1 68	11 33	0 0070
CE401			1 62	5 6	0 0351
CE501			1 52	3 75	0 0750
CE701			1 62	16 0	0 0028
CE801			0 76	3 75	0 0377
CE901			1 34	7 87	0 0129
CRIEPI1-1	0 47	1/20	0 44	6.0	0 0082
CRIEPI1-3			1 05	9 0	0 0075
CRIEPI1-8			0 81	3 0	0 0607
CRIEPI2 1		3/100	1.80	6 0	0 0313
CRIEPI2 2			0 86	9 0	0 0058
CRIEPI2 3			0 66	3 1	0 0473
CRIEPI3-1	0.27	1/20	1.07	9 1	0 0074
CRIEPI3 2			1.05	6 0	0 0196
CRIEPI3-3			0 81	12 0	0 0029
CRIEPI3-4			1 54	3 1	0 1080

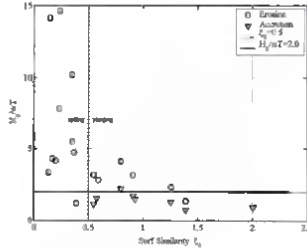

Figure 3-1 Surf similarity parameter and fall velocity parameter versus beach erosion/accretion

3.1.2 Wave Transformation Models

3.1.2.1 Monochromatic wave transformation models

In the EDUNE and CROSS models, a constant ratio of breaker height to water depth inside the surf zone (spilling breaker assumption) was used, which is not applicable on non-monotonic beach profiles such as those containing bar/trough features. For this case, energy dissipation occurs only if $\partial h/\partial y > 0$

One popular simple wave model in the surf zone is Dally, Dean and Dalrymple model (Dally et al , 1984, 1985) Hereafter, it will be referred as D^3 model Other wave models such as those based on Boussinesq equations are very time-consuming and not a good choice for very long time profile evolution simulation The governing equation of the D^3 model is given in Eq I.9 and repeated in Eq 3 3

$$\frac{\partial EC_g}{\partial y} = \frac{K}{h}\left[EC_g - E_t C_g\right] \qquad (3\ 3)$$

where EC_g is energy flux, $E_s C_s$ is the energy flux associated with the stable wave that the breaking wave is striving to attain for the particular water depth, and K is a dimensionless decay coefficient. For increasing K, the breaking wave height dissipates faster and vice versa. Thus, choosing different K values in the D^3 model may approximate different wave breaking types. The stable wave height, H_s is given by

$$H_s = \Gamma h \tag{3.4}$$

where Γ is a dimensionless coefficient. Based on calibration with laboratory data, Dally et al. (1985) suggested $\Gamma = 0.40$ and $K = 0.15$ for applications. Dally et al (1985) presented analytical solutions of the model for beaches of idealized shapes such as uniform depth, uniform slope and equilibrium beach profiles. Figure 3-2 shows an example of the model predicted breaker decay as compared to a laboratory measurement for plane beaches of 1/20, 1/30, 1/65 and 1/80 slopes. The results show that the model appears to provide a good representation of breaking wave decay on plane beaches of laboratory scale. The line $H = 0.78h$ is also plotted in the figures and appears to be a reasonable description of breaker decay only for the 1/30 slope. Figure 3-3 shows another example of the model prediction on a prototype scale bar-trough profile. The simulated wave reaches the stable criterion in the deepest portion of the outermost trough, shoals on the inner bar until the incipient condition is again attained, and then breaks continuously until the shoreline is reached.

3.1.2.2 Random wave models

There exist several random wave models, which can be classified into two groups: one group using a representative wave height with a wave height distribution assumption inside the surf zone, the other group using a wave-by-wave approach.

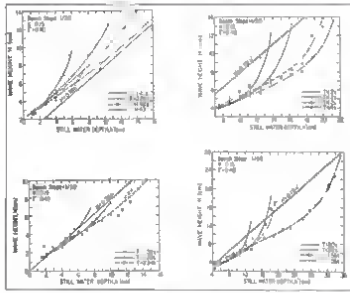

Figure 3 2. Comparison of D^3 model and 0 78 * criterion to laboratory data for 1/20, 1/30, 1/65 and 1/80 beach slope Trend of (H/h') increases with increasing beach slope and increasing incipient condition (decreasing wave steepness) (Dally et al , 1985)

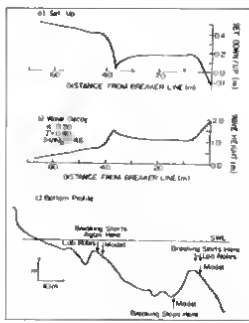

Figure 3-3 Test of D^3 model at prototype scale on large wave tank profile (H = 1 68 m, T = 3 75 s) Wave breaks, reforms shoals, and breaks again (Dally et al , 1985)

Battjes and Janssen (1978) first developed a wave energy dissipation model for random waves. The wave height distribution inside the surf zone was assumed to be a truncated Rayleigh distribution. The average wave energy dissipation was modeled as a bore. The result of the Battjes and Janssen model is

$$D = \frac{\alpha}{4} Q_b f \rho g H_m^2$$

$$\frac{1 - Q_b}{\ln Q_b} = -\left(\frac{H_{rms}}{H_m}\right)^2, \quad H_m = 0.88 k^{-1} \tanh\left(\frac{\gamma k h}{0.88}\right) \tag{3.5}$$

where D is the averaged wave energy dissipation. Q_b is the percentage of breaking waves, H_{rms} is the root-mean-square wave height, H_m is a maximum possible wave height at water depth h, f is the mean wave frequency, k is the wave number, α and γ are two empirical parameters. Later, on the basis of the idea of Battjes and Janssen but with different wave height distribution assumptions, Thornton and Guza (1983), Church and Thornton (1993), Baldock et al. (1598), etc. have developed other random wave models.

In the above-mentioned models, a narrow banded wave spectrum and a form of the wave height distribution inside the surf zone was assumed. However, in nature, the wave spectrum is not always narrow banded and the wave height distribution is very complex, especially inside the surf zone. One method to circumvent this problem is the wave-by-wave approach (Mase and Iwagaki, 1982, Dally and Dean, 1986, Dally, 1992, Larson and Kraus, 1992, Zheng, 1996, Kuriyama and Nakatsukasa, 2000).

In the wave-by-wave method, the random wave field is represented by the collection of a set of individual regular waves. The major assumption inherent in this

approach is that shoaling and breaking are not affected by wave wave interaction At any location, the probability distribution in wave height can be determined from the predicted heights of the individual waves, and wave statistics such as root-mean-square height are easily calculated The wave-by-wave approach has been verified with laboratory and field data (Dally, 1992) and applied to model the undertow and longshore current (Larson and Kraus, 1992, Kuriyama and Nakatsukasa, 2000)

Larson (1995) developed an alternative random wave model that required transformation of only one representative wave height without making any assumptions about the pdf of wave height. Larson (1995) showed that the model results were in reasonable agreement with the wave-by-wave approach.

The wave-by-wave approach is believed to be more similar to natural processes and is incorporated into the cross-shore transport model to simulate the sediment transport processes under random waves A wave spectrum in the offshore boundary needs to be provided to begin the calculation If no real time series data exist, the joint distribution of wave period and heights developed by Longuet-Higgins (1983) can be applied to generate wave height and period series in the time domain

$$p(R,\tau) = L(\nu)\frac{2}{\sqrt{\pi\nu}}\frac{R^2}{\tau^3}\exp\left(-R^2\left[1+(1-\frac{1}{\tau})^2\frac{1}{\tau^2}\right]\right) \qquad (3\,6)$$

where R and τ are normalized wave height and wave period, respectively,

$$R = \frac{H}{2\sqrt{2m_0}}, \qquad \tau = T\frac{m_1}{2\pi m_0} \qquad (3\,7)$$

m_n denotes the nth moment of the spectral density ν is the band width parameter determined by the first three moments of the spectrum

$$\nu = \left(\frac{m_2 m_2}{m_1^2} - 1\right)^{1/2} \tag{3 8}$$

and

$$L(\nu) = \left[\frac{1}{2}\left(1 + \frac{1}{\sqrt{1+\nu^2}}\right)\right]^{1} \tag{3 9}$$

The marginal probability density of wave height R can be determined as

$$p(R) = \int_0^{\infty} p(R,\tau)d\tau = L(\nu)[1 + erf(R/\nu)]R\exp(-R^2) \tag{3 10}$$

where $erf(R/\nu) = \frac{2}{\sqrt{\pi}}\int_0^{R/\nu}\exp(-t^2)dt$ is the error function If $\nu = 0$, Eq (3 10) is the Rayleigh distribution for R For large waves and small ν values, such as shown in Figure 3-4 the distribution of R can be approximated by the Rayleigh distribution Therefore, the cumulative probability of the wave height becomes

$$P(R) = 1 - \exp(-R^2) \tag{3 11}$$

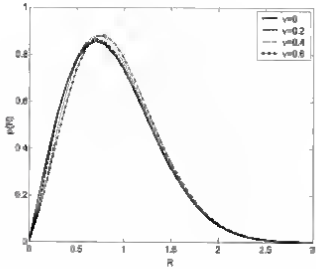

Figure 3-4. The pdf of wave height R compared with the Rayleigh distribution (reproduced from Zheng, 1996)

The distribution of wave period at fixed values of the wave height R is found by dividing Eq (3 6) by Eq (3 10) Integrating with respect to τ and approximating the error function erf(x) with tanh(1 2x) the cumulative probability of wave period is given by

$$P(\tau / R) = \frac{1 + \tanh\left[\frac{1.2R}{\nu}\left(1 - \frac{1}{\tau}\right)\right]}{1 + \tanh\left[\frac{1.2R}{\nu}\right]} \tag{3 12}$$

To simulate a random wave condition, a random number P_1 uniformly distributed between 0 and 1 is generated first A random wave height, R_1 is obtained from Eq (3 11) as

$$R_1 = \sqrt{-\ln(1 - P_1)} \tag{3 13}$$

Then a second random number P_2 is generated, and the corresponding wave period, τ_1, is calculated from Eq (3.12)

$$\tau_1 = \left\{1 - \frac{\nu}{2.4R_1}\ln\left[\frac{P_2\left(1 + \tanh\frac{1.2R_1}{\nu}\right)}{2 - P_2\left(1 + \tanh\frac{1.2R_1}{\nu}\right)}\right]\right\}^{-1} \tag{3 14}$$

The dimensional wave height and wave period can then be determined from Eq (3 7) Zheng (1996) compared the numerical results with Longuet-Higgins's joint density distribution for both narrow ($\nu = 0.1$) band and wide band ($\nu = 0.1$) spectra, and found very good agreement in both cases (Figure 3-5)

3 1.3 Roller Models

When waves break, it has been found that the wave energy dissipation does not occur immediately at the initial breaking point but at some distance landward of the breaker point (Svendsen, 1984) It is within this distance that the decay of organized

wave energy is converted into turbulent kinetic energy that is not dissipated immediately This region is known as the transition region, which is characterized by rapid wave decay and uniform wave setdown, thus indicating that there is also a lag in momentum transfer This phenomenon is observed in both plunging and spilling breakers In many experiments, the bar crests are found somewhat shoreward of the initial breaking points Thus, the inclusion of the transition zone in a profile model has an important effect on the predicted profiles, particularly near the bar features (Nairn et al , 1990; Southgate and Nairn, 1993)

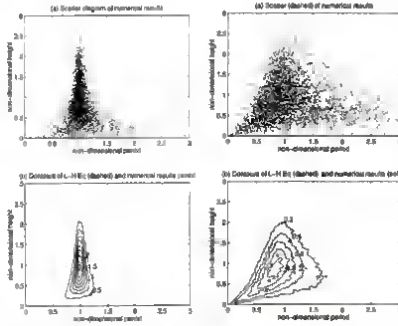

Figure 3 5 Comparison of the numerical results with the density function Eq 3 37 of Longuet-Higgins (Zheng, 1996) A) Narrow band ($\nu = 0.1$) wave spectra. B) Wide band ($\nu = 0.5$) wave spectra.

One concept applied by many researchers to address the lag in energy dissipation is through the surface roller model (Svendsen, 1984, Dally and Brown, 1995, Reniers and Battjes, 1997) The basic idea of the roller model is that the organized wave energy

released at breaking is first transferred to the energy of a roller, which rides on the wave front with the phase speed of the waves The difference in velocity between the roller and the water particles at the wave front causes a shear stress between the roller and underlying wave front. The work done by the shear stress equals the dissipation of roller energy The time needed for the organized wave energy to dissipate through the roller causes a spatial lag between the location of wave breaking and the actual dissipation (Nairn et al., 1990)

The time-averaged energy balance equation that contains contributions from both the organized wave motion and the roller, is expressed as (Nairn et al 1990, Dally and Brown, 1995)

$$\frac{\partial}{\partial y}EC_g + \frac{\partial}{\partial y}E_r C = \varepsilon_r \tag{3.15}$$

where EC_g and E_rC are the energy fluxes associated with the organized wave motion and the roller, respectively; E_r and ε_r are the energy and energy dissipation rate of the roller, respectively Svendsen (1984) expressed the roller energy per unit surface area in terms of the roller cross-section area A_r

$$E_r = \rho A_r C^2 / 2L = \rho A_r C / 2T \tag{3.16}$$

The roller energy dissipation rate, ε_r is modeled as the work performed by the shear stress τ_r between the roller and the organized wave motion.

$$\varepsilon_r = \tau_r C \tag{3.17}$$

Following Nairn et al (1990), the shear stress is deduced by considering the vertical force balance on the roller, which leads to

$$\varepsilon_r = \rho g \frac{A_r}{T} \sin\beta \tag{3.18}$$

where β is the angle of the wave-roller stress vector. Lippmann et al. (1996) showed that the model is insensitive to values of $\beta > 10^{\circ}$.

Several formulations for the roller area A_r have been proposed. Svendsen (1984) related the roller area to the local wave height by

$$A_r = 0.9H^2 \tag{3.19}$$

Deigaard et al. (1991) assumed the roller was similar in size to the aerated region of a steady, fully developed hydraulic jump and modeled the roller area according to

$$A_r = \frac{H^3}{4h\tan\beta} \tag{3.20}$$

If applied in the transition region, because of the dependence on wave height there is no shift in the position of the maximum wave energy dissipation. In attempting to model the shift, Okayasu et al. (1988) adopted the model

$$A_r = \alpha\kappa HL \tag{3.21}$$

in which L is the local wave length, α and κ are empirically prescribed factors that depend upon position in the surf zone. The peak in wave energy dissipation was shifted landward by increasing κ linearly from zero at the breakpoint to a maximum value at the observed end of the transition region and then back to zero at the shoreline. However, this method requires a priori knowledge of the extent of the transition region.

Dally and Brown (1995) proposed a different approach to determine the roller area. In their model, the roller area is not known a priori, but obtained by solving Eq. 3.15 directly by knowing the wave heights using measured data or from wave transformation

models Figure 3-6 shows the calculated roller area using this method in comparison with the models of Svendsen and Deigaard et al The shift between the breakpoint and the location where the roller becomes fully developed is obvious in this new method The momentum equation including roller contribution is

$$\frac{\partial S_{xx}}{\partial y} + \frac{\partial S_{xy}}{\partial y} = -\rho g(h+\bar{\eta})\frac{\partial \bar{\eta}}{\partial y} \tag{3.22}$$

where $$S_{xx} = \frac{3}{2}E\,,\ S_{xy} = 2E_r - \rho C\frac{A_r}{T} \tag{3.23}$$

This equation is used to predict the wave setup/setdown in the model.

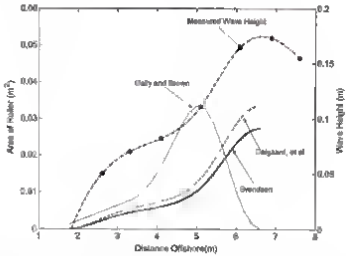

Figure 3-6 Roller area prediction (reproduced from Dally and Brown, 1995)

3.2 Equilibrium Beach Profiles

The equilibrium beach profile theory developed by Dean (1977) is based on uniform wave energy dissipation per unit water volume, D_*, for a given sediment size inside the surf zone

$$\frac{dF}{dy} = hD_* \tag{3.24}$$

where y is directed offshore, and h is the still water depth Thus, different energy dissipation representations may result in different equilibrium beach profiles The shallow water linear wave theory is used in this investigation

3 2.1 EBP under Spilling Breaker Assumption

The spilling breaker assumption, which has been used in EDUNE and CROSS and many other studies, is that the wave height to water depth ratio inside the surf zone is a constant (usually taken as 0.78), $H = \gamma h$ Substituting this definition into Eq 3 24 yields

$$\frac{d}{dy}\left(\frac{1}{8}\rho g\gamma^2 h^2\sqrt{gh}\right) = hD. \tag{3 25}$$

Integrating for h, the relationship between h and y is obtained

$$h = \left(\frac{24D.}{5\rho g\sqrt{g}\,\gamma^3}\right)^{2/3} y^{2/3} = Ay^{2/3} \tag{3 26}$$

which is the equilibrium profile form in Eq 1 1 Here the profile scale factor, A, depends only on the grain size, and later it will be modified to include wave effects

3.2 2 EBP Using D^3 Model

Larson (1988) replaced the spilling breaker assumption with the D^3 model (Eq 1 9) to obtain a modified EBP form (Eq 1 10) Equating Eq 1 9 to Eq 3.21 and solving for H yields

$$H = \left(\frac{8h^2D.}{\rho g\sqrt{gh}K} + \Gamma^2h^2\right)^{1/2} \tag{3 27}$$

Substituting Eq.3 27 back into Eq 3 24 leads to Eq 1 10, which can be rewritten as

$$y = \frac{2}{K}h + \left(\frac{\Gamma^2}{\gamma^2}\right)\left(\frac{5\rho g\sqrt{g}\,\gamma^2}{24D.}\right)h^{3/2} = \frac{2}{K}h + \left(\frac{\Gamma^2}{\gamma^2}\right)\left(\frac{h}{A}\right)^{2/3} \tag{3 28}$$

This relationship includes a linear term that removes the infinite slope at the waterline in Eq 3 26 and a reduction coefficient ($\Gamma^2/\gamma^2 < 1$) that results in a steeper EBP slope if the same profile scale parameter, A, is used as in Eq 3 26

3.2 3 EBP Using Roller Model

In the above derivation of EBPs, the energy dissipation lag discussed in Section 3 1 3 is not included. In the following, the same procedure as Larson (1988) is applied to determine the EBP shape using the surface roller model of Dally and Brown

From Eq 3 18 (where β_d is used to replace $\sin\beta$), equating the roller energy dissipation to Dean's constant energy dissipation per unit volume yields

$$hD_r = \rho g \beta_d \frac{A_r}{T} \tag{3 29}$$

solving for A_r

$$A_r = \frac{hD_r T}{\rho g \beta_d} \tag{3 30}$$

As the first step, the spilling breaker assumption is used to calculate wave energy dissipation inside the surf zone Substituting all into Eq 3 15 yields

$$hD_r = \frac{d}{dy}\left(\frac{1}{8}\rho g \gamma^2 h^2 \sqrt{gh}\right) + \frac{d}{dy}\left(\frac{1}{2}\frac{h^2 D_r}{\beta_d}\right) \tag{3 31}$$

Integrating for h, a similar EBP form to Eq 3 28 can be obtained

$$y = -\left(\frac{5\rho g\sqrt{g}\gamma^2}{24 D_r}\right)h^{3/2} + \frac{1}{\beta_d}h = \left(\frac{h}{A}\right)^{3/2} + \frac{1}{\beta_d}h \tag{3.32}$$

Figure 3 7 presents the resulting EBP with comparison to Eqs 3 26 and 3.28 It shows that all are monotonic profiles

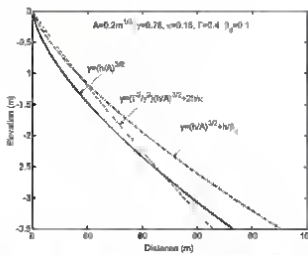

Figure 3-7 Comparison of EBP under different wave transformation models

However, if another wave model such as the D^3 model is used, the wave height to water depth ratio is no longer a constant. Instead, it varies along the profile inside the surf zone. Thus, it is very difficult to obtain an analytical solution for the EBP. If the D^3 model is used, letting $\gamma_r(y) = H/h$, we have

$$hD_* = \frac{K}{8}\rho g\sqrt{g}\left(\gamma_r^2 - \Gamma^2\right)h^{3/2} + \frac{D_*}{2\beta_d}\frac{dh^2}{dy} \tag{3.33}$$

Regrouping Eq.3.33 yields

$$\frac{dh}{dy} = \beta_d\left(1 + \frac{3K}{5A^{3/2}}\left(\frac{\Gamma^2 - \gamma_r^2}{\gamma^2}\right)h^{1/2}\right) \tag{3.34}$$

If the distribution of the wave height to water depth ratio inside the surf zone, $\gamma_r(y)$, is known when the profile reaches equilibrium, the actual EBP shape can be found from Eq.3.34 by numerical integration. A hypothetical example is investigated: initial profile slope 1/15, wave height H = 1.68 m with 11.33 s period and 4.57 m water depth; the profile scale factor A = 0.2 $m^{1/3}$. Because the distribution of $\gamma_r(y)$ is not known in

priori, the developed cross-shore profile model is applied to obtain the final profile and $\gamma_r(y)$. The equilibrium profile is then calculated by substituting $\gamma_r(y)$ into Eq.3.34 and integrating numerically. Figure 3-8 shows the initial and predicted profiles, and Figure 3-9 shows the predicted wave height to water depth ratio and the profile calculated by Eq 3.34. A non-monotonic profile is obtained.

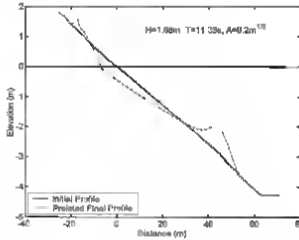

Figure 3-8 Initial and predicted profile for the hypothesis example

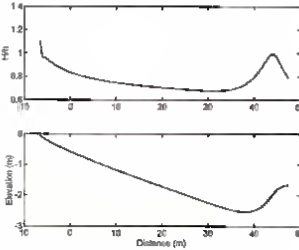

Figure 3-9 Predicted H/h ratio and calculated EBP from Eq 3.31

3.2.4 Reevaluation of the Profile Scale Factor

In the above equilibrium beach profile forms, the profile scale factor A was assumed to be only a function of either grain diameter or its equivalent fall velocity. Moore (1982) examined numerous profiles to quantify the relationship between A and the effective diameter of the sediments across the surf zone. Later, Dean (1987) transformed Moore's relationship of A versus diameter to A versus fall velocity.

$$A = 0.067 w^{0.44} \tag{3.35}$$

Table 3-3 lists the recommended A values versus the median sediment size (reproduced from Dean and Dalrymple, 2002).

Table 3-3. Recommended A values ($m^{1/3}$) (after Dean and Dalrymple, 2002)

D (mm)	0.00	0.01	0.02	0.03	0.04	0.05	0.06	0.07	0.08	0.09
0.1	0.063	0.067	0.071	0.076	0.080	0.084	0.087	0.090	0.094	0.097
0.2	0.100	0.103	0.106	0.109	0.112	0.115	0.117	0.119	0.121	0.123
0.3	0.125	0.127	0.129	0.131	0.133	0.135	0.137	0.139	0.141	0.143
0.4	0.145	0.147	0.148	0.150	0.151	0.153	0.155	0.156	0.158	0.159
0.5	0.161	0.162	0.163	0.165	0.166	0.167	0.168	0.169	0.171	0.172
0.6	0.173	0.174	0.175	0.177	0.178	0.179	0.180	0.181	0.183	0.184
0.7	0.185	0.186	0.187	0.188	0.189	0.190	0.190	0.191	0.192	0.193
0.8	0.194	0.195	0.196	0.196	0.197	0.198	0.199	0.200	0.200	0.201
0.9	0.202	0.203	0.204	0.204	0.205	0.206	0.207	0.208	0.208	0.209
1.0	0.210	0.211	0.212	0.212	0.213	0.214	0.215	0.216	0.216	0.217

A limitation in the above relationship is that wave conditions are not included. Thus, this representation cannot explain one phenomenon that occurs in natural beaches: the profiles are of milder slope in the winter, compared to the summer conditions associated with milder and less steep waves. The fall velocity parameter includes information of both sediment size and wave conditions. The hypothesis tested here is that there exists a relationship between the profile scale factor A and the fall velocity parameter H_b/wT.

$$A = f(D_{50}) \cdot F(\frac{H_b}{wT}) \tag{3.36}$$

where the first term is determined from Table 3-3, and the second term is a modification term which is a function of the fall velocity parameter To investigate this modification function, the large-scale wave flume experimental data from LWT (Kraus and Larson, 1988), CRIEPI (Larson and Kraus, 1989), LWF'96/97 (Dette et al , 1998) and LIP11D (Roelvink and Reniers, 1995) are analyzed The detailed descriptions of these experiments are included in the following chapters for model calibration and verification purposes. Among them, LWT and CRIEPI used monochromatic waves, while the experiments in LWF'96/97 and LIP11D were conducted with random waves

The analysis procedure is as follows first using the D^3 model or from the measurements, determine the breakpoints and the corresponding breaking wave heights (significant wave heights are used in the case of random wave conditions) in the final measured profiles; then, applying the least-square method from the shoreline positions up to the breakpoint positions, determine the best-fit A values by assuming that the final profiles are in equilibrium (although some of them may not be). Figure 3-10 shows one example from CE300 in the LWT experiments A plot of the fall velocity parameter and the ratio of the best-fit A values to the recommended values in Table 3-3 are presented in Figure 3-11

Upon further investigation of the experimental data, the following are believed to be partially responsible for a major portion of the scatter: (1) there may be an effect the initial slope on the final equilibrium profiles, the initial slope ranges from 1:50 to 1:10; (2) some profiles have not reached equilibrium, particularly those lower data points on the left in Figure 3-11, because these cases all have initial mild slopes under small wave

action and the test durations are short (the time scale of profile accretion is much longer than erosion), (3) the final profiles have multiple bars and a wide trough landward of the primary bar in tests such as CE500, CE501, CRIEPI3-4, CRIEPI4-3 and CRIEPI6-1. An attempt is made to fit these profiles just to the second breakpoint near the inner bars, with better results than the original (Figure 3-12). Figure 3-13 shows an example of the adjustment in CE500.

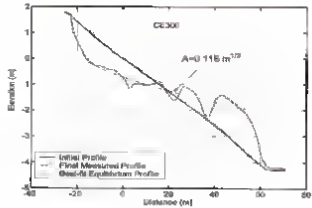

Figure 3-10 Best-fit equilibrium beach profile for CE300. The A value based on Table 3-2 is 0.106m$^{1/3}$.

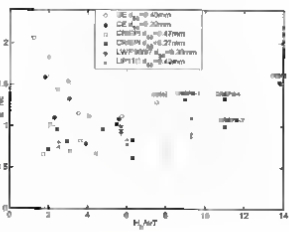

Figure 3-11 Relationship between the fall velocity parameter and the ratio of the best-fit A values to the recommended A values

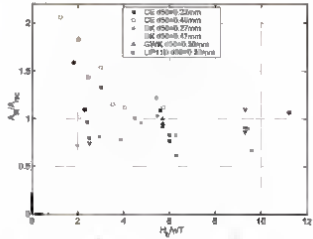

Figure 3-12 Modified relationship between the fall velocity parameter and the ratio of the best-fit A values to the recommended A values

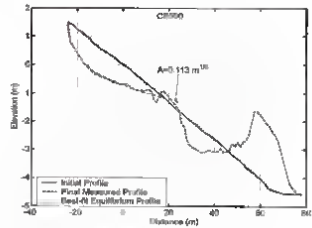

Figure 3-13 Modified best-fit equilibrium profile for CE500 The A value based on Table 3-2 is 0 106 $m^{1/3}$

Figure 3-14 shows the relationship based only on the LWT profiles (all commenced with an initial slope of 1:15) and most of the final profiles in this experiment had almost achieved equilibrium As Figure 3 14 illustrates, a reasonable fit to the data is

$$F(\frac{H_b}{wT}) = 0.868 + 1.406\left(\frac{H_b}{wT}\right)^{-1} \qquad (3.37)$$

This equation will be included in the model to modify the profile factor, A, in the determination of uniform wave energy dissipation per unit volume, D. Of special interest, seasonal profile changes can be interpreted using Eq 3 37 from winter to summer, the A value becomes larger with the fall velocity parameter decreasing, thus the profile becomes steeper in summer and the shoreline advances seaward

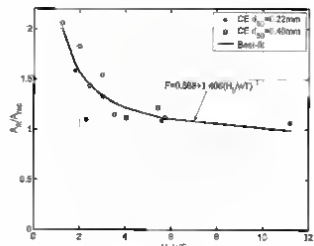

Figure 3 14 Best-fit equation for modification function F, LWT data only

3.3 Cross-Shore Profile Evolution Model

As discussed in Dean and Dalrymple (2002), an equilibrium profile represents a balance of destructive and constructive forces acting on the beach Of those forces recognized, the dominant destructive force inside the surf zone is the high turbulence level caused by wave breaking. The transport models based on wave energy dissipation and equilibrium beach profile concepts, such as EDUNE, SBEACH and CROSS capture this force. Although these models lack detailed descriptions of the physical processes related to sediment transport, they have yielded reasonable, useful and encouraging results, particularly for storm wave conditions which cause beach and dune erosion.

Thus, the model developed in this research uses the same strategy with some modifications made based on recent and additional analysis

3.3.1 Global Consideration of Transport Rate Exponents

In the transport rate relationship (Eq 3 1), two different exponent (n) values have been used n =1 (EDUNE and SBEACH), and n=3 (CROSS) The experimental data from LWT (Kraus and Larson, 1988) are examined to investigate this relationship

In the case of n = 1, Eq 3 1 can be integrated from the shoreline position y_s (where the wave energy is assumed to be close to zero) to the wave breaking point y_b (assuming no wave energy dissipation outside the surf zone),

$$\int_{y_s}^{y_b} hQ\,dy = K\int_{y_s}^{y_b}(hD - hD_*)\,dy \tag{3 38}$$

This leads to Eq 3 39, the relationship between the total wave energy entering the surf zone and the total sediment transport (determined from the profile measurements)

$$\overline{Q} = K\left[\frac{\left(EC_g\right)_b}{A} - D_*\right] \tag{3 39}$$

where $$A = \int_{y_s}^{y_b} h\,dy \qquad \overline{Q} = \int_{y_s}^{y_b} Qh\,dy \Big/ A \tag{3 40}$$

Figure 3-15 shows the results for case CE300, CE400 and CE401, where the calculation has been carried out at the times the measured profiles are available However, for n = 3, direct integration is impossible unless the distribution of wave energy dissipation is known Thus, the D^3 model is applied to predict the wave energy transformation within the surf zone Eq 3 1 is then integrated numerically The results are presented in Figures 3-16 and 3-17 for n = 1 and n = 3, respectively

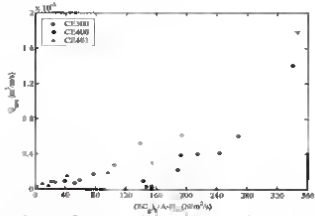

Figure 3-15 Investigation of transport relationship, Eq 3 1, for n = 1.

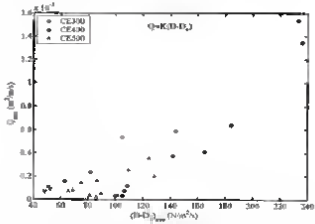

Figure 3-16 Transport rates versus energy dissipation, n = 1, D^3 model

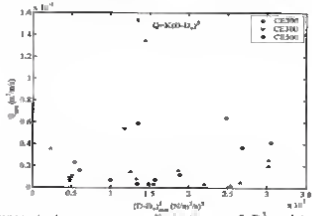

Figure 3-17 Transport rates versus energy dissipation, n = 3, D^3 model

From the above comparisons, n = 1 appears to be the better representation of the relationship between transport rates and wave energy dissipation. However, from physical considerations, n = 3 is considered to be consistent with both Froude number and the fall velocity parameter modeling similarity criteria (Zheng, 1996, Zheng and Dean, 1997). Some discrepancies may be due to the inaccuracy of modeling wave energy dissipation and determination of transport rates from measured profiles. Thus, both of these two n values are included in the model for further investigation.

3.3.2 Transport Rates

A modified Eq. 3.1 that includes the gravity effect is used to obtain the transport rates inside the surf zone.

$$Q = K(D - D_* + \alpha \frac{dh}{dy})\left|D - D_* + \alpha \frac{dh}{dy}\right|^n \tag{3.41}$$

where α is a gravity coefficient, which equals to D_* / m according to Dean (1991), m is the beach face slope. Three different wave energy dissipation models have been examined and compared in Section 3.2: spilling breaker assumption, D^3 model and roller model. The first two models cannot treat the transition zone directly and the resulted equilibrium profiles are monotonic. In the program SBEACH, the transport rates in the transition zone are considered to decay exponentially from the plunge point to the break point. In contrast, Lee et al. (1996) assumed a Gaussian distribution in that region. On the other hand, the roller model, especially the formula of Dally and Brown (1995), can directly account for the lag of energy dissipation and a non-monotonic equilibrium profile can be reached. Thus, the D^3 model coupled with the roller model of Dally and Brown is chosen in the present study to predict the wave height transformation and energy dissipation inside the surf zone.

3.3.3 Numerical Modeling Process

3.3.3.1 Grid system

Two types of grid representations of the physical domain have been used for cross-shore numerical modeling as shown in Figure 3-18. In the first type shown in Figure 3-18A, the cells are finite increments of the distance variable y, whereas in the second type shown in Figure 3-18B the computational cells are formed by finite increments of the depth variable, h. The advantage of the first type is that it can easily represent bar profiles, thus it is chosen in the present model with a staggered representation such that the depth, h is located at the center of each cell and the transport, Q, is at the grid boundaries. H and C_g are at the Q-points, while D is at the h-points. The cross-shore coordinate, y, is directed offshore, thus positive Q indicates offshore transport.

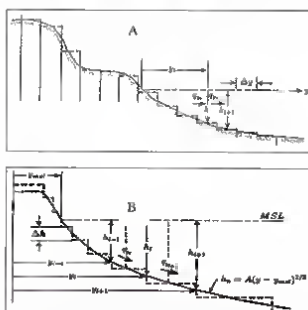

Figure 3-18. Two types of grids employed in numerical modeling of cross-shore sediment transport and profile evolution. A) Grid with y and t as the independent variables and h dependent. B) Grid with h and t as the independent variables and y dependent.

3.3.3.2 Governing equations

The governing equations in the model are listed below for convenient reference

- D^3 Model

$$\frac{\partial EC_g}{\partial y} = \frac{K}{h+\bar{\eta}}\left[EC_g - EC_{gs}\right] \tag{3.42}$$

- Dally and Brown's roller model

$$\frac{\partial}{\partial y}EC_g + \frac{\partial}{\partial y}E_r C = \varepsilon_r$$

$$E_r C = \frac{1}{2}\rho C^2 \frac{A_r}{T},\ \varepsilon_r = \rho g \beta_d \frac{A_r}{T} \tag{3.43}$$

- Momentum equation

$$\frac{\partial S_{xx}}{\partial y} + \frac{\partial S_{xy}}{\partial y} = -\rho g h \frac{\partial \bar{\eta}}{\partial y}$$

$$S_{xx} = \frac{3}{2}E,\ S_{xy} = 2E_r - \rho C\frac{A_r}{T} \tag{3.44}$$

- Transport model

$$Q = K\left(D - D_* + \alpha\frac{dh}{dy}\right)\left|D - D_* + \alpha\frac{dh}{dy}\right|^{2} \tag{3.45}$$

- Continuity equation

$$\frac{dh}{dt} = \frac{dQ}{dy} \tag{3.46}$$

where h includes wave setup/setdown, which is calculated by iteration.

3.3.3.3 Numerical solution scheme

There are two types of numerical solutions available the ' explicit ' and "implicit" methods. The explicit method solves the transport and continuity equations sequentially whereas the implicit method solves these two equations simultaneously The primary advantage of the explicit method is simplicity in formulation and programming and also the ease of incorporating different transport rate formulations, however, in order to avoid numerical instabilities, very small time steps can be required. The implicit method

allows much larger time steps while maintaining the solution stable The implicit scheme is employed to solve the governing equations in the present model The finite difference equations for each module are presented below In these equations, the index i is used to denote the number of a specific grid point and increases offshore. Linear wave theory and shallow water assumptions are applied to calculate wave related quantities

For the wave module, the numerical calculations start at the seaward end of the grid and proceed onshore Wave setup is included in the water depth as an unknown, thus an iteration procedure is needed until the wave setup calculation meets certain accuracy criteria From a specific Q point to the next, Eqs 3 42 to 3 44 are solved numerically one after another. The difference equation for Eq 3 42 is

$$\frac{(EC_g)_{i+1}-(EC_g)_i}{\Delta y}=\frac{K}{h_i}\left[\frac{1}{2}[(EC_g)_{i+1}+(EC_g)_i]-(E_iC_{gi})_i\right] \tag{3 47}$$

where $$(EC_{gi})_i=\frac{1}{8}\rho g[\Gamma h_i]^2\frac{C_{gi}+C_{gi+1}}{2} \tag{3 48}$$

and Δy is the space step From Eq.3 47, the energy flux at point i is,

$$(EC_g)_i=\frac{1}{1+B_i}\left[(EC_g)_{i+1}(1-B_i)+B_i(EC_{gi})_i\right] \tag{3 49}$$

with $$B_i=\frac{K\,\Delta y}{2h_i} \tag{3 50}$$

After the energy flux has been calculated, the corresponding wave height is determined as

$$H_i=\left[\frac{8(EC_g)_i}{\rho g C_g}\right]^{1/2} \tag{3.51}$$

The difference equation for the roller model (Eq.3 43) is calculated to determine the roller area,

$$\frac{(EC_g)_{i+1}-(EC_g)_i}{\Delta y}+b_1[(A_rC^2)_{i+1}-(A_rC^2)_i]=b_2(A_{r_i}+A_{r_i}) \tag{3 52}$$

where $$b_1=\frac{\rho}{2T\Delta y},\ b_2=\frac{\rho g\beta_d}{2T} \tag{3.53}$$

Using the wave height and the roller area, wave setup/setdown is given from Eq 3 44, expressed in finite difference form as

$$\overline{\eta}_i=\overline{\eta}_{i+1}+\frac{1}{\rho g h_i}\left[(S_{xx}+S_{xy})_{i+1}-(S_{xx}+S_{xy})_i\right] \tag{3 54}$$

Once the desired accuracy is reached, the energy dissipation per unit volume for the roller model at each Q-point is determined by

$$D_i=\frac{2}{(h_i+h_{i-1})}\varepsilon_r \tag{3.55}$$

The transport rate distribution within the surf zone is calculated from Eq 3 45, written in difference form at the (m+1)th time step,

$$Q_i^{m+1}=K\left(D_i^{m+1}-D_*+\alpha\frac{h_i^{m+1}-h_{i-1}^{m+1}}{\Delta y}\right)\left|D_i^{m+1}-D_*+\alpha\frac{h_i^{m+1}-h_{i-1}^{m+1}}{\Delta y}\right|^{n-1} \tag{3 56}$$

Rewriting

$$h_i^{m+1}=h_i^m+\Delta h_i^{m+1} \tag{3 57}$$

$$D_i^{m+1}=D_i^m+\frac{\partial D_i}{\partial h_i}\Delta h_i^{m+1}+\frac{\partial D_i}{\partial h_{i-1}}\Delta h_{i-1}^{m+1} \tag{3 58}$$

The roller area is assumed to be constant over a time step From Eq 3.55,

$$\frac{\partial D_i}{\partial h_i}=\frac{\partial D_i}{\partial h_{i-1}}=-\rho g\beta_d\frac{A_{ri}}{T}\frac{2}{(h_i+h_{i-1})^2} \tag{3.59}$$

Thus, Eq 3 56 becomes,

$$Q_i^{m+1} = K\left[\left(D_i^m - D_* + \alpha\frac{h_i^m - h_{i-1}^m}{\Delta y}\right) + \left(\frac{\partial D_i}{\partial h_{i-1}} - \frac{\alpha}{\Delta y}\right)\Delta h_{i-1}^{m+1} + \left(\frac{\partial D_i}{\partial h_i} + \frac{\alpha}{\Delta y}\right)\Delta h_i^{m+1}\right]$$

$$\times\left|\left(D_i^m - D_* + \alpha\frac{h_i^m - h_{i-1}^m}{\Delta y}\right) + \left(\frac{\partial D_i}{\partial h_{i-1}} - \frac{\alpha}{\Delta y}\right)\Delta h_{i-1}^{m+1} + \left(\frac{\partial D_i}{\partial h_i} + \frac{\alpha}{\Delta y}\right)\Delta h_i^{m+1}\right|^{n-1} \qquad (3\ 60)$$

When n is an odd number (1 or 3), the absolute sign in the equation can be dropped. For a small time increment, the value of $\Delta h / h$ is much less than 1. Neglecting higher order terms after expanding Eq 3 60, the linearized finite difference transport equation is expressed as

$$A_i^* \Delta h_{i-1}^{m+1} + B_i^* Q_i^{m+1} + C_i^* \Delta h_i^{m+1} = G_i^* \qquad (3\ 61)$$

$$A_i^* = -nK\left|D_i^m - D_* + \alpha\frac{h_i^m - h_{i-1}^m}{\Delta y}\right|^{n-1}\left(\frac{\partial D_i}{\partial h_{i-1}} - \frac{\alpha}{\Delta y}\right)$$

$$B_i^* = 1.0$$

$$C_i^* = -nK\left|D_i^m - D_* + \alpha\frac{h_i^m - h_{i-1}^m}{\Delta y}\right|^{n-1}\left(\frac{\partial D_i}{\partial h_i} + \frac{\alpha}{\Delta y}\right)$$

$$G_i^* = K\left(D_i^m - D_* + \alpha\frac{h_i^m - h_{i-1}^m}{\Delta y}\right)\left|D_i^m - D_* + \alpha\frac{h_i^m - h_{i-1}^m}{\Delta y}\right|^{n-1}$$

However, for an even number such as n = 2, the absolute sign in Eq.3 60 is difficult to expand. Thus, a different finite difference scheme is used,

$$Q_i^{m+1/2} = K\left[\left(D_i^m - D_* + \alpha\frac{h_i^m - h_{i-1}^m}{\Delta y}\right) + \left(\frac{\partial D_i}{\partial h_{i-1}} - \frac{\alpha}{\Delta y}\right)\Delta h_{i-1}^{m+1} + \left(\frac{\partial D_i}{\partial h_i} + \frac{\alpha}{\Delta y}\right)\Delta h_i^{m+1}\right]$$

$$\times\left|\left(D_i^m - D_* + \alpha\frac{h_i^m - h_{i-1}^m}{\Delta y}\right)\right| \qquad (3\ 62)$$

where $Q_i^{n+1/2} = \frac{Q_i^{n+1} + Q_i^n}{2}$. After expanding Eq 3 62, a similar equation with similar coefficients as in Eq 3 61 is obtained

The discrete form of the sediment continuity equation (Eq 3 46) is

$$\frac{\Delta h_i^{n+1}}{\Delta t} = \frac{Q_{i+1}^{n+1} - Q_{i-1}^{n+1} + Q_{i+1}^n - Q_{i-1}^n}{2\Delta y} \tag{3 63}$$

which can be rewritten as

$$A_i Q_{i-1}^{n+1} + B_i \Delta h_i^{n+1} + C_i Q_{i+1}^{n+1} = G_i \tag{3 64}$$

$$A_i = \frac{\Delta t}{2\Delta y},\ B_i = 1.0,\ C_i = -A_i,\ G_i = \frac{\Delta t}{2\Delta y}\left(Q_{i+1}^n - Q_{i-1}^n\right)$$

Eqs.3 61 and 3 64 are tridiagonal equations and can be solved simultaneously by the standard double sweep method Two boundary conditions are needed in the model The seaward limit is taken as the breaking point (y_{ie}), where the transport rate is considered to be zero Actually some sediment movement exists seaward of the breaking point, which is a limitation of the model The other boundary is the maximum point of uprush (y_{ib}) in the case of no seawall nor overwash The transport is also set to zero at this boundary Starting from the seaward boundary, four new sets of variables are calculated as

$$E_i = -\frac{A_i}{B_i + C_i E_{i+1}^*},\ F_i = \frac{G_i - C_i F_{i+1}^*}{B_i + C_i E_{i+1}^*},\ E_i^* = -\frac{A_i^*}{B_i^* + C_i^* E_i},\ F_i^* = \frac{G_i^* - C_i^* F_i}{B_i^* + C_i^* E_i} \tag{3 65}$$

with the boundary conditions. $F_{ie}^* = Q_{ie}$ and $E_{ie}^* = 0$ Therefore the current transport rates and the profile changes are determined as

$$\begin{aligned} \Delta h_i &= E_i Q_i + F_i & ib \le i \le ie \\ Q_i &= E_i^* \Delta y_{i-1} + F_i^* & ib+1 \le i \le ie-1 \end{aligned} \tag{3 66}$$

3 3.3.4 Wave runup

The uprush limit is based on the wave runup Hunt (1958) proposed an equation for the wave runup as a function of bed slope, wave height and wave steepness in the study of seawall and breakwater design, expressed as

$$R = H_b \frac{\tan\beta}{\sqrt{H_b / L_0}} \tag{3 67}$$

where R is the wave runup height, $\tan\beta$ is the average bed slope from the runup limit to the incipient breaking point

3 3 3.5 Limiting onshore and offshore slopes

The program adopts the idea of CROSS (Zheng, 1996, Zheng and Dean 1997) and allows specification of maximum onshore and offshore slopes These limitations are required at the upper limit of runup where seaward or landward transport can cause the angle of repose of the profile to be exceeded above this elevation Slopes exceeding the allowed can also occur at the seaward end of the computational domain where the most seaward active contour is displaced seaward, thus creating a locally steep slope At each time step, the program checks and if it is determined that a local slope exceeds the specified values, avalanching occurs with the sand redistributed to the adjacent contours until the maximum allowable slope is reached The allowable slopes from Zheng (1996) are taken as 0 18 and 0 22 for onshore and offshore slope, respectively, based on large wave flume data.

3.3.3-6 Random waves

In the case of random wave conditions, the wave-by wave approach is applied in the model The wave heights and corresponding wave periods are generated as described

in Section 3 1.2.2. The total sediment volume transport at a point, V_i, in a time step Δt is

$$V_i = \sum_{k=1}^{nw} Q_{k,i} T_k \tag{3 68}$$

where $Q_{k,i}$ is calculated by Eq 3 45 using the generated wave height H_k and wave period T_k, and nw is the number of waves included in the time span of Δt The assumption is that the profile does not change immediately after each single wave action The finite difference transport equation for random waves, similar to Eq 3 61 is

$$A_i^* \Delta h_{i-1}^{m+1} + B_i^* V_i^{m+1} + C_i^* \Delta h_i^{m+1} = G_i^* \tag{3 69}$$

$$A_i^* = -nK \sum_{k=1}^{nw} \left[\left| D_{k,i}^m - D_* + \alpha \frac{h_i^m - h_{i-1}^m}{\Delta y} \right|^{n-1} \left(\frac{\partial D_{k,i}}{\partial h_{i-1}} - \frac{\alpha}{\Delta y} \right) T_k \right]$$

$$B_i^* = 1.0$$

$$C_i^* = -nK \sum_{k=1}^{nw} \left[\left| D_{k,i}^m - D_* + \alpha \frac{h_i^m - h_{i-1}^m}{\Delta y} \right|^{n-1} \left(\frac{\partial D_{k,i}}{\partial h_i} + \frac{\alpha}{\Delta y} \right) T_k \right]$$

$$G_i^* = K \sum_{k=1}^{nw} \left[\left(D_{k,i}^m - D_* + \alpha \frac{h_i^m - h_{i-1}^m}{\Delta y} \right) D_{k,i}^m - D_* + \alpha \frac{h_i^m - h_{i-1}^m}{\Delta y} \Bigg|^{n-1} T_k \right]$$

The discrete form of the continuity equation for random waves becomes

$$A_i V_i^{m+1} + B_i \Delta h_i^{m+1} + C_i V_{i+1}^{m+1} = G_i \tag{3 70}$$

$$A_i = \frac{1}{2\Delta y},\ B_i = 1.0,\ C_i = -A_i,\ G_i = -\frac{1}{2\Delta y}\left(V_{i+1}^m - V_i^m\right)$$

CHAPTER 4
MODEL CALIBRATION WITH LABORATORY EXPERIMENTS

4.1 Introduction

Application of the cross-shore model discussed in Chapter 3 requires quantification of several coefficients. To reduce the number of free variables and facilitate the calibration process, the coefficients in the wave and roller model, namely decay coefficient K, stable wave coefficient Γ, and roller dissipation coefficient β_d, are taken as the suggested values at this stage, that is, $K = 0.15$, $\Gamma = 0.4$, and $\beta_d = 0.1$. Thus, two coefficients are to be determined, the exponent, n, and the transport coefficient, K. The linear (n = 1) and nonlinear (n = 2, 3) transport relationships are used for comparison of model prediction with several large-scale laboratory experiments. The similarities for these models are that they should converge to the same target profile for unchanging wave conditions and unlimited time. The only difference is that the evolution with larger n value will evolve more rapidly at the beginning and more slowly later than the relationship with smaller n values.

As an objective criterion for judging agreement between the simulated and measured profile, the root mean-square of the difference between measured and calculated depths is used

$$RMS = \sqrt{\frac{1}{N}\sum_{i=1}^{N}(h_i^m - h_i^p)^2} \qquad (4.1)$$

in which superscripts m and p refer to measured and predicted profiles, respectively, and N is the number of data points. The errors between the predicted and observed profile

depths are obtained at the times for which measured profile information is available. The best-fit K value is determined as the value yielding the overall least RMS error. In order to avoid scale effects on profile evolution, only large-scale wave flume experiments are used. Dette et al. (2002) provided a detailed overview of the existing large wave flumes in the world and the profile evolution related experiments available from these flumes. Three different laboratory data sets were available and are examined in this study for the present model calibration: "Large Wave Tank" (LWT) experiments in 1956/1957 and 1962 by Saville (data are from Kraus and Larson, 1988), the Large Wave Flume of the Central Research Institute of Electric Power Industry (CRIEPI) in 1982 (Kajima et al. 1982, Larson and Kraus, 1989), and German wave flume experiments (GWK) in Hannover, Germany, in 1986/1987 (Dette and Uliczka, 1987) and in1996/97 as part of the MAST III-SAFE project (Dette et al., 1998). Among them, LWT and CRIEPI were carried out with monochromatic waves, GWK had both monochromatic and random waves.

4.2 LWT Experiments

4.2.1 Description of Experiments

Two series of movable-bed model experiments on beach profile change were conducted in the tank of the Beach Erosion Board 1956/57 and 1962 (reported by Kraus and Larson, 1988). The two series differ mainly in the grain size of the bed material used. Nine major tests were run with each of two sand sizes using essentially the same water depth and wave conditions. Tests for a given grain size were characterized by waves of varying steepness producing either accreting or eroding profiles. All tests were with monochromatic waves. The experiments included extensive profile surveys during

each test to document the approach to equilibrium. Only limited hydraulic measurements were made, mainly wave heights at incipient breaking and run up heights.

The experiments were conducted when the tank was located at Dalecarlia Reservation in Washington, DC. The concrete tank was 194 m long, 4.6 m wide, and 6.1 m deep. The initial profile slope for all tests but two was 1:15. The wave periods ranged between 3.75 and 16.0 s and generated wave heights between 0.55 and 1.68 m in the horizontal part of the tank. The wave height and period were held constant except in one case when the water depth was varied in order to simulate a tide (Test 911). The water depths ranged from 3.5 to 4.6 m and two grain sizes were used with median diameters of 0.22 mm in 1956/57 and 0.4 mm in 1962, respectively. Tests 510 and 610 were conducted from an initial profile that was non planar and Test 110 was a repetition run of Test 100. Of the 15 generic cases studied (plane initial slope, different wave and sediment conditions), eight terminated with erosional profiles (Tests 100, 300, 400, 500, 700, 401, 501, and 901) and seven with accretionary profiles (Tests 200, 600, 101, 201, 301, 701, and 801).

In Test 100, the profile eroded back to the end of the tank. The water level in Test 700 varied during the experiment. In all the accretionary cases, a majority of sand was carried onshore from offshore of the surf zone, however, the model calculation domain is ended at the breaking point, thus cannot predict these onshore transports. Thus, only five erosional cases (Tests 300, 400, 500, 401 and 501) are used for the model calibration. Table 4-1 summarizes the conditions of the tests and the corresponding fall velocity parameters based on the breaking wave heights.

4.2.2 Modeling Results

The best-fit K values for both linear (n = 1) and nonlinear (n =2, 3) transport relationships of the five LWT tests are listed in Table 4-2. It appears that transport relationship with n = 2 provides overall least root-mean-square errors and best fits to the observed profile evolution.

The comparisons of predicted and measured profile evolutions are presented in Figure 4-1 to Figure 4-5 for the five cases, respectively. In each case, the profiles at four different times are compared. A primary breaking point bar is predicted at each case, but no secondary inshore bar is generated. Also the model cannot predict the wide trough area after the primary offshore bars. The nonlinear relationships predict a faster profile evolution at the beginning and slower later, as the measured profiles show the same trend.

Table 4-1 Summary of the LWT experiment tests used for model calibration.

Test No	Grain size (mm)	Wave height (m)	Wave period (s)	Water depth (m)	Duration (hrs)	H_b wT
300	0.22	1.68	11.33	4.27	50	5.53
400		1.62	5.6	4.42	40	10.0
500		1.52	3.75	4.57	100	12.27
401	0.40	1.62	5.6	4.42	66	5.36
501		1.52	3.75	4.57	60	6.57

Table 4-2 Best-fit K values for LWT experiments

Test No	n = 1		n = 2		n = 3	
	Best-fit K (m^4/N)	Error (m)	Best-fit K (m^5s/N^2)	Error (m)	Best-fit K (m^6s^2/N^3)	Error (m)
300	1.3×10^{-6}	0.361	0.79×10^{-8}	0.343	0.58×10^{-10}	0.348
400	2.0×10^{-6}	0.250	1.4×10^{-8}	0.203	0.99×10^{-10}	0.222
500	1.0×10^{-6}	0.381	1.1×10^{-8}	0.365	1.1×10^{-10}	0.393
401	0.83×10^{-6}	0.267	0.47×10^{-8}	0.261	0.27×10^{-10}	0.270
501	0.98×10^{-6}	0.303	0.71×10^{-8}	0.306	0.62×10^{-10}	0.319

4.3 CRIEPI Wave Flume Experiments

The wave flume is operated by the Central Research Institute of Electric Power Industry in Japan between 1979 and 1983 (Kajima et al., 1982). It is made of reinforced concrete, and is 205 m long, 3.4 m wide, and 6 m deep in the 115 m-long upwave flat section, which is joined to a shoreward section of 1/15 slope. As in the LWT experiments, two different median grain sizes were employed, although slightly coarser in the CRIEPI experiments (0.27 and 0.47 mm). A majority of the tests started from a plane beach slope, but the initial slope was varied, ranging from 1:50 to 1:10. Both erosional and accretionary cases were investigated. Only monochromatic waves were used in the experiments keeping the water level fixed during a test. Plunging, spilling, and surging breaking waves were observed, although plunging breakers occurred in the majority of cases. The experimental program consisted of 24 monochromatic tests with wave periods ranging between 3.0 and 12.0 s and generated wave heights between 0.3 and 1.8 m.

Extensive surveys were carried out during the experiments at a very high spatial resolution (at least every 50 mm, sometimes every mm), which allowed for the study of micro-scale features such as ripples. Larson and Kraus (1989) used the CRIEPI data to quantify and model beach profile evolution. Of the 17 tests identified as giving distinct responses corresponding to bar or berm profiles, Tests 1-8, 2-1, 3-1, 3-2, 3-4, 4-2, 4-3, 5-2, 6-1, and 6-2 produced bar profiles and Tests 1-1, 1-3, 2-2, 2-3, 3-3, 4-1, and 5-1 produced berm profiles. Here, Test 6-2 with a 0.27 mm median grain size is selected to calibrate the model and the results are presented in Table 4-3. Figure 4-6 shows the comparisons between the measured and the best fit predicted profiles for four time series

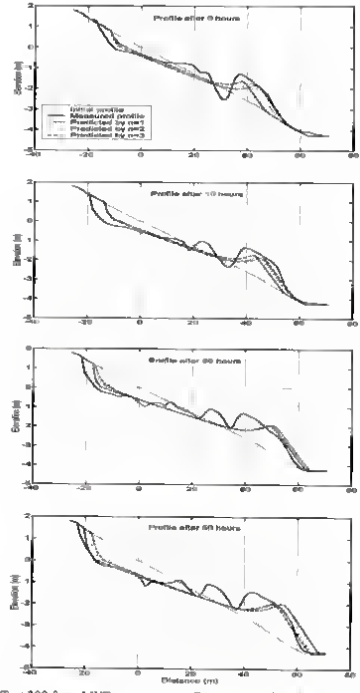

Figure 4-1 Test 300 from LWT experiments. Comparison of predicted to observed profiles at different times for the best-fit K values for n = 1, 2 and 3

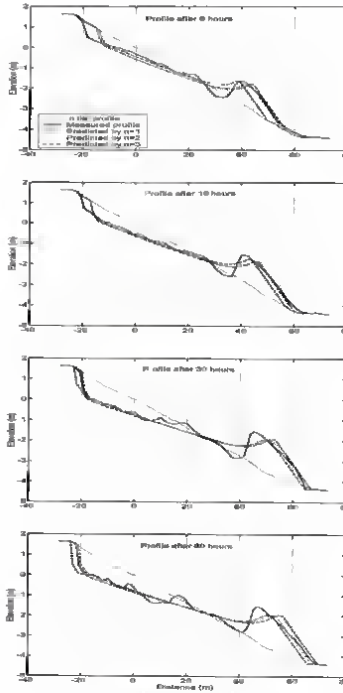

Figure 4-2. Test 400 from LWT experiments - Comparison of predicted to observed profiles at different times for the best-fit K values for n = 1, 2 and 3

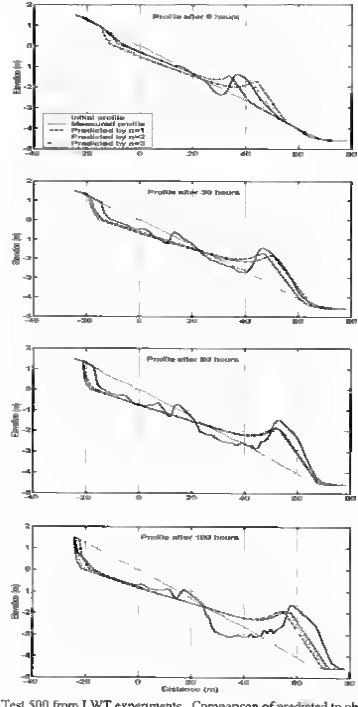

Figure 4-3 Test 500 from LWT experiments Comparison of predicted to observed profiles at different times for the best fit K values for n = 1, 2 and 3

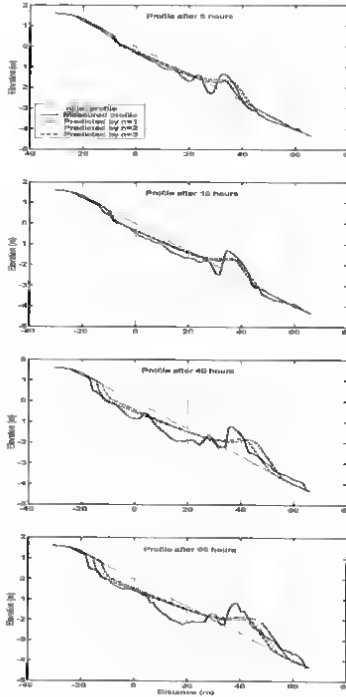

Figure 4-4 Test 401 from LWT experiments Comparison of predicted to observed profiles at different times for the best-fit K values for n = 1, 2 and 3

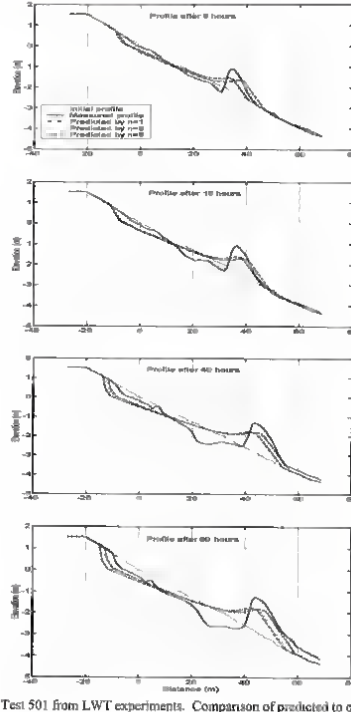

Figure 4-5 Test 501 from LWT experiments. Comparison of predicted to observed profiles at different times for the best-fit K values for n = 1, 2 and 3

Table 4-3 Best-fit K values for CRIEPI experiment

Test No	Test cond		n = 1		n = 2		n = 3	
	H (m)	T (s)	Best fit K (m^4/N)	Error (m)	Best fit K (m^5s/N^2)	Error (m)	Best-fit K (m^8s^2/N^3)	Error (m)
6-2	1 12	7 5	2.3×10^{-6}	0.186	1.2×10^{-8}	0 181	0.7×10^{-10}	0 201

4.4 German Large Wave Flume

The German "large wave flume" in Hannover is 324 m long, 7 m deep and 5 m wide. Since 1986 a series of beach profile experiments have been conducted in the flume. Only tests from 1986/1987 and 1996/1997 were available for the present study.

4.4.1 1986/1987 Experiments

The purpose of the first set of experiments in 1986/1987 was to study beach and dune erosion under monochromatic and random waves (Dette and Uliczka, 1987). Two of these experiments were conducted with the same constant wave conditions and different initial profiles. Regular waves with a wave height of 1.5 m and a period of 6 s were generated in a water depth of 5 m. The sand used for both experiments had a mean diameter of 0.33 mm, which corresponds to a fall velocity of 5 cm/s. Two initial profiles, "dune without foreshore" and "dune with foreshore", were used. The "dune without foreshore" had a dune crest of 2 m above still water level and a seaward slope of 1:4 down to the channel floor. The "dune with foreshore" had a slope of 1:4 from the dune crest of 2 m above still water level to 1 m water depth followed by a slope of 1:20 down to the channel floor.

Here, the case "dune without foreshore" is used for model calibration. Table 4-4 provides the results and Figure 4-7 presents the comparisons between predicted and measured profiles at four different time series.

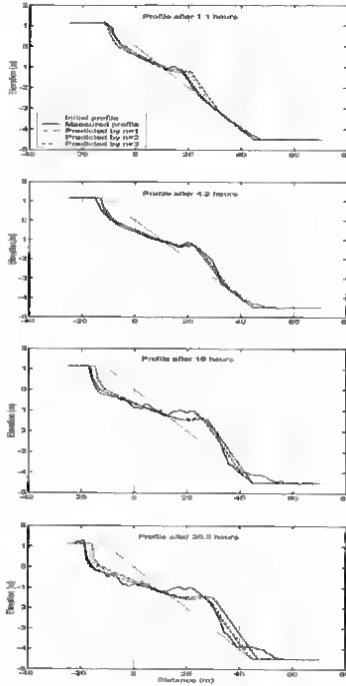

Figure 4-6 Test 6-2 from CRIEPI experiments (initial slope 1:10) Comparison of predicted to observed profiles at different times for the best-fit K values for n = 1, 2 and 3

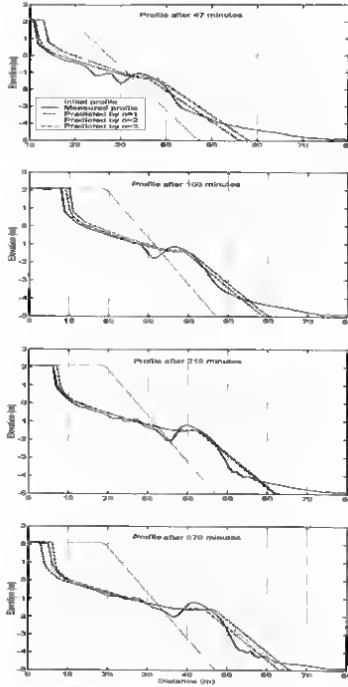

Figure 4-7. Case 'dune without foreshore' under regular wave conditions in German wave flume experiments (initial slope 1:4). Comparison of predicted to observed profiles at different times for the best-fit K values for n = 1, 2 and 3

Table 4-4 Best-fit K values for German wave flume 1986/1987 experiment

Test	n = 1		n = 2		n = 3	
	Best-fit K (m^4/N)	Error (m)	Best-fit K (m^5s/N^2)	Error (m)	Best-fit K (m^8s^2/N^3)	Error (m)
Dune w/o foreshore	2.3×10^{-6}	0.379	0.79×10^{-8}	0.313	1.5×10^{-11}	0.306

4.4.2 1996/1997 Experiments

From November to December 1996, February to March 1997 and June to August 1997, in conjunction with the MAST III SAFE project, experiments were carried out in the Grosser Wellenkanal in Hannover to study the development of the underwater profile and sand losses from the beach by various water level and wave conditions (Dette et al. 1998; Dette et al., 2002). The tests were divided into two major phases focusing on beach and dune stability under given conditions with variable sea levels.

In Test Phase I, attention was concentrated on beach stability without structural aid. The beach was formed from sands with a median diameter of 0.3 mm and a fall velocity of 0.042 m/s. The underwater profile from 4 m above the flume floor was shaped to the equilibrium profile $h = 0.12y^{2/3}$. The beach above the still water level (4 m above the flume floor) had slopes of 1:20, 1:15, 1:10, and 1:5. The initial profile geometries of Test Phase I are shown in Figure 4-8. Each test slope was first subjected to normal wave and water level conditions using a TMA spectrum with $H_{m0} = 0.65$ m and $T_m = 5$ s. This initial test lasted until the profile reached an equilibrium state for the selected wave parameters and reused as the initial profile for the profile change due to storm surge conditions by raising the water level by 1 m (channel floor +5 m) and generating storm waves (TMA spectrum with $H_{m0} = 1.2$ m and $T_m = 5$ s). The peak period for the generated TMA spectra was 6.6 s (normal and storm conditions). The spectral length was

15 min and consisted of 165 waves. Figure 4-9 presents the initial and final measured profiles under storm wave condition in Test Phase 1

The model calibration uses the wave-by-wave random wave model discussed in Chapter 3. The best-fit K values for the four tests under storm wave conditions are summarized in Table 4-5 and the comparisons between predicted and measured profile evolutions are shown in Figure 4-10 to Figure 4-13, respectively. The developed bars near the normal water line (4 m above the floor) are not generated by the model. The linear transport relationship provides an overall better fit than the nonlinear relationships.

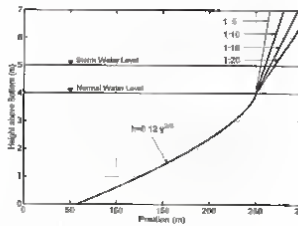

Figure 4-8 Profile geometries for beach stability experiments in Test Phase 1 of German 1996/1997 experiments

Table 4-5 Best-fit K values for German flume 1996/1997 experiments

Test No	n = 1		n = 2		n = 3	
	Best-fit K (m^4/N)	Error (m)	Best-fit K (m^5s/N^2)	Error (m)	Best-fit K (m^6s^2/N^3)	Error (m)
A9 (1:20)	0.99×10^{-6}	0.0676	0.68×10^{-8}	0.0728	0.47×10^{-10}	0.0758
B2 (1:10)	2.5×10^{-6}	0.0765	1.6×10^{-8}	0.0828	1.5×10^{-10}	0.0883
C2 (1:5)	1.7×10^{-6}	0.0721	0.81×10^{-8}	0.0834	0.75×10^{-10}	0.0919
H2 (1:15)	1.3×10^{-6}	0.0662	0.66×10^{-8}	0.0765	0.36×10^{-10}	0.0841

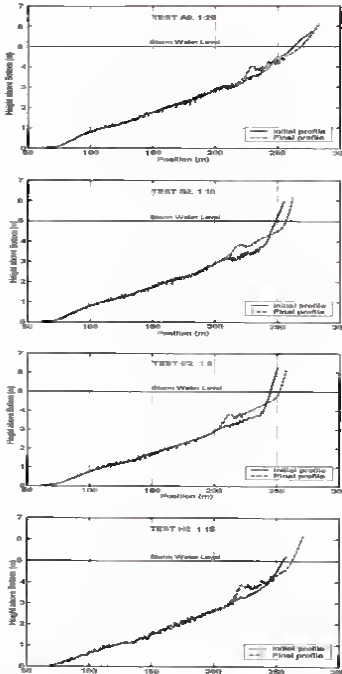

Figure 4-9 The initial and final observed profiles to Test Phase I of German wave flume 1996/1997 experiments.

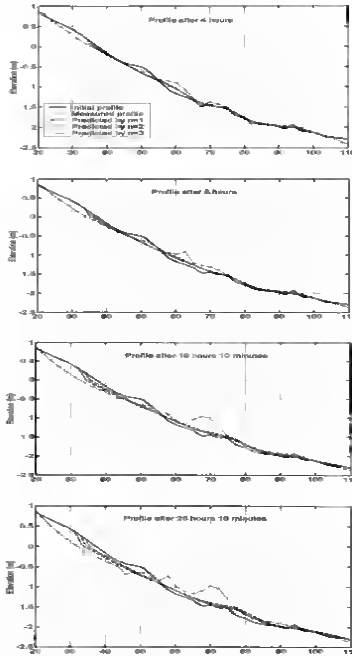

Figure 4-10 Test A9 from German wave flume1996/1997 experiments (initial slope 1 20) Comparison of predicted to observed profiles at different times for the best fit K values for n = 1 2 and 3

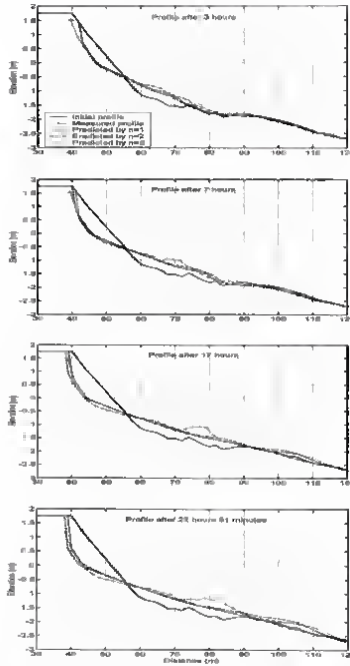

Figure 4-11 Test B2 from German wave flume1996/1997 experiments (initial slope 1:10) Comparison of predicted to observed profiles at different times for the best-fit K values for n = 1, 2 and 3

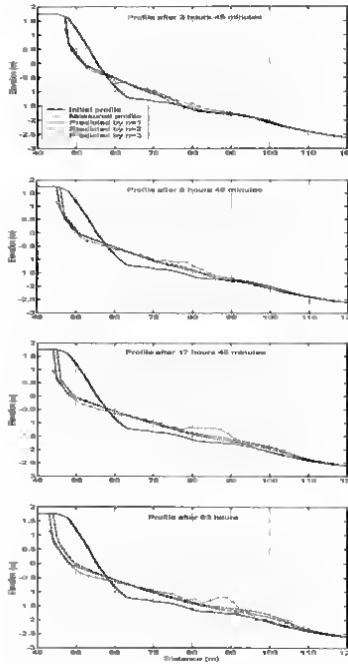

Figure 4-12 Test C2 from German wave flume1996/1997 experiments (initial slope 1:5) Comparison of predicted to observed profiles at different times for the best-fit K values for n = 1, 2 and 3

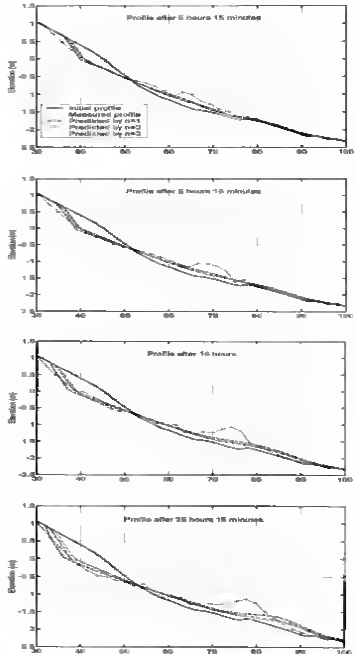

Figure 4-13 Test H2 from German wave flume1996/1997 experiments (initial slope 1:15) Comparison of predicted to observed profiles at different times for the best-fit K values for n = 1, 2 and 3

4.5 Summary of Laboratory Calibration

A total of eleven large-scale experiments from three different wave flumes are employed for the model calibration and comparison of the linear and nonlinear transport relationships. Seven of these tests were conducted with monochromatic wave conditions and the other four were carried out with random waves. These tests are characterized with different sediment sizes, initial profiles, and incident wave conditions.

The minimum root-mean-square errors between predicted and measured profiles are used as the objective in the calibration procedure. The experimental conditions and the best-fit results are summarized in Table 4-6. Note that the best-fit K values obtained are based on total time series available for each individual test, not just one particular measured profile. The average best-fit K value of the linear relationship ($n = 1$) is 1.72×10^{-6} m^4/N, with a variation from −52% to 133%, whereas the best-fit K values range from −49% to 72% of the average value of 0.93×10^{-8} m^6s/N^2 for $n = 2$ and from −78% to 121% of the average value of 0.68×10^{-10} m^8s^2/N^3 for $n = 3$, respectively. The nonlinear relationship with $n = 2$ has a narrower range than that for $n = 1$ and 3. Of the eleven tests, the nonlinear relationship with $n = 2$ has the best fit for six of seven monochromatic wave cases, while $n = 1$ provides the best fit for four random wave cases.

To further investigate the transport relationship, the best-fit K values (shown in Figures 4-14 to 4-17) for each individual measured profile are determined using the same criteria for LWT tests 300, 400, 500 and CRIEPI test 6-2. In most cases, the best-fit K values for $n = 1$ decrease with time, and increase with time for $n = 3$, but have no apparent trend for $n = 2$. If the transport coefficient in the model is assumed to be a constant, the model with $n = 2$ can have a better simulation of the profile change history

Table 4-6. Summary of laboratory calibration

Case		H (m)	T (s)	d_{50} (mm)	Best-fit K			Error (m)		
					$n=1$ (m^4/N)	$n=2$ (m^5s/N^2)	$n=3$ (m^6s^2/N^3)	$n=1$	$n=2$	$n=3$
LWT	300	1 68	11 33	0 22	1.3×10^{-6}	$0\ 79\times10^{-8}$	$0\ 58\times10^{-10}$	0 361	0.343	0.348
	400	1 62	5 6	0 22	$2\ 0\times10^{-6}$	$1\ 4\times10^{-8}$	$0\ 99\times10^{-10}$	0 250	0 203	0.222
	500	1 52	3 75	0 22	$1\ 0\times10^{-6}$	$1\ 1\times10^{-8}$	$1\ 1\times10^{-10}$	0 381	0.365	0.393
	401	1 62	5 6	0 40	$0\ 83\times10^{-6}$	$0\ 47\times10^{-8}$	$0\ 27\times10^{-10}$	0 267	0 261	0 270
	501	1.52	3 75	0 40	$0\ 99\times10^{-6}$	$0\ 71\times10^{-8}$	$0\ 62\times10^{-10}$	0 303	0 306	0 319
CRIEPI	6-2	1 12	7 5	0 27	2.3×10^{-6}	1.2×10^{-8}	$0\ 70\times10^{-10}$	0 186	0 181	0.201
German LWF	dwf	1.50	6 0	0.33	$4\ 0\times10^{-6}$	$0\ 79\times10^{-8}$	$0\ 15\times10^{-10}$	0 381	0 313	0 308
	A9	1.20	5 0	0.30	$0\ 99\times10^{-6}$	0.68×10^{-8}	$0\ 47\times10^{-10}$	0 0676	0.0728	0.0758
	B2	1.20	5 0	0.30	$2\ 5\times10^{-6}$	1.6×10^{-8}	$1\ 5\times10^{-10}$	0 0765	0 0828	0 0883
	C2	1 20	5 0	0.30	$1\ 7\times10^{-6}$	$0\ 8\ 1\times10^{-8}$	$0\ 75\times10^{-10}$	0 0721	0 0834	0 0919
	H2	1.20	5 0	0.30	$1\ 3\times10^{-6}$	$0\ 66\times10^{-8}$	$0\ 36\times10^{-10}$	0 0662	0 0765	0 0841
Averages					$1\ 72\times10^{-6}$	$0\ 93\times10^{-8}$	$0\ 68\times10^{-10}$			

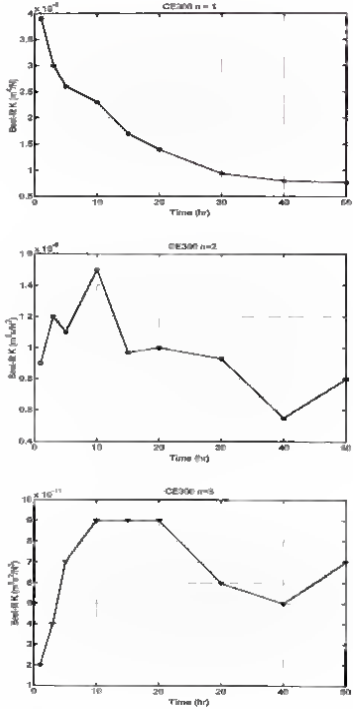

Figure 4-14 Best-fit K values with time for LWT Test 300 with n = 1, 2 and 3

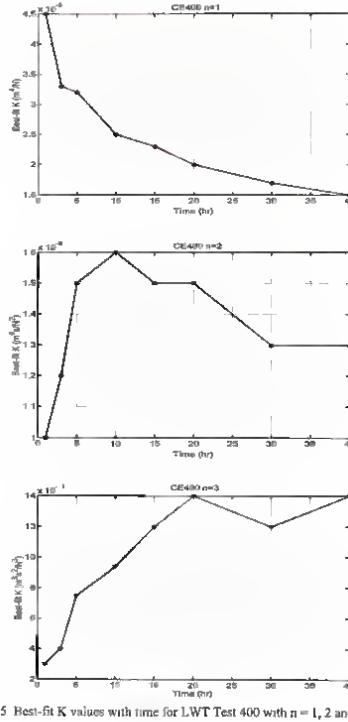

Figure 4-15 Best-fit K values with time for LWT Test 400 with n = 1, 2 and 3

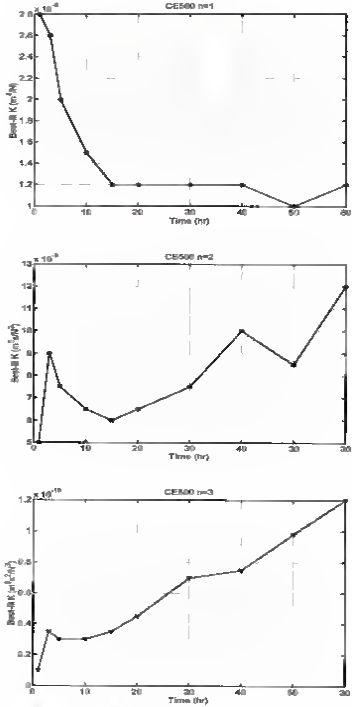

Figure 4-16 Best fit K values with time for LWT Test 500 with n = 1, 2 and 3

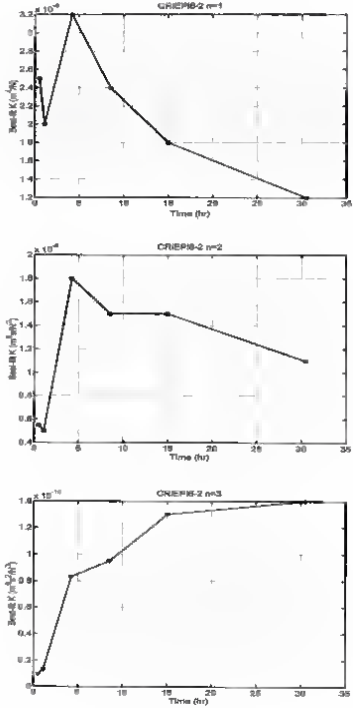

Figure 4-17 Best-fit K values with time for CREEP1 Test 6-2 with n = 1, 2 and 3

Another parameter characterizing modal skill is the profile foreshore volumetric erosion (Zheng, 1996, Zheng and Dean, 1997). Figure 4-18 shows comparisons of the measured and the best-fit predicted eroded volume for the above-investigated tests. The best-fit RMS errors are presented in Table 4-7. The transport relationship with n = 2 gives the best fit for Tests CE300 and CE400, while n = 1 has the best fit for Tests CE500 and CRIEPI6.2. One unusual feature in CE500 case is that there is a rapid change in the eroded volume after 60 hours wave action. If excluding the profile evolution after 60 hours, n = 2 gives the best fit eroded volume for this test.

Based on these results, it is determined that the nonlinear transport relationship with n = 2 is more appropriate in the cross-shore profile model. The transport coefficient $K = 0.93\times10^{-8}$ m^6s/N^2 is adopted according to the average of the best-fit K values in the eleven tests.

Table 4-7 Best-fit RMS errors of eroded volume (unit: m^2).

	n = 1	n = 2	n = 3
CE300	3.19**	1.57	2.48
CE400	2.67	0.67	1.73
CE500	1.64	2.23	3.18
CE500*	1.79	0.90	1.16
CRIEPI	1.24	1.85	3.29

* The measurements after 60 hours are excluded in the calculation.
** The RMS error between predicted and measured eroded volume, defined as Eq. 4.1 except change profile depth to eroded volume.

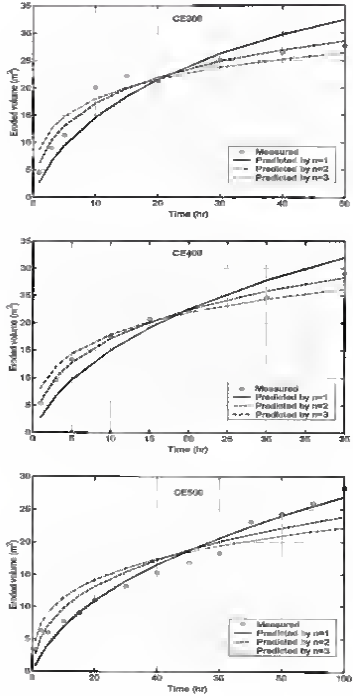

Figure 4-18 Comparison of best-fit to observed eroded volumes

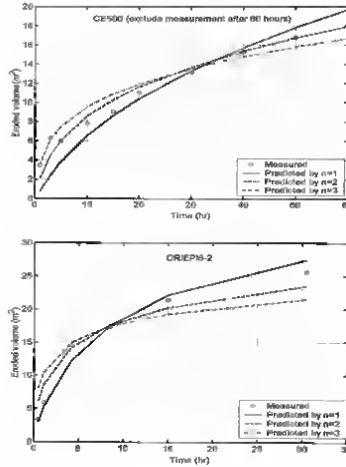

Figure 4-18 Continued

CHAPTER 5
MODEL EVALUATION AND SENSITIVITY ANALYSIS

In Chapter 4 eleven large scale wave flume laboratory tests were selected to calibrate the developed cross-shore profile model. Based on the calibration results, the nonlinear transport relationship with n = 2 was found to yield the overall least root mean-square error for profile evolution. The average best-fit K value of 0.93×10^{-6} m^5/N^2 was recommended for model application. The purpose of this chapter is to evaluate the cross-shore model with the recommended average K value. First, the predicted profile evolutions with the average K value are compared with the results of the individual best-fit K values using the same laboratory data in Chapter 4. Then a sensitivity analysis is performed to quantify the influence of various model parameters and empirical coefficients on the simulation results. Predictions of the model are also examined for varying water levels and different initial profile slopes.

5.1 Evaluation of K value with Laboratory Experiments

The eleven experiments described in Chapter 4 are included in the evaluations of the cross-shore model with the fixed average K value. The input values of several parameters in the model are summarized below:

- The breaking index, $\gamma = 0.78$.
- The decay coefficient, K, and stable wave height coefficient, Γ, in the D^3 wave model are taken as 0.15 and 0.4, respectively.
- The dissipation coefficient, β_r, in the roller model is set to 0.1.
- The limiting onshore and offshore slopes for avalanching are 0.18 and 0.22, respectively.

The deviation of the profile depth root-mean-square errors (defined in Eq 4.1) between the results of the average K value and the individual best-fit K value is chosen as the model evaluation parameter

$$Dev = \frac{RMS_f - RMS_b}{RMS_b} \tag{5.1}$$

where Dev denotes a non-dimensional deviation, RMS is the root mean-square error of the profile depth, the subscript f and b represent the results of the model prediction with the average and best-fit K values, respectively. If the predictions with the average K value are exactly identical to those of the best-fit K values, the deviation in Eq 5.1 is zero. Generally, the sign of Dev is positive since the model with best-fit K values should yield less error than that with fixed values.

The model results of the root-mean-square errors are presented in Table 5-1 for the eleven experiments. Figures 5.1 to 5-11 show the comparisons of the predicted profiles for these experiments. It is seen that the predictions with the average K value provide fits to the measured profiles which are nearly as good as these with the best-fit K values for each experiment. Although the best-fit K values range from –49% to 72% of the average K value, ten out of eleven deviations of the root-mean-square errors are less than 10%, and eight of the eleven are within 5%.

The model predicts bar profiles in the seven monochromatic wave tests, although the wide trough area in Case 500 and 501 are not produced. However, the model does not generate the double bars present in the LWT experiments. In the random wave tests, the predicted bars are not very clear as in the observed profiles. The reason could be that the generated random waves in the controlled laboratory conditions are much different than those generated randomly in the model.

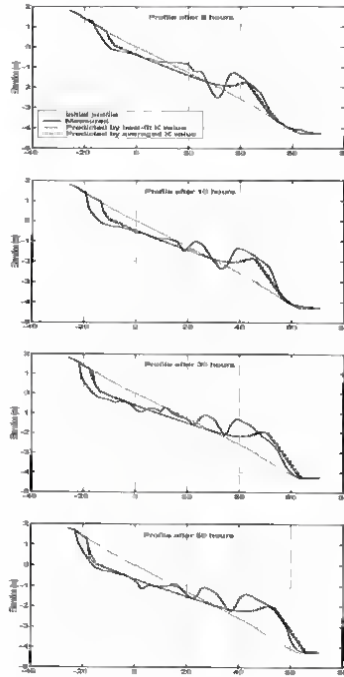

Figure 5-1 Test 300 from LWT experiments Comparison of measured and predicted profiles by the model with the best-fit and average K values.

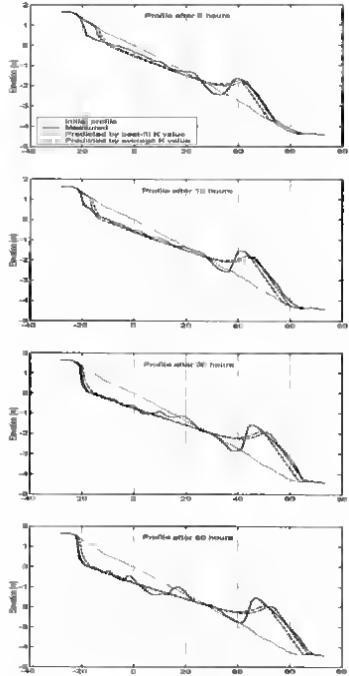

Figure 5-2. Test 400 from LWT experments Comparison of measured and predicted profiles by the model with the best-fit and average K values

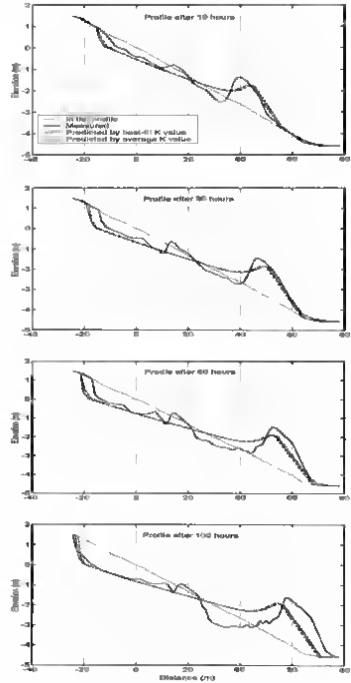

Figure 5-3 Test 500 from LWT experiments. Comparison of measured and predicted profiles by the model with the best-fit and average K values.

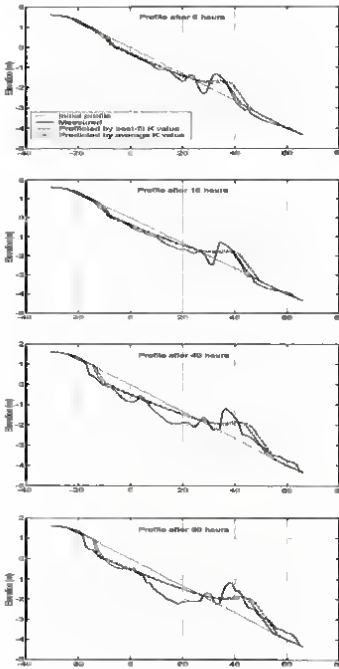

Figure 5-4 Test 401 from LWT experiments Comparison of measured and predicted profiles by the model with the best-fit and average K values.

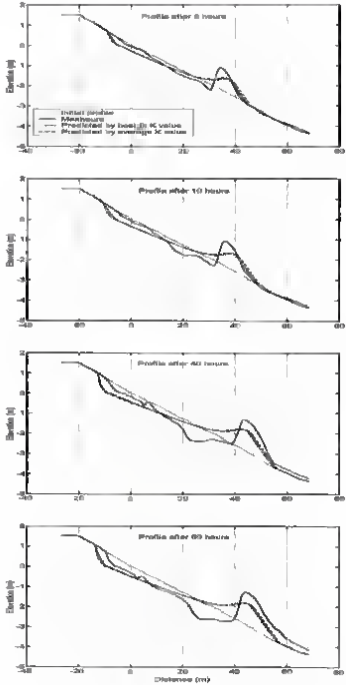

Figure 5-5 Test 501 from LWT experiments Comparison of measured and predicted profiles by the model with the best-fit and average K values

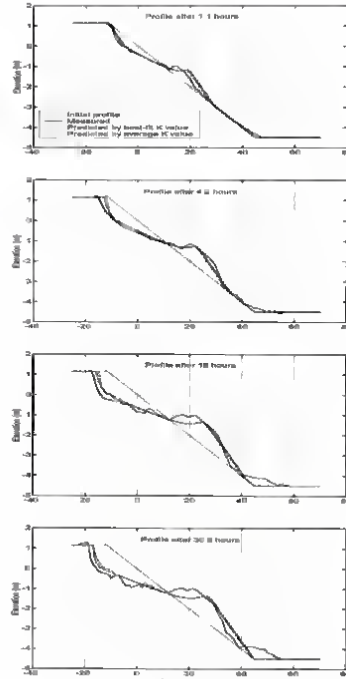

Figure 5-6. Test 6-2 from CRIEPI experiments Comparison of measured and predicted profiles by the model with the best-fit and average K values

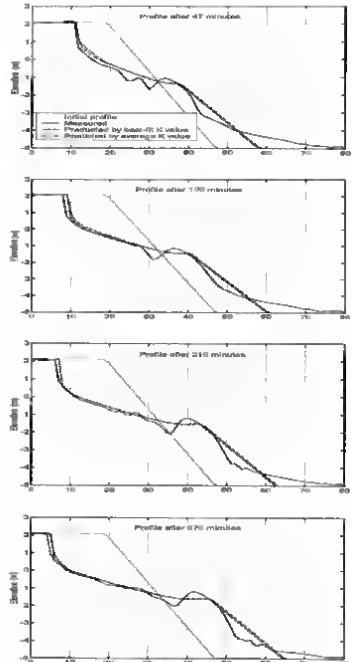

Figure 5.7 Case "dune without foreshore" under regular wave conditions in German wave flume experiments. Comparison of measured and predicted profiles by the model with the best-fit and average K values.

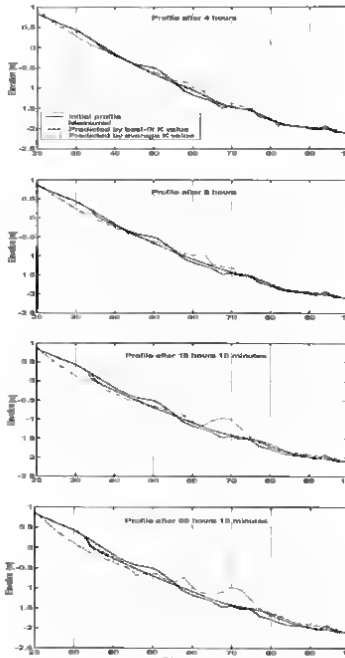

Figure 5-8 Test A9 from German wave flume 1996/1997 experiments Comparison of measured and predicted profiles by the model with the best-fit and average K values.

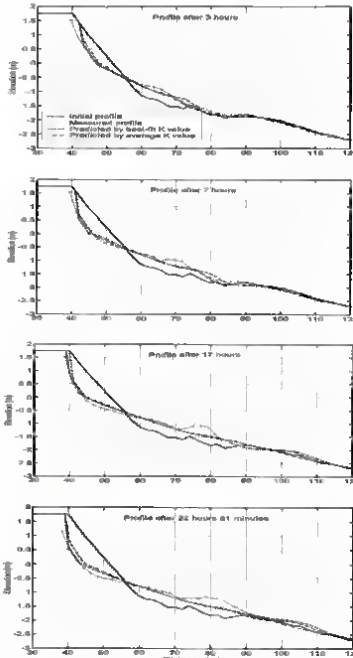

Figure 5-9 Test B2 from German wave flume 1996/1997 experiments Comparison of measured and predicted profiles by the model with the best-fit and average K values.

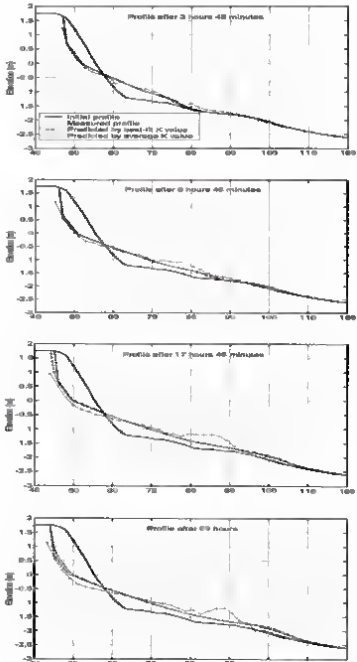

Figure 5-10 Test C2 from German wave flume 1996/1997 experiments Comparison of measured and predicted profiles by the model with the best-fit and average K values

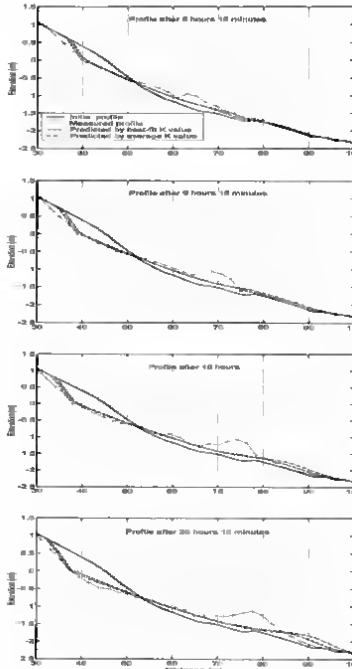

Figure 5-11 Test H2 from German wave flume 1996/1997 experiments. Comparison of measured and predicted profiles by the model with the best-fit and average K values

Table 5-1 Root-mean-square errors of profile depths predicted by the model with best-fit and average K values and the corresponding deviations.

Test		Best fit K value		Average K value	
		K (m^3s/N^2)	RMS_b (m)	RMS_f (m)	Dev
LWT	300	0.79×10^{-3}	0.343	0.345	0.005
	400	1.4×10^{-3}	0.203	0.238	0.17
	500	1.1×10^{-3}	0.365	0.370	0.014
	401	0.47×10^{-3}	0.261	0.279	0.069
	501	0.71×10^{-3}	0.306	0.308	0.0065
CRIEPI	6-2	1.2×10^{-3}	0.181	0.186	0.028
German LWF	dwf	0.79×10^{-3}	0.313	0.321	0.026
	A9	0.68×10^{-3}	0.072	0.073	0.0027
	B2	1.6×10^{-3}	0.082	0.089	0.085
	C2	0.81×10^{-3}	0.0776	0.077	0.0026
	H2	0.66×10^{-3}	0.0731	0.0751	0.027

5.2 Sensitivity Analysis of Model Parameters

Sensitivity analysis provides valuable information regarding the physical implications of the model parameters and their relative effects on the results. In the following, the influence of the principal model parameters on beach evolution is discussed by reference to eroded volume for a specific case (CRIEPI 6-2).

5.2.1 Influence of Breaking Index γ

The breaking index determines the offshore boundary position of the model. Larger γ values indicate the breaking point moves onshore, and vice versa. Figure 5-12 illustrates the eroded volume as a function of time for various values of γ. A smaller value of γ implies larger beach erosion due to a wider surf zone and thus more material movement from the inshore to attain equilibrium.

5.2.2 Influence of D^3 Breaking Wave Model Parameters

To quantify the importance of variations in the wave height calculation, the wave decay coefficient K is varied. Figure 5-13 shows the evolution of eroded volume for

different values of K. A smaller value of K indicates that the wave heights decay slowly after breaking and thus propagate a greater distance landward. From Eq. 3.31, a smaller value of K gives a flatter shape of the equilibrium beach profile and thus requires redistribution of a greater amount of sand before equilibrium is attained. On the other hand, a smaller value of the stable wave height coefficient Γ results in a steeper equilibrium beach profile and a smaller eroded volume, since less material has to be moved from the inshore to attain equilibrium. Figure 5-14 illustrates the effect of varying the stable wave height coefficient on the eroded volume.

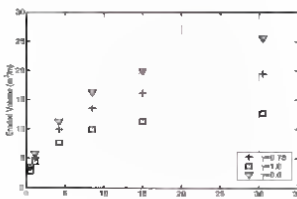

Figure 5-12 Effect of breaker index on eroded volume

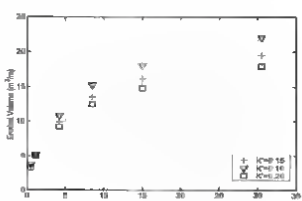

Figure 5-13 Effect of wave decay coefficient on eroded volume

5.2.3 Influence of Roller Model Coefficient

The dissipation coefficient β_d in the roller model determines the roller energy dissipation. A larger β_d value implies steeper equilibrium beach profile slope from Eq 3.31, thus causing less volume erosion inshore (Figure 5-15).

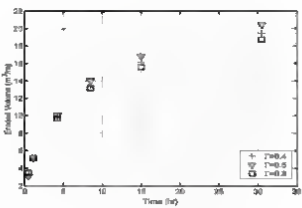

Figure 5-14 Effect of stable wave height coefficient on eroded volume.

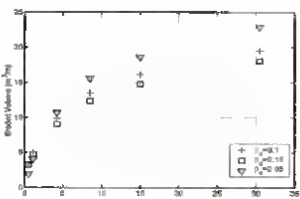

Figure 5-15 Effect of roller model coefficient on eroded volume.

5.2.4 Influence of Equilibrium Energy Dissipation

The equilibrium energy dissipation per unit volume D_* is a function of grain size through the profile parameter A. A smaller value of D_*, occurring for finer grain size,

corresponds to a flatter equilibrium beach profile, thus requiring more sand to be moved before equilibrium is attained In the model, a modification of the A values (Table 3-2) is made (Eq 3 34) to account for the wave effects on equilibrium beach profile. Figure 5-16 illustrates the influence of varying equilibrium energy dissipation on eroded volume. The three A values are 0 119 $m^{1/3}$ from Table 3-2, 0.136 $m^{1/3}$ calculated from Eq.3.33, and best-fit value of 0 114 $m^{1/3}$ in the fitting process of Section 3.2.4.

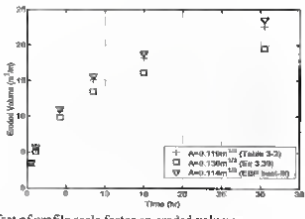

Figure 5 16 Effect of profile scale factor on eroded volume

5 2.5 Influence of Wave Height and Period

The effect of an increase in wave height on beach erosion is obvious since a larger wave height involves a larger amount of wave energy for the beach profile to dissipate in a state of equilibrium and also displace the offshore boundary condition seaward The eroded volume inshore will increase significantly as wave height increased.

Figure 5 17 shows the evolution in time of eroded volume for various wave periods The model is absolutely insensitive to wave period. Although wave period appears in the roller model (Eq.3 19) and the profile scale factor modification (Eq.3 33), the effect of wave period on profile evolution is extremely small One reason may be that the linear wave theory for shallow water conditions is applied in the numerical model

However, it becomes very difficult to program an implicit solution scheme if intermediate water conditions are considered

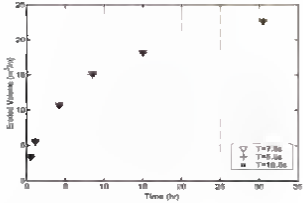

Figure 5-17 Effect of wave period on eroded volume

5.2.6 Influence of Limiting Onshore and Offshore Slopes

These slopes are introduced into the model to determine slope avalanching. Figures 5-18 and 5-19 illustrate the effects of varying limiting onshore and offshore slopes, m_{ss} and m_{sf}, on profile erosion, respectively. It shows that smaller limiting slopes causes more erosion and vice versa. However, further increasing the limiting offshore slope, the beach erosion does not change in this case. The rational is for a smaller limiting slope, more sediment need to be redistributed from the dune and beach area to reach that slope, thus causing more erosion.

5.3 Effect of Varying Water Level

Tests 901 and 911 performed in the LWT experiments were unique and focused on investigating the influence of a tide (variable water level) on profile evolution. A sinusoidal tide with amplitude of 0.45 m and a period of 12 hour was used in Test 911 whereas the water level was constant for Test 901. Figure 5-20 shows the measured profiles for the two tests after 40.3 hours of wave action. Overall, the resulting profile

shape is quite similar in the two cases, although the bar is somewhat larger for Test 911 This is probably caused by the increased possibility for the waves to erode higher up on the foreshore due to the water level variation.

This case provides an opportunity to evaluate model predictions of profile change induced by constant incident waves with a realistic variation in water level. The predicted profiles after 40 3 hours for these two tests are also shown in Figure 5-20 The predicted profile with variable water level has more erosion in the foreshore and the primary breaking bar is offshore of the bar position of the constant water level case, and a small second bar feature joint with the primary bar is also produced by the model

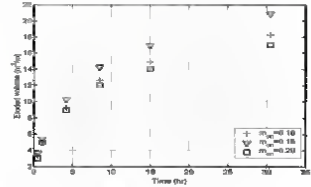

Figure 5-18 Effect of on-shore limiting slope on eroded volume.

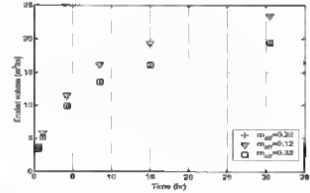

Figure 5-19 Effect of offshore limiting slope on eroded volume.

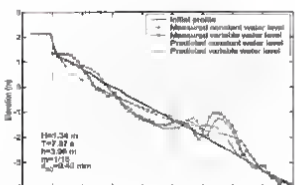

Figure 5-20 Comparison of observed and predicted profile evolution for variable water level

5.4 Initial Beach Slope Effect

Beach nourishment projects are usually constructed with an initial plane beach slope. According to Dean's equilibrium beach profile theory, the profile with an initial slope steeper than the equilibrium slope will cause beach erosion and shoreline recession. On the other hand, an initial mild slope will result in beach accretion and shoreline advancement. The model is tested here to investigate the final equilibrium profile shape with regard to different initial plane slopes. The wave conditions and sediment size are held constant (H = 1.12 m, T=7.5 s, h=4.5 m and d_{50} = 0.27 mm). The four slopes tested are 1/4, 1/10, 1/50, and 1/100, respectively. Figure 5-21 compares the predicted final profiles after 1000 hours of constant wave action. Accretionary profiles are produced from the mild initial slopes (1/100 and 1/50), while erosive profiles are generated from the steep initial slopes (1/10 and 1/4). The final profiles have the same slopes to the bar crests, which indicates that the initial slope has no effect on the equilibrium profile shape, but determines the transport direction. The slopes in beach nourishment projects usually range from 1:20 to 1:10.

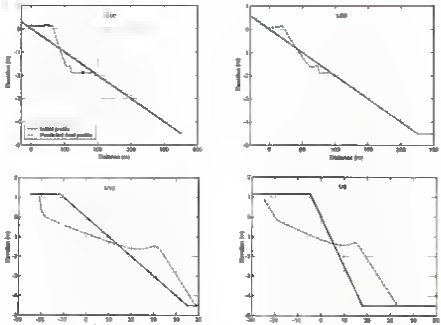

Figure 5-21 Comparisons of equilibrium beach profile for different initial beach slopes.

5.5 Summary of Model Evaluation

The model results (n = 2) with the fixed average K value were compared with those with individual best-fit K values for the eleven large-scale wave flume experiments used for calibration. The deviations between the fixed K value and best-fit K values are found to be very small (below 10% in 10 out of eleven cases).

The model is somewhat sensitive to most of the model parameters. One exception is the input wave period, to which the model is not sensitive at all. The varying water level (such as tide, storm surge) on profile evolution can be represented by the model. It is also found that the initial beach slope has no influence on the equilibrium beach profile shape, although it affects the sediment transport direction. This is expected since this is a closed loop model and should converge to a target profile.

Overall, the cross-shore model with a nonlinear transport relationship (n = 2) has the capacity to generate bar features as well as accretionary profiles. It performs reasonably well for beach erosion in both regular and irregular waves. In the next chapter, more large-scale laboratory data as well as some field data are applied to further test and demonstrate the model applications

CHAPTER 6
MODEL APPLICATION

In this Chapter more large-scale laboratory experiment data and field data are employed to examine the performance of the cross shore model which has been developed. Comparisons with predictions of SBEACH and CROSS models are also included.

6.1 Laboratory Experiments Studies

Measures of model performance used for analysis of laboratory experimental data are based on the statistical fit of the calculated profiles to the measured profile for a given simulation. The residual parameter, Res, used by Zheng and Dean (1995), provides a relative measure of the difference between the measured and calculated profiles as compared to the amount of actual change that has occurred over a given range of the profile. The residual parameter is given by:

$$Res = \frac{\sum_{j=1}^{N_p} (h_{pj} - h_{mj})^2}{\sum_{j=1}^{N_p} (h_{ij} - h_{mj})^2} \qquad (6.1)$$

where h is the profile elevation, N_p is the number of points across the profile, the subscripts "p", "m" and "i" denote predicted, measured and initial, respectively. Smaller values of Res correspond to a better fit. The minimum possible value of Res is zero, which indicates a perfect simulation. If no changes occurred, the value of Res is 1. Bar generation and migration are of primary interest in the laboratory experimental results. So just SBEACH model is used here to compare with the current model.

6.1.1 SUPERTANK Project

6.1.1.1 Background

The SUPERTANK project was carried out in August and September 1991 at the O. H. Hinsdale Wave Research Laboratory, Oregon State University (Kraus and Smith, 1994). SUPERTANK was a multi-institutional effort to obtain detailed information on beach profile response to waves with special emphasis on surf and swash zone processes. The project generated an extensive data set consisting of wave transformation, velocities, profile surveys, and sediment transport across the profile for a large number of test cases.

The channel used in the SUPERTANK project was 104 m long, 3.7 m wide, and 4.6 m deep. A digitally controlled hydraulic wave generator capable of generating random or monochromatic waves was located at one end of the tank. The wave generator faced a 76-m beach profile constructed of 600 m^3 of sand. Sand for the profile was obtained from the Oregon coast and had a median grain size of 0.22 mm. Data collected during the SUPERTANK study were gathered by a dense array of wave gauges, current meters, sediment concentration profilers, pressure gauges, video cameras, and other instruments. A summary of the data sets collected at SUPERTANK is provided by Smith and Kraus (1995). During the project, waves were run for fairly short periods (e.g. 10, 20, 40, or 70 min) in order to avoid leaching in the tank and to keep the amount of data collected at a manageable level. Random waves with broad- and narrow-banded spectra were run with zero-moment wave heights in the range 0.2-1.0 m and with peak spectral periods in the range 3-10 s.

The test conditions investigated in the present study are summarized in Table 6-1. The developed model with the recommended K values and other default parameters is applied to these tests, and the results are compared to those predicted by SBEACH.

(version 2 0) The default value for the transport coefficient in SBEACH is 1.75×10^{-6} m^4/N and other input parameters are also taken as the suggested default values.

Table 6-1 Summary of the tests conditions in the SUPERTANK project.

Test No	Description	Wave height H_{mo} (m)	Wave period T_p (s)
ST_I0	Equilibrium erosion (random)	0 8	3 0
ST_G0	Equilibrium erosion (monochromatic)	0.8	3.0
ST_J0	Narrow mound	0 7	3 0
ST_K0	Broad mound	0.7	3 0

6 1.1.2 Equilibrium erosion (random waves)

The equilibrium erosion cases were the first tests performed during SUPERTANK. The initial profile was a planar beach and was subjected to varying wave conditions including both random and monochromatic waves. The first few equilibrium tests produced significant erosion at the foreshore and developed an offshore bar. During later tests, the amount of erosion decreased as the profile approached an equilibrium shape.

Figure 6 1 shows the initial, measured and calculated profiles for the first case, P1A. The test resulted in removal of material from the upper profile and deposition in an offshore bar. Although the calculated results from both models show similar trends compared to the measurements, both models overpredict the amount of erosion at the foreshore. Offshore movement of the bar is overestimated. The current model predicts the bar-trough system, whereas SBEACH does not.

6 1 1.3 Equilibrium erosion (monochromatic waves)

Figure 6-2 shows model results for an equilibrium erosion case involving monochromatic waves. For this case both models overestimate the amount of foreshore erosion. The location of the bar is fairly well produced, although details of the bar and

trough development are not predicted SBEACH predicts better bar generation than the current model

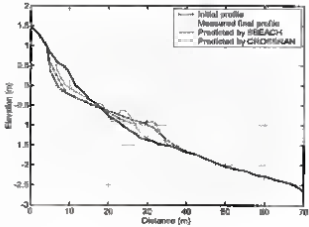

Figure 6-1. Result of model simulation, SUPERTANK P1A.

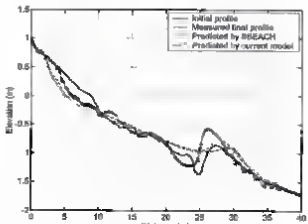

Figure 6-2 Result of model simulation, SUPERTANK PGA.

6.1 1.4 Narrow-crested mound

For this set of test cases, a narrow-crested mound was constructed in the offshore region of the profile. Wave breaking at the mound caused a significant amount of energy dissipation, reducing the amount of incident wave energy that reached the foreshore

Tests were run with both random and monochromatic waves. Figure 6-3 shows the results for the random wave case, PJA. Waves in this test produced significant erosion at the mound. Erosion was greater on the shoreward side of the mound with some sediment being transported down the shorsward-facing slope. Both models overestimated the mound erosion. SBEACH predicted the entire mound crest being uniformly lowered.

Figure 6-4 shows the results for the monochromatic wave test, PJC. The uniform breakpoint of the monochromatic waves produced an increase in elevation of the mound crest corresponding to the formation of an offshore bar. A nearshore bar also formed from deposition of eroded foreshore sediment. In contrast to the observed profile changes, SBEACH predicts little change in shape of the offshore mound and no inshore bar. The predicted profile by the current model has large change in the mound, with most of sediment being transported onshore, and the location of the predicted nearshore bar is situated farther offshore than the measured bar.

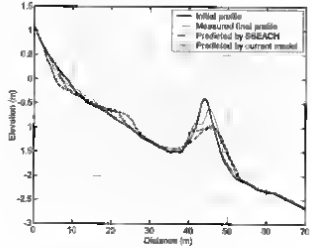

Figure 6-3 Result of model simulation, SUPERTANK PJA.

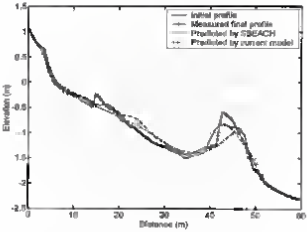

Figure 6-4 Result of model simulation, SUPERTANK PJC

6 1.1.5 Broad-crested mound

This test was similar to the previous test, except that more sand was added to create a wider mound in the offshore to examine the effect of mound width on wave dissipation

As shown in Figure 6 5, the random wave test case PKA produced a trough at the offshore end of the mound, with material being deposited on the offshore slope of the mound Little profile change was observed elsewhere. The SBEACH simulation erodes the entire mound with most of the eroded material being deposited across the offshore slope of the mound As a result of the lower mound height, the SBEACH simulation allowed more wave energy to reach the foreshore, causing erosion to be overestimated at the foreshore The current model also predicts entire mound erosion, but approximately half the material from the mound is transported onshore to build up the foreshore portion of the profile Little foreshore erosion is predicted by the current model.

The monochromatic wave test (case PKC) produced a trough on the offshore end of the broad-crested mound and reduced the height of the entire mound crest, as observed in Figure 6-6 The sediment removed from the mound was deposited in a bar at the offshore

end of the mound crest. SBEACH produces slightly more lowering of the mound than was observed, and formation of a bar at the offshore end of the mound is predicted, but the observed trough is not produced. Similar to the random wave case, the current model overpredicts the mound erosion and onshore transport of the eroded material from the mound crest.

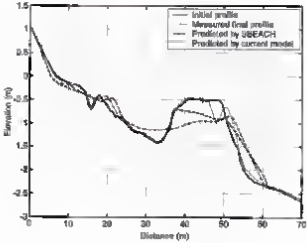

Figure 6-5 Result of model simulation, SUPERTANK PKA

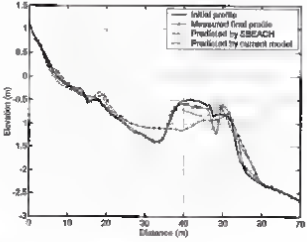

Figure 6-6 Result of model simulation, SUPERTANK PKC

Figure 6-7 presents the calculated residuals for the SUPERTANK selected cases From the results the predicted profile changes under both monochromatic and random waves have some differences from the laboratory measurements, especially during the offshore mound tests. Some wave generated sediment transport mechanisms are not understood nor included in both numerical models such as wave plunging, sediment advection and diffusion near the breaking point. The residuals of current model are almost the same as SBEACH in P1A, PGA and PJA cases, but have larger values in PJC, PKA and PKC cases due to more overprediction of mound erosion

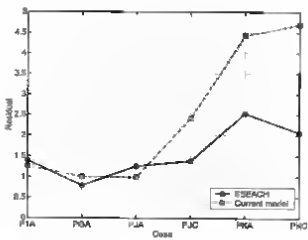

Figure 6-7. Residuals for SBEACH and current modal SUPERTANK experiments.

6.1.2 LIP 11D Delta Flume Experiments

6.1.2.1 Background

In spring of 1993 from April to June, within the framework of the European Large Installation Plan (LIP), detailed measurements of hydrodynamics and sediment transport in the surf zone were undertaken in the Delft Hydraulics Delta Flume. The tests (code 11D and thus denoted LIP 11D) were designed and overseen by researchers from the universities of Catalunya, Liverpool, Padova and Thrace. The objective of the

experiments was to generate high-quality and high resolution data on the hydrodynamics and sediment transport dynamics of a natural 2DV beach under equilibrium, erosive and accretive conditions. Special attention was paid to long wave effects and near bottom resolution. A first overview of the experiments is presented in Arcilla et al. (1994). The data have been reported by Roelvink and Reniers (1995).

Two initial beach geometries, starting with a near-equilibrium Dean-type beach without (Test 1) and with the presence of a low dune (Test 2), using a median grain diameter of 0.22 mm, were used in the project (Figure 6-8). The dune foot was located just above the still water level to investigate the effect of upper boundary condition on the profile development. For each of these two geometries the following three wave conditions were tested: slightly erosive, highly erosive and strongly accretive. Narrow-banded random waves with a JONSWAP spectrum were chosen such that the combination of wave steepness at peak frequency, bottom slope and water level would result in a stable, erosive and accretive beach consecutively. During each of these stages, the water level and wave conditions were kept constant. This sequence of conditions could be interpreted as a schematization of the natural development of a storm, represented by the different sea states. The duration (number of wave hours) of each state was determined by the test duration and number of possible wave hours per day, but was chosen to be at least long enough to obtain accurate sediment transport estimates from the profile measurements. A summary of all test conditions is presented in Table 6-2, in which incident wave heights, periods, water levels and durations are described.

6.1.2.2 Test 1 (without dune)

Under the first wave condition (1a), the initial profile changes into a mildly barred profile (Figure 6-9). The sediment transport within the surf zone is predominantly

offshore directed, while the sediment transport is directed onshore outside the surf zone During the highly erosive wave condition (1b), the bar region becomes more pronounced and at the same time the bar is moving offshore, as shown in Figure 6-10 During the accretive wave condition (1c), the bar crest becomes more pronounced, now propagating in the onshore direction (Figure 6-11). The profile changes in the trough and swash zone are small compared to the two previous conditions

SBEACH predicts foreshore erosion in all three cases but no bar is formed. However, the sediment transport direction predicted by the current model in the foreshore region is predominantly onshore for all wave conditions. The reason is that the initial profile slope is milder than the anticipated equilibrium beach profile slope (Eq 3 31), thus causing onshore sediment movement according to the EBP concept

Table 6 2. Summary of test conditions in LIP 11D project.

Test code	Initial geometry	H_{mo} (m)	T_p (s)	Water level (m)	Duration (hr)
1a	Dean-type	0 9	5	4 1	12
1b	Result of 1a	1 4	5	4 1	18
1c	Result of 1b	0 6	8	4 1	13
2a	Dean type with dune	0 9	5	4 1	12
2b	Result of 2a	1 4	5	4 1	12
2c	Result of 2b	1 4	5	4 6	18
2c	Result of 2c	0 6	8	4.1	21

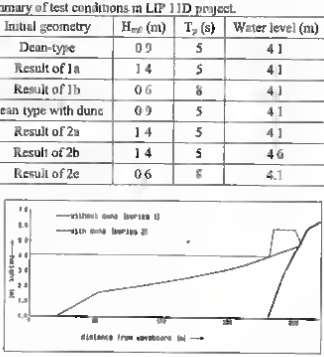

Figure 6-8 Initial beach geometry of LIP 11D experiments (Roelvink and Reniers, 1995)

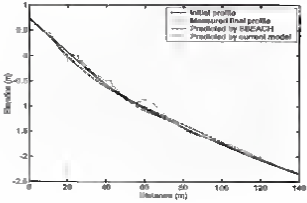

Figure 6-9 Result of model simulation, LIP 11D Test 1a.

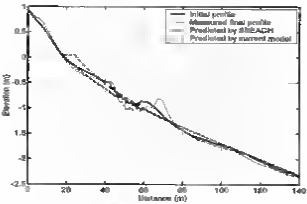

Figure 6-10 Result of model simulation, LIP 11D Test 1b

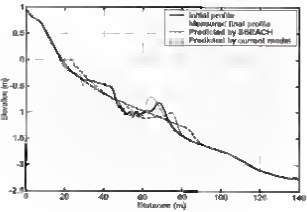

Figure 6-11 Result of model simulation, LIP 11D Test 1c.

6.1.2 3 Test 2 (with dune)

The observed and predicted profile evolutions in the case with a low dune are presented in Figures 6-12 to 6-15 Starting with the mildly erosive wave conditions, the measured changes in the bottom profile are similar to the case without the dune. During the highly erosive wave condition of Test 2b the bar feature grows while moving offshore Increasing the water level (2c) results in a strong attack on the low dune, resulting in significant changes in the bottom profile A second bar develops closer to the shore whereas the outer bar decreases in amplitude and progresses in the onshore direction. Lowering the water level to its original position and using an accretive wave condition (2c) rebuilds the outer bar and diffuses the inner bar

As in Test 1, beach erosion in the foreshore is predicted by SBEACH model in all four cases and a flat profile shape is generated The current model also predicts almost flat profiles in 2a and 2b tests, with some dune erosion occurring due to the slope adjustment in the model There are two bars reproduced by the current model in case 2c. But the bar positions are offshore of those observed The model predictions in Test 2c are similar to those for Test 1c

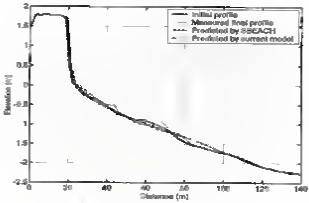

Figure 6-12 Result of model simulation, LIP 11D Test 2a.

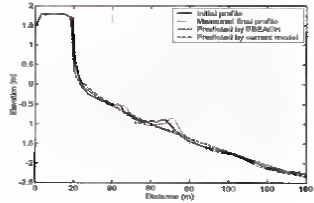

Figure 6-13 Result of model simulation, LIP 11D Test 2b

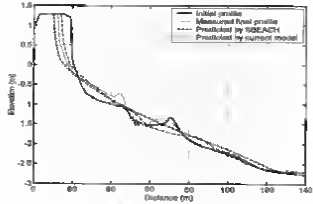

Figure 6-14 Result of model simulation, LIP 11D Test 2c.

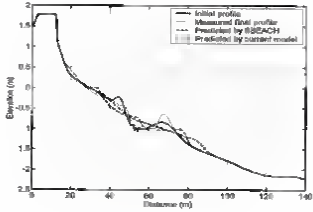

Figure 6-15 Result of model simulation, LIP 11D Test 2c

Figure 6-16 shows the residuals of the model prediction for all tests in LIP 11D experiments. The residuals of SBEACH and CROSS are almost the same except in Test 2a for which the SBEACH residual is the smaller of the two. However, the transport is in opposite direction during the tests without dune.

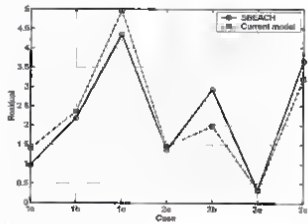

Figure 6-16. Residuals for SBEACH and current model, LIP 11D experiments

6.2 Field Studies

Profile response at the foreshore and dune is important in engineering applications of numerical models, where model estimates of erosion are used to determine the storm effects on structures and properties adjacent to the shoreline. Thus, measures of model performance for field cases focus on its capabilities to predict the response of the dune and foreshore after storms. These measures investigated in this study include volume change at the foreshore and recession of a special contour.

Volume change at the foreshore is computed as the net gain or loss in volume per unit beach width above some specified elevation. In this study, the National Geodetic Vertical Datum (NGVD) is used as the reference elevation. Contour recession provides information on how well a model predicts the erosion of a dune or berm and the loss of

beach width resulting from a storm A representative beach contour located between the reference elevation (NGVD) and the dune crest is selected for each field case. Recession of the selected contour from its initial position on the profile is determined from the measured data and compared with simulation results. In addition, the residual error (Eq 6 1) between measured and predicted profiles is also investigated.

Field cases selected for this study are based on the availability of data records of beach profile surveys, wave and water level information, and sediment grain size information. The most recognized and applied field data set in the literature is Ocean City, Maryland (a series of storms from October 1991-January 1992) (Stauble et al , 1993) The profile changes after Hurricane Eloise 1975 and Hurricane Opal 1995 in the Panhandle Coast of Florida are also investigated.

6.2-1 Ocean City, Maryland

6.2 1 1 Background

Ocean City, MD, is located on Fenwick Island, a north-south oriented sandy barrier Island of the central Delaware-Maryland-Virginia coast. The island extends from Indian River Inlet, Delaware, on the north to Ocean City Inlet on the south and is backed by Isle of Wight and Assawoman Bays The Ocean City beach was nourished by the state of Maryland in 1988, and the Federal Government in 1990 and 1991 to protect the city against storm damage (Stauble et al , 1993) The project layout is shown in Figure 6-17. Both projects were constructed from beach-quality material taken from Borrow Areas 2 and 3. The representative grain sizes from Borrow Areas 2 and 3 are 0 25 mm and 0 35 mm, respectively The fill constructed by the State of Maryland consisted of approximately 2 7 million cubic yards (2 1 million cubic meters) of material placed along

the entire project area. The total amount of material placed in the Federal project was 3 8 million cubic yards (2 9 million cubic meters)

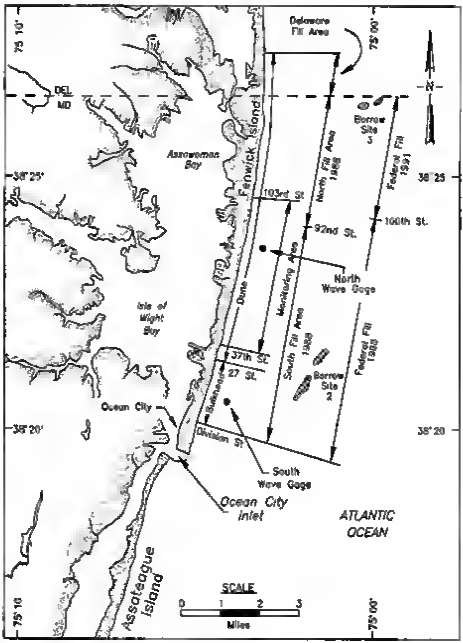

Figure 6-17 The Ocean City beach nourishment project layout (Stauble et al , 1993)

From late October 1991 to early January 1992 after the project, the beach at Ocean City was impacted by a series of severe storms. The series of storms, which included the October 30, 1991 "Halloween storm", November 11, 1991 storm, and January 4, 1992 storm, caused extensive erosion of the constructed foreshore and dune at Ocean City. As part of the project monitoring effort, beach profile data at ten locations along the shoreline were collected which enabled the analysis of the erosional effects of the series of storms. The wave height, wave period and storm surge time history were measured by two gages located directly offshore of Ocean City in a water depth of 10 m. Water depths and profile elevations used are referenced to NGVD, which lies 0.02 m below mean water level for Ocean City.

Six survey lines located at 37th, 45th, 56th, 63rd, 74th, and 103rd Streets have both pre-storm and post-storm measured profiles available and are simulated in this study for all three major storms. In the analysis of the profile changes, the net volume gained or lost between surveys are quite different from zero, which is considered to be due to gradients in longshore sediment transport. To remove this effect, each post-storm profile is adjusted by shifting the profile horizontally a distance Δy to yield zero net volume change (Zheng, 1996, Zheng and Dean, 1997). The value of Δy is calculated by

$$\Delta y = \frac{1}{h_{total}} \int_{y_0}^{y_m} (h_{mb} - h_{ma}) dy \tag{6.2}$$

where subscripts mb and ma denotes profile elevation measured before and after storms, respectively, y_0 and y_m are the offshore distance coordinates at the baseline and offshore profile change limit, respectively, and h_{total} is the total elevation of the active post-storm profile. The sign of Δy is positive for a seaward translation.

Based on results of sediment analyses performed during the monitoring program, a median sediment grain size of 0 35 mm is selected as a representative value for all beach profiles in the numerical simulation

6.2 1.2 Halloween storm

The northeast storm of October 29 – November 2, 1991 (the "Halloween Storm") produced high waves and water levels at Ocean City, with a peak significant wave height of about 3 m and a peak water elevation of about 1.5 m NGVD. Figure 6-18 shows the measured significant wave height, peak spectral wave period and storm surge time histories for this storm. Pre-storm profiles were collected in June 1991 and post-storm surveys were performed shortly after the storm. The June surveys were assumed to adequately represent the conditions of the upper beach profiles prior to the storm, as no other significant erosion events occurred between June and October. Table 6-3 presents the net volume change per unit beach width calculated between surveys for each profile and the corresponding beach shifting adjustment calculated from Eq 6 2. Five profiles exhibited a net loss of material while one profile (103rd Street) gained material.

The model predictions with default input parameters for SBEACH, CROSS and current model are presented in Appendix B for all six profiles. Figures 6-19 and 6-20 show one example of the comparison of the calculated results for the profile at 63rd street with the original and shifted profile, respectively. Good agreement is obtained above the NGVD datum. Below datum, the measured profile exhibits a convex shape with a nearshore step, whereas the calculated profiles by all three models show more concave shape with a bar situated offshore by SBEACH and the current model. The measured beach step may be attributed to beach recovery prior to the surveys during the waning storm conditions, an effort not included by the models.

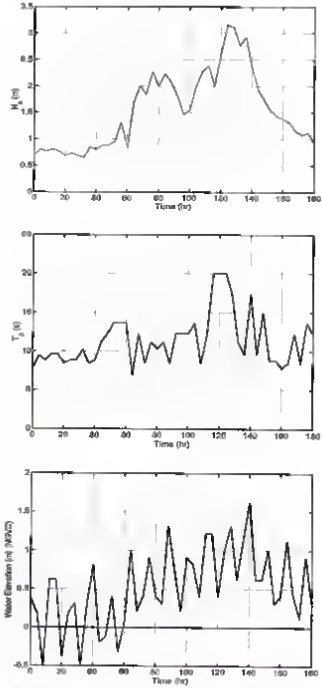

Figure 6-18 Significant wave height, peak wave period and water level time history for the Halloween 1991 storm, Ocean City, MD (Stauble et al , 1993)

Table 6-3 Measured volume changes during the Halloween storm and adjustment Δy

Street No	Volume change (m^3/m)	Adjustment Δy (m)
37th	-59 445	4 766
45th	-75 055	6 237
56th	-47 160	3 801
63rd	-38 539	3 159
74th	-59 611	4.997
103rd	99 197	-7 687

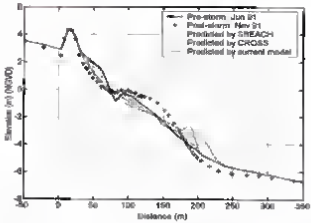

Figure 6-19 Comparison of calculated and original measured profile of the Halloween storm for the profile at 63rd street, Ocean City, MD

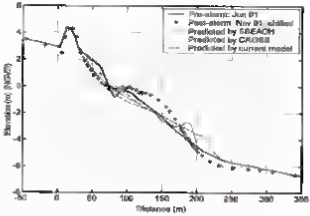

Figure 6-20 Comparison of calculated and shifted measured profile of the Halloween storm for the profile at 63rd street, Ocean City, MD

Figures 6-21 to 6-23 compare volume changes above NGVD, recessions of +1.5 m contour, and residuals for the measured and simulated profiles for each profile (street), respectively. In the figures, "without adjustment" means data given by the original measured post-storm profiles, while "with adjustment" means data resulting from horizontally shifted post-storm profiles. The calculated volume changes and contour recession by all models are closer to the measured results with adjustment. On average, the current model results are similar to those by SBEACH. Some differences between SBEACH and the current model may be due to the current model not including sediment transport in swash zone and overwash, which are incorporated in SBEACH model. The residuals by CROSS are smaller than the other two models which may be interpreted that CROSS has the better overall profile prediction. However, after examining the calculated profiles, it is believed that the major differences are caused by the offshore profile shape predictions. CROSS cannot produce bars and generates a flat offshore profile, which occurs in the measured profiles in coincident due to beach recovery. The largest residual discrepancy is at the 56th street, where CROSS predicts minor profile changes while SBEACH and the current model have beach erosion at the pre-storm nearshore step area and deposition offshore.

6.2.1.3 November-January storms

The November-January (NJ) storms include the November 11, 1991 storm and the January 4, 1992 storm, with the measured significant wave height, peak wave period and storm surge level shown in Figures 6-24 and 6-25, respectively. In this case, these two storms are combined together in the simulation because no beach profile measurement data are available between these two storms.

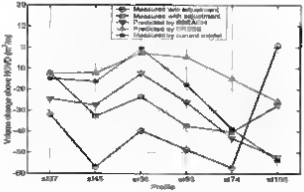

Figure 6-21 Comparison of measured and simulated volume change above NGVD for the Halloween storm, Ocean City, MD

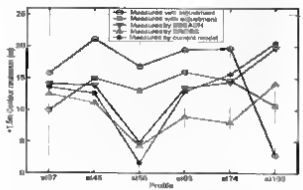

Figure 6-22 Comparison of measured and simulated recession of the +1.5m contour for the Halloween storm, Ocean City, MD

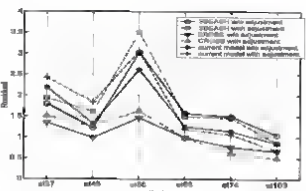

Figure 6-23 Residuals for SBEACH and current model for the Halloween storm, Ocean City, MD

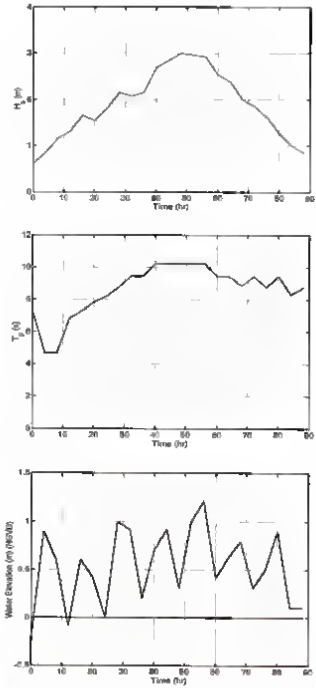

Figure 6-24 Significant wave height, peak wave period and water level time history for the November 1991 storm, Ocean City, MD (Stauble et al., 1993)

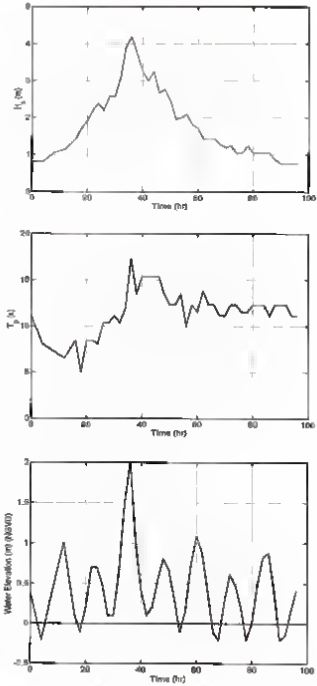

Figure 6-25 Significant wave height, peak wave period and water level time history for the January 1992 storm, Ocean City, MD (Stauble et al , 1993).

As observed in the figures, high waves and water levels lasted approximately 3 days for both storms. The November storm had a peak significant wave height of about 3 m and water elevation of about 1 2 m NGVD The January storm is much more severe, with a peak wave height and water level of 4 m and 2 m NGVD, respectively The meteorological characteristics of the January 1992 storm contrast significantly with those of the Halloween Storm. Whereas the Halloween Storm was a very large, slow-moving maritime winter cyclone, the January storm was a small, rapidly developing, fast-moving event (Stauble et al , 1993)

The beach profiles measured after the Halloween storm served as pre-storm profiles for the NJ storm set. Beach surveys performed shortly after the January storm provided post-storm profiles for comparison with model results. Table 6-4 presents the net volume change per unit beach width calculated between surveys for each profile and the corresponding beach shifting adjustment after the NJ storm. A large gain in material was observed on profiles at 37th and 103rd street, whereas volume was conserved reasonably well on the other profiles.

Measured beach response to the NJ storm series shows that four of the six profiles experienced overwash of the dune, and SBEACH produces dune overwash in each of the four cases, whereas CROSS and the current model do not. Figures 6-26 and 6-27 illustrate the comparison of simulated results for the profile at 63rd street with original and shifted profiles, respectively. It is noted that although substantial erosion occurred at the dune, erosion on the lower foreshore profile was minimal A berm above NGVD was developed on the profile Profiles at 45th, 74th and 103rd street demonstrated similar features.

Table 6-4 Measured volume changes during the NJ storm and adjustment Δy

Street No	Volume change (m^2/m)	Adjustment Δy (m)
37th	136 853	-10 860
45th	36 6162	-3 155
56th	-15.365	1 230
63rd	-4.221	0 367
74th	3.513	-0 323
103rd	91 420	-7 517

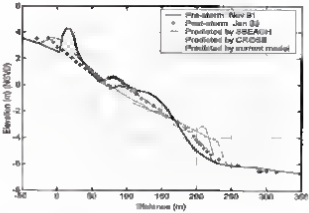

Figure 6-26. Comparison of calculated and original measured profile of the NJ storm for the profile at 63rd street, Ocean City, MD

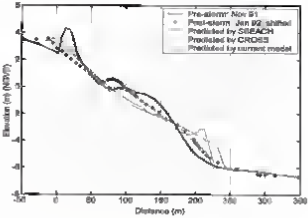

Figure 6-27. Comparison of calculated and shifted measured profile of the NJ storm for the profile at 63rd street, Ocean City, MD

Volume changes above NGVD, recessions of +1.5 m contour, and residuals of profile changes are presented respectively in Figures 6-28, 6-29 and 6-30 for the NJ storm. As for the Halloween storm case, the current model predictions are similar to SBEACH results and the differences could be improved by incorporating swash zone transport and overwash into the model. Little change is observed across the entire subaerial at the 56th street profile in both observed and predicted results by SBEACH and CROSS which is indicated by volume change and contour recession. The current model predicts some onshore sediment movement from the pre-storm profile near NGVD and thus has volume accretion and contour advancement above NGVD. Contour recession is underpredicted by all three models at the 63rd and 74th streets, which are located in the area of the erosional hotspot (Wise et al. 1996). The better residual results from CROSS are believed to be the same reason as mentioned for the Halloween storm.

6.2.2 Panhandle Coast of Florida

Several severe storms have struck the Panhandle Coast of Florida (Figure 6-31) the past century. Here beach erosion caused by Hurricanes Eloise and Opal are examined.

6.2.2.1 Hurricane Eloise

Background. Hurricane Eloise continuing its strengthening after sweeping over the Dominican Republic, Cuba, and adjacent waters, and regaining its hurricane force on the morning of September 22, 1975 in the central Gulf of Mexico about 300 nautical miles south of New Orleans, struck the Florida northwest coast in the early morning of September 23, 1975. Its center crossed the shoreline about midway between Fort Walton Beach in Okaloosa County and Panama City Beach in Bay County at a forward speed of better than 20 knots towards the northeast. Hurricane Eloise was classified 3 on a scale of 5 by the National Hurricane Center.

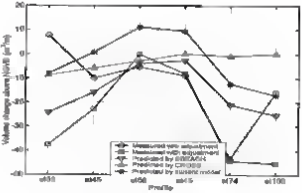

Figure 6-28 Comparison of measured and simulated volume change above NGVD for the NJ storm, Ocean City, MD

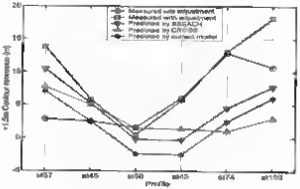

Figure 6-29 Comparison of measured and simulated recession of the +1 5m contour for the NJ storm, Ocean City, MD

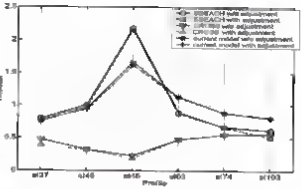

Figure 6-30 Residuals for SBEACH and current model for the NJ storm, Ocean City, MD

Hydraulic conditions Hurricane Eloise was a rapidly moving storm, lasting less than 20 hours There are no open coast storm surge measurements available. Numerical estimates ranged from 8 4 feet (2 56 m) at the western end of Walton County to 9 6 feet (2 93 m) at the eastern end of the county (Kriebel, 1986) Figure 6-32 shows the predicted storm surge hydrograph near the western end of Walton County used by Kriebel (1986) to verify his dune erosion model The storm surge at other sites was determined by multiplying a constant over the surge hydrograph in Figure 6-32 for each profile A representative significant breaking wave height of 12 feet (3 66 m) and peak period of 11 seconds were used in Kriebel (1986)

Figure 6-31 Panhandle Coast of Florida (Leadon et al , 1998)

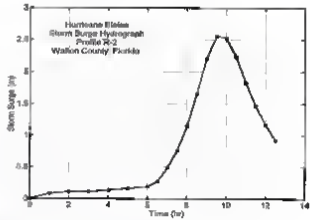

Figure 6-32 Estimated storm surge hydrograph near the western end of Walton County for Hurricane Eloise (reproduced from Kriebel 1986)

Profile response Under the Florida Coastal Construction Setback Line Program, the coastal areas primarily affected by Hurricane Eloise in Bay, Walton and Okaloosa Counties were surveyed in October 1973, with beach dune profiles at approximately every 1000 feet, and offshore soundings every 3000 feet Post-storm surveys were conducted within 2-4 weeks after the storm in October 1975 in Walton County

The entire Walton County had suffered severe beach-dune erosion during the storm However, the measured profiles showed that there was great variability in pre-storm profile forms and in storm erosion response of individual profiles In areas where the beach was wide with gentle slope and gradually merged into the dunes, there was little erosion, whereas in the neighboring areas with steeper beach slope and rapid dune rise, severe erosion took place Such instances indicate that gradual wave energy dissipation reduces the erosion potential on the beach. Also over 20 profiles showed a net gain of sand between the two available surveys Such variability in profile response can be attributed in part to three sources of uncertainty: (1) pre-storm profile modification between October 1973 and Hurricane Eloise, (2) localized longshore transport effects during the storm, causing areas of local accretion and accentuated erosion, and (3) non-uniform beach recovery between the storm and the post-storm surveys A sand ridge near and above the mean sea level on the post-storm profiles in Walton County was found to be about 1 5-2.5 feet (0 46-0 76 m) high and 50 feet (15 m) wide On average 50 ft^3/ft ($4.7m^3/m$) had returned to the beach face prior to the post storm survey (Chiu, 1977) No offshore bar was formed on the post-storm profiles which may be because the storm was so fast-moving that there was not enough time to form the bar or a barely formed bar was eliminated by waves between the storm and the survey

Numerical simulation A reference profile, line R-41, which has been used in other dune erosion verification studies (Hughes and Chiu 1981, Vellinga 1983, Kriebel 1986), is chosen to investigate the model performance on Hurricane Eloise. Due to lack of offshore profile measurement, the pre-storm profile is constructed as in Kriebel (1986) above NGVD, the actual measurement is applied, offshore, a $Ay^{2/3}$ profile is assumed. The scaling parameter A, based on the effective grain size of 0.262 mm, is 0.184 $ft^{1/3}$ (0.123 $m^{1/3}$). The hydraulic conditions of Kriebel (1986) are also adopted

The pre-storm and post-storm profiles are shown in Figure 6-33. All three models underestimate the dune erosion substantially. The above-mentioned first two factors in profile response may explain the extra measured erosion.

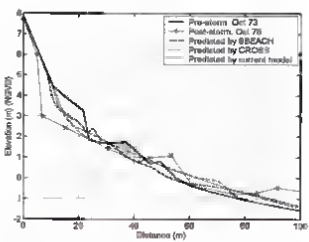

Figure 6-33. Comparison of calculated and measured profile of the Hurricane Eloise for the profile at R-41, Walton County, FL

6.2.2.2 Horricane Opal

Background Hurricane Opal, which struck the Panhandle Coast of Florida on October 4, 1995, was one of the most severe hurricanes to impact Florida during the past century. Opal reached category 4 status as it approached landfall on October 4, 1995

with maximum sustained surface winds reaching 150 mph Hurricane Opal caused more structural damage along the Florida coast than all hurricanes and tropical storms combined since 1975 Severe damage occurred across the entire Panhandle region with coastal flooding extending along the central Florida Gulf coast region southward all the way through Key West

Hydraulic conditions. There were several NOAA stations that recorded data as Opal passed through the Gulf and onto land (Figure 6-34). Wave data collected at the offshore buoy station 42036, which is nearest to the Florida coast, is shown in Figure 6-35 The data at this station shows the dramatic increase in wave height and dominant wave period as Opal traveled across the Gulf, even though Opal's track was quite a significant distance west of this station.

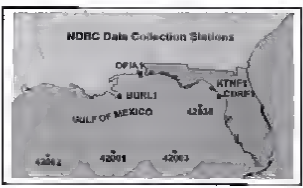

Figure 6-34. NOAA data collection stations that recorded Opal data (Leadon et al., 1998)

Storm surge data obtained from a National Ocean Survey tide gage located on the Panama City Beach Pier (near Monument line R-40) is shown in Figure 6-36 The peak storm surge elevation is shown at +2.53 m above the NGVD datum The tide gage collected this data near the seaward end of the pier several hundred feet seaward of the shoreline. A storm surge model estimated a peak storm surge at the shoreline to be from +3 7 to +4 9 m (NGVD) (Leadon et al., 1998) which is consistent with a number of high

water marks surveyed in the Panhandle by FDEP staff and other surveyors following Opal

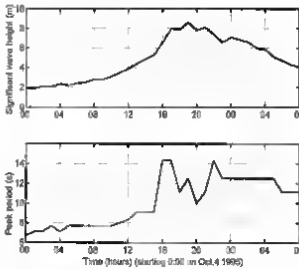

Figure 6-35 Wave data at NDBC buoy 42036 during passage of Opal (data from NDBC website www.ndbc.noaa.gov)

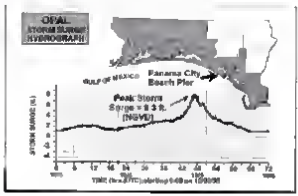

Figure 6-36 Storm surge hydrograph for Hurricane Opal at Panama City Beach (Leadon et al., 1998)

Beach and dune erosion Hurricane Opal's substantial storm surge and breaking waves severely eroded the beach and dune system throughout the Panhandle Coast Beach erosion resulted in a significantly lower beach and a shoreline that retreated

landward Areas of high, continuous dunes experienced substantial recession while in areas with lower dune topography experienced dune overtopping in which sand material was transported inland as overwash

Beach and offshore profile data were collected by the Bureau of Beaches and Coastal Systems, FDEP, in March of 1995 in Bay County and in June of 1995 in Walton County The post-storm beach and dune profiles data were collected in October 1995, in many cases within 4-5 days of Opal's October 4th landfall In addition, the Mobile District of the U S Army Corps of Engineers obtained a high-resolution bathymetric survey of the offshore region in the vicinity of their planned beach restoration project at Panama City Beach (unfortunately these data are unavailable) Typical examples of profile comparisons for Bay County which include the offshore survey are presented in Figure 6-37 (original Figures 43 and 44 in Leadon et al. 1998) The detailed analysis of beach and dune erosion and structural damage along the Panhandle Coast after Hurricane Opal are given by Leadon et al (1998)

Numerical simulation Several profiles from Panama City Beach in Bay County are selected to compare the numerical model predictions with measured profiles. The sand grain size is taken as 0 26 mm. The WIS data at Station 182 (Figure 6-38) is coupled with the storm surge information in Figure 6-36 as the input hydraulic conditions. Figures 6-39 and 6-40 show two examples of the results from profile R-21T and R-41, respectively As in the Hurricane Eloise case, all three models underestimate the dune erosion substantially The outer bars on the pre-storm profiles are not totally eroded by SBEACH and the current model However, in the observed profile shown in Figure 6-37 for R-21T, the original bar was totally smoothed out by the storm.

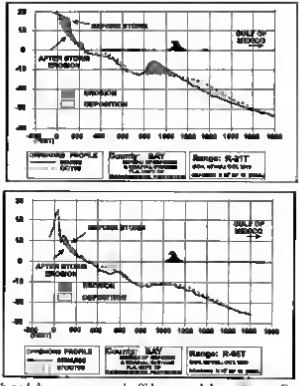

Figure 6-37 Beach and dune erosion and offshore sand deposition in Bay County after Hurricane Opal 1995 (Leadon et al., 1998)

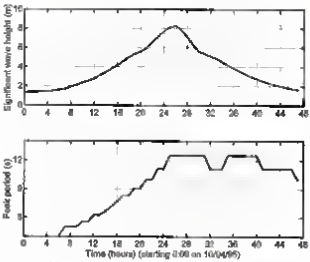

Figure 6-38 Wave conditions of Hurricane Opal for model application in Bay County (data from WIS website http://frf.usace.army.mil/wis/)

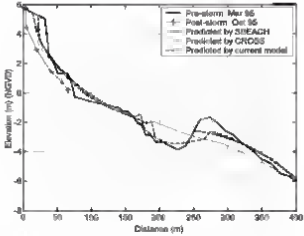

Figure 6-39 Comparison of calculated and measured profiles for Hurricane Opal, profile at R-21T, Bay County, FL.

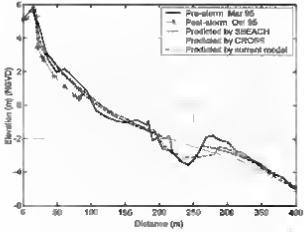

Figure 6-40 Comparison of calculated and measured profiles for Hurricane Opal, profile at R-41, Bay County, FL

6.3 Summary

This chapter has presented the model application to both controlled large-scale laboratory experiments (SUPERTANK and LIP 11D) and field data (Ocean City, MD, Hurricane Eloise and Hurricane Opal) for storm erosion, and compared the results with the profile evolution models SBEACH and CROSS. Quantities chosen to evaluate the

model performance include residual of profile change, volume change above selected elevation, and recession of a selected contour

In the laboratory experiments studies, because the focus is on the bar profile generation and migration under different wave conditions, and CROSS model could not represent bar profiles, only comparison with SBEACH and residuals of profile change are investigated. For the simulation of storm erosion at Ocean City, MD, an adjustment is made by shifting the entire profile horizontally a distance to yield zero net volume change to approximate removal of longshore sediment transport effects. This adjustment may not be appropriate for the upper beach profile and dune region because the longshore processes primarily affect the subaqueous profiles From the results, it appears that the residuals are less affected by the shifting adjustment, while the eroded volumes and contour recessions are affected more significantly by the shift. For Hurricanes Eloise and Opal, there is no profile adjustment due to lack of offshore profile measurements.

The results show that the current model with default parameters provides fairly reasonable agreement in most cases with the measurements and model results of SBEACH Both models could produce bar features offshore, although the bar crest is more pronounced in the current model than SBEACH The differences between CROSS and the current model and SBEACH are believed to be mainly due to different wave energy dissipation representations CROSS uses the simple, spilling breaker assumption inside the surf zone, while the current model and SBEACH incorporate more physically sound dissipation mechanisms. The discrepancy of volume losses of all three models on field data is believed to be somewhat mainly due to longshore transport effects during storms

CHAPTER 7
SUMMARY CONCLUSIONS AND RECOMMENDATIONS

7.1 Summary

A numerical model is developed to investigate the use of a roller model for bar generation in the nearshore region and to better represent the time history of cross-shore profile evolution. The cross-shore sediment transport relationship in the model is based on equilibrium beach profile concepts. The wave transformation model by Dally et al (1984) and the roller model by Dally and Brown (1995) are applied to predict the wave height and roller energy dissipation inside the surf zone, respectively. Profile evolution under random waves is simulated by the wave-by-wave approach which does not require assumptions of wave height distribution inside the surf zone in order to represent bar profiles, a grid system is used that can include representation of bar features readily. An implicit, double sweep scheme is adopted to solve the sediment transport and continuity equations numerically. An effort is made to account for the wave effects on equilibrium beach profiles using the fall velocity parameter (H/wT). The two unknowns in the cross-shore sediment relationship are the transport coefficient, K, and the exponent, n, in $Q = K(D - D_*)|D - D_*|^{n-1}$. Up to eleven large-scale wave flume laboratory experiments from three different facilities are incorporated to calibrate and compare the sediment transport relationships (K and n = 1, 2 and 3). The best fit transport coefficients are determined as the value yielding the overall least square error of profile changes in each case. Based on the calibration results, it is found that the non linear transport relationship

with n = 2 provides the best representation of profile evolution for monochromatic waves, a result reinforced in investigating eroded volume evolution with time. For the four irregular wave tests, n = 1 provides the best fit.

The performance of the model is evaluated by the difference between the errors of profile change predicted by the model with fixed and best-fit K values using the same laboratory experimental data as in the model calibration. The predictions of the model with fixed and best-fit K values are quite close for the eleven experiments. Sensitivity analyses are also conducted to investigate the effects of several model input parameters on the model performance. The model is then applied to other large-scale wave flume experiments (SUPERTANK and LIP 11D) and field data (Halloween storm 1991, November 1991 and January 1992 storm at Ocean City, Maryland, Hurricane Elaine and Opal at the Panhandle Coast of Florida). The model predictions are compared with two other models (SBEACH and CROSS) with default input parameters for all three models. In the Ocean City simulation, in order to reduce longshore transport effects, an adjustment is made by shifting the entire active profile horizontally a distance to yield a zero net volume change for each post-storm profile. In the Hurricane Elaine and Opal cases, there is inadequate offshore profile measurements to conduct such an adjustment. Three different measures are proposed to evaluate the agreement between measurements and predictions: residual parameter for profile change, volume change and contour recession above NGVD.

7.2 Conclusions

The present numerical model is able to simulate beach profile evolution under both monochromatic and random wave conditions. Based on the investigation conducted and results developed herein, the following conclusions are offered:

(1) The inclusion of a surface roller model with a realistic breaking wave model provides a rational basis for bar generation. The roller model captures the lag between initial wave breaking and maximum wave energy dissipation. A new equilibrium beach profile shape is developed, which can represent bar profiles.

(2) Modification of the profile scale factor to include a dependency on the fall velocity parameter (H/wT) accounts for the effects of wave characteristics on beach profile shape and provides an explanation for seasonal shoreline changes in nature.

(3) The exponent, n = 2, in the sediment transport equation provides better agreement to the laboratory data than values used in previous closed loop models (n = 1 and 3) under monochromatic waves. The determined transport relationship better represents time scales of profile evolution under different initial profile and wave conditions. The transport coefficient K of 0.93×10^{-6} m^6s/N^2 is recommended for model application.

(4) The transport relationship with n = 1 provides the best-fit to random wave tests. The reason probably is that the generated waves using the wave-by-wave approach are different than the actual wave series generated in the wave flumes, although this issue requires further investigation.

(5) The model is somewhat sensitive to most of the model input parameters with the exception of wave period. The model insensitivity to wave period may be due to the shallow water wave environment in which this model is applied. It is also found that the initial beach slope has no influence on the final equilibrium beach profile shape, although it affects the sediment transport direction and the time required for equilibration.

(6) The units of the sediment transport coefficient K, when interpreted by Froude scaling, has units of $(length)^{1/2}$. Thus when applying this model to field situations, it is advisable to calibrate the K value if possible or to consider scaling based on consideration of field and model scales.

(7) Available field data contain an unknown amount of recovery due to onshore sediment transport occurring before the post-storm surveys and some net volume changes along the profiles due to longshore sediment transport gradients.

7.3 Recommendations for Future Study

Several features of the present work merit further consideration and can be readily investigated or incorporated into the model for investigation. The profile changes between the wave set-up limit to the runup limit (the swash zone) in the model are treated to adjust the slope once the limiting slope is reached. To better represent the profile changes in this region and its subsequent effects on surf zone profile changes, the detailed swash mechanisms and the corresponding sediment transport need to be represented.

By incorporating surface roller into the wave energy dissipation, a bar trough profile can be generated. However, the detailed profile evolution near the bar-trough area is not well simulated. On observed profiles, shoreward slope of the bar is much steeper, and the bar is much wider than predicted by the model. In some cases, multiple bars are formed inside the surf zone. Some adjustments on sediment transport near the wave breaking point may provide improvement. The convergence between offshore transport inside the surf zone and on shore transport outside the surf zone due to wave asymmetry may contribute to bar growth. Lack of transport representation outside of the surf zone also limits the model capability to simulate on shore bar migration and beach recovery in summer wave conditions.

Another model improvement should be to better represent the wave period effects on profile evolution. From the investigation on measured profiles under different period waves in Chapter 1, it is clear that wave periods have an influence on cross-shore sediment transport, especially long period waves (as in Figure 1-7). This effect needs further investigation and incorporation into the model although the effect of wave parameters (H/wT) on the profile scale parameters, A represents one contribution to this goal

The sediment transport and resulting profile change under random waves are treated by the wave-by-wave approach, which has the advantage of no wave height distribution assumption requirements inside the surf zone However, wave interaction effects on sediment transport are not taken into account. Some studies have shown that long waves (infragravity waves) generated by wave interactions can have a significant influence on sediment transport. Further effort is required to determine the best approach of including this effect in closed loop energy dissipation based models

The representations of cross-shore sediment transport and profile evolution under two other commonly met conditions, overwash caused by a severe storm and beach-structure interaction in front of shore parallel structures, are requirements for a model to be labeled as a complete and "good" beach profile evolution model Although these two issues have been included in the SBEACH model, they were treated in ad hoc fashions A rational understanding of these processes and incorporating them into the current model is another main focus in further model development.

APPENDIX A
FORTRAN PROGRAM CODE LISTING

```
!**********************************************************************
!                          PROGRAM ICRPEM FOR
! THIS PROGRAM SOLVES THE ONE-DIMENSIONAL CROSS-SHORE PROBLEM OF
!              PROFILE EVOLUTION  USING Y,T AS FREE VARIABLES
!                        METHOD OF SOLUTION  IMPLICIT
!                        RANDOM WAVES  WAVE-BY WAVE
!                              IN METRIC UNIT
!**********************************************************************

!-----------------------------------------------------------------------
! DIST-->DIRECTED OFFSHORE
!
! STAGGERED GRID (SBEACH)
!          h,D Fs IN WATER DEPTH GRID
!          Q H F L,CG,SETUP IN TRANSPORT GRID
!
! WAVE MODEL INCLUDES
!          Dally  W R. (1992) random wave model  wave-by-wave
!-----------------------------------------------------------------------
!
!REFERENCE:
!
!DALLY  W.E., 1987   "WAVE TRANSFORMATION IN THE SURF ZONE "
!          DOCTORAL DISSERATATION       UNIVERSITY OF FLORIDA GAINESVILLE,FL
!DALLY  W.R., 1992.  "RANDOM BREAKING WAVES  FIELD VERIFICATION OF A
!          WAVE-BY WAVE ALGOKITHM FOR ENGINEERING APPLICATION "
!          COASTAL ENGINEERING 1992, VOL 16,369-397
!ZHENG,J   1996     "IMPROVED CROSS-SHORE SEDIMENT TRANSPORT RELATIONSHIP
!          AND MODELS " DOCTORAL DISSERTATION  UNIVERSITY OF
!          FLORIDA,GAINESVILLE,FL
!-----------------------------------------------------------------------

PROGRAM ICRPEM

IMPLICIT NONE
EXTERNAL RAN9
DOUBLE PRECISION RAN9
!-------------------------variables definition-----------------------------
DOUBLE PRECISION  ALLOCATABLE   DIST( ),DPT( ),DIST1( ),DPT1( ),DFTC( ) WAVH(:),DISP( ), &
  SETUP( ),Q( ) Q0( ) TOUT( ),SI( ),TTID( ) HWAVE( ) TWAV( ),PWAV( ), DH( ), &
  AROLL( ),AF( ),BF( ),C( ) D( ) AS( ) BS( ),CS( ),DS( ) E( ),F( ) ES( ),FS( )
INTEGER, ALLOCATABLE   :: SKIPINDEX(:)
DOUBLE PRECISION   RHO GRAV BKAPPA DT,DY,APROF,HOFF PERIOD,KQ1 W
DOUBLE PRECISION   KDALLY GAMMA,BETAD BSL,SLOFF,SLON TIDA UNIT SWL,NU,DHMAX
DOUBLE PRECISION   THC SC,R HDIN,TMIN HB OPTF  B1 B2,CDF OMEGA,DSTAR,DSTARP
INTEGER   IWAVTYPE NTIMES NGRID,NTID NTOUT NWAVE,IRANDOM,ISTOP
INTEGER   IRC,IBC,ICC,IR,IB,IE,IT,IJMAX,IT IS,IL
COMMON /COM1/RHO,GRAV,BKAPPA DT,KQ1,DY
COMMON /COM2/IRC,IBC,IEC
COMMON /COM3/PERIOD HOFF,APROF W,BETAD KDALLY,GAMMA,BSL

!-------------------------files definition----------------------------------
```

```
OPEN(3 FILE='CRWANG.INP',STATUS='OLD')                  !INPUT PARAMETERS FILE
OPEN(4,FILE='inprofce300.DAT' STATUS='OLD')             !INITIAL PROFILE
OPEN(5 FILE='SSUR.DAT' STATUS='OLD')                    !STORM SURGE
OPEN(1 FILE='WAVE.DAT' STATUS='OLD')                    !WAVE HEIGHT AND PERIOD SERIES
OPEN(6,FILE='OUTPROF.OUT')                              !OUTPUT PROFILE
OPEN(7 FILE='TRANS.OUT')                                !OUTPUT TRANSPORT
OPEN(8,FILE='WSETP.OUT')                                !OUTPUT SETUP
OPEN(9 FILE='OUTPAR.OUT')                               !OUTPUT INPUT DATA

!-------------------------output formation ------------------------------------
31 FORMAT(/1X,'RHO=',F12.4,'G=',F12.4,'KAPPA=',F12.4 'A=',F12.4,'K=',E12.5,/)
32 FORMAT(1X,'DT=',F12.4 'DY=',F12.4,/)
34 FORMAT(1X,'BSL=',F12.4 'SLOPE=',F12.4,'SLON=',F12.4,'TIDA=',F12.4,/)
36 FORMAT(2(5X,E12.5))
37 FORMAT(3(5X,E12.5))

!------------------------------ read data ---------------------------------------
READ(3 *)IWAVTYPE
READ(3 *)NTIMES,NGRID,NTOUT,NTID,NWAVE
READ(3 *)RHO,GRAV,BKAPPA,DT,DY
READ(3 *)KQ1,APROF,W,NU
READ(3 *)BSL,SLOPE,SLON,TIDA,UNIT,SWL
READ(3 *)KDALLY,GAMMA,BETAD

IF( NOT ALLOCATED(TOUT)) ALLOCATE(TOUT(NTOUT+1))
IF( NOT ALLOCATED(TTID)) ALLOCATE(TTID(NTID+1))
IF( NOT ALLOCATED(S))    ALLOCATE(S(NTID+1))
IF( NOT ALLOCATED(DIST)) ALLOCATE(DIST(NGRID+1))
IF( NOT ALLOCATED(DPT))  ALLOCATE(DPT(NGRID+1))
IF( NOT ALLOCATED(TWAV)) ALLOCATE(TWAV(NWAVE+1))
IF( NOT ALLOCATED(HWAV)) ALLOCATE(HWAV(NWAVE+1))
IF( NOT ALLOCATED(PWAV)) ALLOCATE(PWAV(NWAVE+1))

DO I=1,NTOUT
        READ(3 *)TOUT(I)                        !TIME TO OUTPUT PREDICTED RESULTS
END DO
DO I=1,NGRID
        READ(4 *)DIST(I),DPT(I)                 !INITIAL PROFILE
        DIST(I)=DIST(I)*UNIT
        DPT(I)=-(DPT(I)+SWL)*UNIT
END DO
DO I=1,NTID
        READ(5 *)TTID(I),S(I)                   !STORM SURGE
END DO
DO I=1 NWAVE
        READ(1 *)TWAV(I),HWAV(I),PWAV(I)        !WAVE HEIGHT AND PERIOD SERIES
END DO

!-------------------------output input data-------------------------------------
WRITE(9 *)'-------------------OUTPUT OF PARAMETERS-------------------'
WRITE(9 *)NTIMES= NTIMES
WRITE(9,31)RHO,GRAV,BKAPPA,APROF,KQ1
WRITE(9,32)DT,DY
WRITE(9,34)BSL,SLOPE,SLON,TIDA
WRITE(9 *)'-------------------INITIAL INPUT PROFILE-------------------'
WRITE(9 *)'NGRID=' NGRID
WRITE(9,36)DIST(I) -DPT(I) I=1,NGRID)
WRITE(9 *)'-------------------STORM SURGE INPUT-------------------'
WRITE(9 *)'NTID=' NTID
WRITE(9,36)(TTID(I),S(I),I=1 NTID)
!-------------------interpolate input profile-----------------------------
IIMAX=INT((DIST(NGRID)-DIST(1))/DY)+1
```

```
WRITE(*,*)'NGRID=',NGRID ' IIMAX=',IIMAX

IF( NOT ALLOCATED(DIST)) ALLOCATE(DIST(IIMAX+1))
IF( NOT ALLOCATED(DPT)) ALLOCATE(DPT(IIMAX+1))
CALL PROFINTERP(IIMAX,NGRID DIST,DPT,DY,DIST1 DPT1)
DEALLOCATE(DIST)
DEALLOCATE(DPT)
NGRID=IIMAX
!WRITE(0,30)(DIST1(I)/UNIT_DPT1(I)/UNIT I=1 NGRID)

!-------------------array size definations-------------------------
IF( NOT ALLOCATED(WAVH))          ALLOCATE(WAVH(NGRID+2))
IF( NOT ALLOCATED(SETUP))         ALLOCATE(SETUP(NGRID+2))
IF( NOT ALLOCATED(DPTC))          ALLOCATE(DPTC(NGRID+2))
IF( NOT ALLOCATED(DISP))          ALLOCATE(DISP(NGRID+2))
IF( NOT ALLOCATED(AROLL))         ALLOCATE(AROLL(NGRID+2))
IF( NOT ALLOCATED(BKINDEX)) ALLOCATE(BKINDEX(NGRID+2))
IF( NOT ALLOCATED(Q0))            ALLOCATE(Q0(NGRID+2))
IF( NOT ALLOCATED(Q))             ALLOCATE(Q(NGRID+2))
IF( NOT ALLOCATED(A))             ALLOCATE(A(NGRID+2))
IF( NOT ALLOCATED(B))             ALLOCATE(B(NGRID+2))
IF( NOT ALLOCATED(C))             ALLOCATE(C(NGRID+2))
IF( NOT ALLOCATED(D))             ALLOCATE(D(NGRID+2))
IF( NOT ALLOCATED(E))             ALLOCATE(E(NGRID+2))
IF( NOT ALLOCATED(F))             ALLOCATE(F(NGRID+2))
IF( NOT ALLOCATED(AS))            ALLOCATE(AS(NGRID+2))
IF( NOT ALLOCATED(BS))            ALLOCATE(BS(NGRID+2))
IF( NOT ALLOCATED(CS))            ALLOCATE(CS(NGRID+2))
IF( NOT ALLOCATED(DS))            ALLOCATE(DS(NGRID+2))
IF( NOT ALLOCATED(ES))            ALLOCATE(ES(NGRID+2))
IF( NOT ALLOCATED(FS))            ALLOCATE(FS(NGRID+2))
IF( NOT ALLOCATED(DH))            ALLOCATE(DH(NGRID+2))

!initial transport rates
DO I=1 NGRID+1
        Q(I)=0.0
END DO
DSTAR=5.0/24.0*APROF**( 5*RHO*GRAV**1.5*0.78**2.0

!-----------------------------------------------------------------
!                       -time loop-
!-----------------------------------------------------------------
IRANDOM=95433435
DO IT=1 NTIMES
!------ determine storm surge (twels, HRMS AND TM at offshore boundary:HOFF T
  THC=IT*DT/3600.0
  SC=0.0
  IF(NTID.NE.0)CALL INTEP(TTID,S,THC,SC NTID)
  CALL INTEP(TWAV,HWAV,THC,HOFF NWAVE)
  CALL INTEP(TWAV,PWAV,THC,PERIOD NWAVE)
  DO I=1,NGRID
          DPTC(I)=DPT(I)+SC+TIDA
  END DO

!------ INITIAL ARRAYS
  DO I=1,NGRID+1
          DH(I)=0.0; Q0(I)=Q(I); Q(I)=0.0; SETUP(I)=0.0;
          A(I)=0.0  B(I)=0.0  C(I)=0.0  D(I)=0.0, E(I)=0.0; F(I)=0.0
          AS(I)=0.0  BS(I)=0.0  CS(I)=0.0  DS(I)=0.0, ES(I)=0.0; FS(I)=0.0
          WAVH(I)=0.0  BKINDEX(I)=0; DISP(I)=0.0; AROLL(I)=0.0
  END DO
```

```
!---- DETERMINE MONO WAVES OR RANDOM WAVES
  IF(IWAVTYPE.EQ.1) THEN ~RANDOM WAVES
          !RANDOM wave height and period generation
          OMEGA=1.0-EXP(-(0.78*DPTC(NGRID)**2.0/(HDFF)**2.0)
          CDF=RAN(IRANDOM)
          HBIN=SQRT(-DLOG(1.0-CDF*OMEGA))
          CDF=RAN(IRANDOM)
          B1=CDF*(1.0+TANH(0.8*HBIN/NU))-1.0
          B2=1.0-NU/(2.4*HBIN)*DLOG((1.0+B1)/(1.0-B1))
          HBIN=HBIN*HOFF/SQRT(2.0)
          TBIN=PERIOD/B2
          HOFF=HBIN
          PERIOD=TBIN
  ELSE IMOND WAVES
          HDFF=HOFF
          PERIDD=PERIOD
  END IF

!---- wave height transformation and energy dissipation
  CALL DALLYROLLER2(NGRID,DPTC,WAVH,BKINDEX,DISP,SETUP,JSTOP,AROLL)

!---- add setup into water depth
  DO I=1,NGRID
          DPTC(I)=DPTC(I)+0.5*(SETUP(I)+SETUP(I+1))
  END DO

!------determine the first breaking wave height and water depth
  DO I=NGRID+1,1,-1
          IF(BKINDEX(I).EQ.1)THEN
                  HB=WAVH(I)
                  DPTB=DPTC(I-1)
                  GOTO 999
          END IF
  END DO

!------determine runup, runup point, shoreline, break-point
999  CALL RUNUP(IT,NGRID,DPTC,DISTL,HB,PERIOD,DPTB,IR,IB,IE,R)
  IRC=IR
  IBC=IB !STOP
  IEC=IE
!---- double sweep method
  distarp=distar*(0.888+1.406/(hb/wo/period))**1.5

  ! determine coefficients
  CALL COEFF(A,B,C,D,AS,BS,CS,DS,DPTC,Q0,NGRID+1,WAVH,DISP,AROLL,DSTARP)
  CALL FSWEEP(A,B,C,D,E,F,AS,BS,CS,DS,ES,FS,Q,NGRID+1,IBC,IEC)
  CALL SSWEEP(E,F,ES,FS,DPTI,DH,Q,IBC,IEC,NGRID+1)

!---- EXAMINE WHETHER DH<1
  DHMAX=0.0
  DO I=1,NGRID
          IF(ABS(DH(I)).GT.DHMAX) DHMAX=ABS(DH(I))
  END DO
  IF(DHMAX.GE.1.0) STOP 'DH>1...REDUCE TIME STEP'

!------ smooth profiles to limit slope
  IS=IEC
  IL=NGRID
  CALL SMOOTH(DISTI,DPTI,IS,IL,BSL,NGRID)
  IS=IEC-6
  IL=NGRID
  CALL SMOOTH(DISTI,DPTI,IS,IL,SLOPE,NGRID)
```

```
  IS=2
  IL=NGRID
  CALL SMOOTH(DISTI DPTI,IS,IL,SLON NGRID)

!----- output profile at given time
  DO JT=1 NTOUT
        IF(THC.EQ TOUT(JT))THEN
                WRITE(6,36)(DISTI(I)/UNIT -DPTI(I)/UNIT I=1 NGRID)
                WRITE(7,36)(DISTI(I) Q(I),I=1,NGRID)
                WRITE(8,36)(DISTI(I),SETUP(I) I=1 NGRID)
        END IF
  END DO
   WRITE(*,*)IT=',IT,IRC,IEC
END DO !TIME_LOOP

!-------------------------------------------------------------------------
DEALLOCATE(TOUT); DEALLOCATE(TITD); DEALLOCATE(S)
DEALLOCATE(TWAV); DEALLOCATE(HWAV); DEALLOCATE(PWAV)
DEALLOCATE(DISTI); DEALLOCATE(DPTI) DEALLOCATE(WAVH)
DEALLOCATE(SETUP) DEALLOCATE(DISP), DEALLOCATE(DH)
DEALLOCATE(Q0) DEALLOCATE(Q), DEALLOCATE(DPTC)
DEALLOCATE(SKINDEX); DEALLOCATE(AROLL) DEALLOCATE(A)
DEALLOCATE(B); DEALLOCATE(C), DEALLOCATE(D)
DEALLOCATE(E); DEALLOCATE(F) DEALLOCATE(AS)
DEALLOCATE(BS) DEALLOCATE(CS) DEALLOCATE(DS)
DEALLOCATE(ES), DEALLOCATE(FS)
CLOSE(UNIT=1)
CLOSE(UNIT=3)
CLOSE(UNIT=4)
CLOSE(UNIT=5)
CLOSE(UNIT=6)
CLOSE(UNIT=7)
CLOSE(UNIT=8)
CLOSE(UNIT=9)

STOP
END     PROGRAM ICRIPEM

!**************************************************************************
!**                          DALLY AND BROWN (1995) ROLLER MODEL          **
!**      USING LINEAR WAVE THEORY AND SHALLOW WATER ASSUMPTION            **
!**                          INCLUDING SETUP/SETDOWN                      **
!**                                DALLYROLLER2                           **
!**************************************************************************
SUBROUTINE DALLYROLLER2(IMAX,DP WAVH IB,DISP,SETUP ISTOP,AROLL)
  IMPLICIT NONE
  DOUBLE PRECISION PARAMETER   BETAC=1.0 EPS=0.001
  INTEGER IMAX I ISTOP IWAVE
  DOUBLE PRECISION DIMENSION (IMAX)   DP
  DOUBLE PRECISION DIMENSION (IMAX+1)   DISP,DPH WAVH,AROLL,SETUP,CG,N
  INTEGER, DIMENSION (IMAX+1) :: IB
  DOUBLE PRECISION   KDALLY GAMMA,BKAPPA,HOFF,DT,APROF,DSL,KQ1 W BETAD
  DOUBLE PRECISION   PERIOD GRAV,RHO,ZZ,ZZ2,DY,DP8 WD1-WD2,BB,DPFS
  DOUBLE PRECISION   AA,AB,AC,AD,AE,AF,WAVNUM,SETUPOLD,SETUPNEW,PI
  COMMON /COM1 RHO,GRAV BKAPPA,DT,KQ1 DY
  COMMON /COM3/ PERIOD HOFF,APROF,W BETAD,KDALLY,GAMMA,BSL

  BB=1.0/8.0*RHO*GRAV
  PI=ACOS(-1.0)
  DPFS=0.2
  IWAVE=0 !0/1
```

```
!------------DETERMINE AVERAGE DEPTH BETWEEN NEIGHBORING CELLS
DPH(1)=DP(1)
DO I=2,IMAX
        DPH(I)=0.5*(DP(I-1)+DP(I))
END DO
DPH(IMAX+1)=1.01*DP(IMAX)

!------------VALUES @OFFSHORE BOUNDARY
WAVH(IMAX+1)=HOFF
IB(IMAX+1)=0  !0/1=NONBREAKING/BREAKING
AROLL(IMAX+1)=0.0
CALL DSP(DPH(IMAX+1),PERIOD,WAVNUM,CG((IMAX+1),N(IMAX+1))
SETUP(IMAX+1)=-HOFF**2*WAVNUM/(8.0*SINH(2.0*WAVNUM*DPH(IMAX+1)))

!------------SPACE LOOP
DO I=IMAX,1,-1
        ZZ=1.0
        ZZ2=1.0
        DPB=WAVH(I+1)/BKAPPA  !BREAKER DEPTH

        WD1=DPH(I+1)+SETUP(I+1)
        SETUPOLD=SETUP(I+1)
35              WD2=DPH(I)+SETUPOLD
        IF(WD2.LT.DFFS)THEN
                ISTOP=I+1
                RETURN
        END IF

        CALL DSP(WD2,PERIOD,WAVNUM,CG(I),N(I))

        !determine whether wave break or not  set ib(I)
        IF(DPB.LT.WD1.AND.IB(I+1).EQ.0) GOTO 30 !NO BREARING
        IB(I)=1
        GOTO 38
30              ZZ=0.0
30              IF(WAVH(I+1).LE.GAMMA*WD1)THEN
                ZZ2=0.0
                IB(I)=0
        END IF

        !-----calculate wave height
        IF(WAVE.EQ.1)THEN                       !-----H=0.78h
                IF(IB(I).EQ.0)THEN
                        WAVH(I)=WAVH(I+1)**SQRT(CG(I+1)/CG(I))
                ELSE
                        WAVH(I)=BKAPPA*WD2
                END IF
        ELSE                                    !-----Dally's wave model
                AA=ZZ2*ZZ*KDALLY*DY/(DP(I)+SETUP(I+1))
                AB=1.0+0.5*AA
                AC=1.0-0.5*AA
                AD=IB*WAVH(I+1)**2*CG(I+1)
                AE=IB*(GAMMA*(DP(I)+SETUP(I+1)))**2*(CG(I)+CG(I+1))/2.0
                AF=(AD*AC+AE*AA)/AB
                IF(AF.LE.0.0)AF=0.0
                WAVH(I)=SQRT(AF/IB*CG(I))
        END IF

        !-----calculate roller area..Dally and Brown's model
        IF(IB(I).EQ.0)THEN
                AROLL(I)=0.0
        ELSE
```

```
                AA=RHO*BETAC**2*(CG(I+1)/N(I+1))**2-RHO*GRAV*BETAD*DY
                AB=AROLL(I+1)*AA/(2.0*PERIOD)
                AC=8.0*(WAVH(I+1)**2*CG(I+1)-WAVH(I)**2*CG(I))
                AD=((CG(I)/N(I))**2*RHO*BETAC**2+RHO*BETAD*DY*GRAV)/(2.0*PERIOD)
                AROLL(I)=(AB+AC)/AD
        END IF
        IF(AROLL(I).LT.0.0) AROLL(I)=0.0

        !----calculate wave setup/setdown  include roller effect
        AB=RHO*BETAC**2/PERIOD*(AROLL(I+1)*CG(I+1)/N(I+1)-AROLL(I)*CG(I)/N(I))
        AC=8.0*(WAVH(I+1)**2/(2.0*N(I+1)-0.5)-WAVH(I)**2/(2.0*N(I)-0.5))
        AD=RHO*GRAV*(DP(I)+SETUP(I+1))
        SETUPNEW=SETUP(I+1)+(AB+AC)/AD

        !----determine whether reach the desired accuracy on setup
        IF(ABS(SETUPNEW-SETUPOLD)/SETUPOLD.GT.EPS)THEN
                SETUPOLD=(SETUPNEW+SETUPOLD)/2.0
                GOTO 35
        END IF
        SETUP(I)=SETUPNEW

        !----calculate roller energy dissipation
        AA=DFR(I)+SETUP(I)
        DISP(I)=GRAV*RHO*BETAD*AROLL(I)/(PERIOD*AA)

  END DO

RETURN
END


!**********************************************************************
!**      WAVE LENGTH CALCULATION USING DISPERSION RELATIONSHIP       **
!**                          LINEAR WAVE THEORY                      **
!**********************************************************************
SUBROUTINE DSP(DPT,WAVPRD,WAVNUM,CG,N)
  IMPLICIT NONE
  DOUBLE PRECISION   DPT,WAVPRD,WAVNUM,CG,N
  DOUBLE PRECISION   GRAV,PI,PI2,SGM,WLO,WLOLD,WLNEW,WKH
  INTEGER   CHOICE

  CHOICE=2

  GRAV=9.81
  PI=ACOS(-1.0)
  PI2=2.0*PI
  IF(CHOICE.EQ.1)THEN
          SGM=0.0001
          WLO=GRAV*WAVPRD**2/PI2 !WAVE LENGTH AT DEEP WATER
          WLOLD=WLO
 20       WAVNUM=PI2/WLOLD
          WLNEW=WLO*TANH(WAVNUM*DPT)
          IF(ABS(WLNEW-WLOLD).LE.SGM)GO TO 10
          WLOLD=(WLOLD+WLNEW)/2.0
          GO TO 20
 10       WLNEW=(WLOLD+WLNEW)/2.0
          WAVNUM=PI2/WLNEW
          WKH=WAVNUM*DPT
          N=0.5*(1.0+2.0*WKH/SINH(2.0*WKH))
          CG=N*WLNEW/WAVPRD
  ELSE
          N=1.0
```

```
        CG=SQRT(GRAV*DPT)
        WAVNUM=PI2/(CG*WAVPRD)
  END IF

RETURN
END



!*****************************************************************
!**                    INTERPOLATE PROFILES                     **
!*****************************************************************
SUBROUTINE PROFINTEP(IIMAX,IMAX,DIST,DPT,DY,DISTI,DPTI)
  IMPLICIT NONE
  INTEGER   IIMAX,I,IIMAX
  DOUBLE PRECISION DIMENSION (IIMAX)  DIST,DPT
  DOUBLE PRECISION DIMENSION (IIMAX)  DISTI,DPTI
  DOUBLE PRECISION   DY,YA,HIC

  DISTI(1)=DIST(1)
  DPTI(1)=DPT(1)
  DO I=2,IIMAX
        DISTI(I)=DISTI(I-1)+DY
        YA=DISTI(I)
        CALL INTEP(DIST,DPT,YA,HIC,IMAX)
        DPTI(I)=HIC
  END DO

RETURN
END


!*****************************************************************
!**                SUBROUTINE INTEP- INTERPOLATION OF DATA      **
!                          LINEAR INTERPOLATION                 **
! X MUST BE INCREASE WITH INDEX,THAT IS X1 > X2 > X3 > X4>...> Xn **
!*****************************************************************
SUBROUTINE INTEP(X,Y,XC,YC,IMAX)
  IMPLICIT NONE
  INTEGER   IMAX,I,IC,ICM
  DOUBLE PRECISION DIMENSION (IMAX)  X,Y
  DOUBLE PRECISION   XC,YC,DEN,A1,A2

  DO I=2,IMAX
        IC=I
        ICM=I-1
        IF(X(IC).GE.XC)THEN
                DEN=X(IC)-X(ICM)
                A1=(XC-X(ICM))/DEN
                A2=1.0-A1
                YC=A1*Y(IC)+A2*Y(ICM)
                RETURN
        END IF
  END DO
RETURN
END


!*****************************************************************
!**                        SUBROUTINE RUNUP                     **
!*****************************************************************
```

```
SUBROUTINE RUNUP(IT,IMAX,HC,Y,HB,T,DPTB,IR,IB,IE,R)
  IMPLICIT NONE
  INTEGER   IT,IMAX,IR,IB,IE,IRO,IBO,IEO,N
  DOUBLE PRECISION DIMENSION (IMAX)  HC,Y
  DOUBLE PRECISION   HB,T,DPTB,R,RHO,GRAV,BKAPPA,DT,KQ1,DY
  DOUBLE PRECISION   A1,SLOPE,PI,L0
  COMMON /COM1/ RHO,GRAV,BKAPPA,DT,KQ1,DY

  R=0.1
  PI=ACOS(-1.0)
  L0=GRAV*T**2/2.0/PI
  A1=SQRT(HB/L0)
  DO N=1,50
        CALL ILIM(IT,IMAX,HC,R,DPTB,IR,IB,IE,IRO,IBO,IEO)
        SLOPE=(HC(IE)-HC(IR))/(Y(IE)-Y(IR))
        R=HB*SLOPE/A1
  END DO
RETURN
END


!*****************************************************************************
!**                                SUBROUTINE ILIM                          **
!*****************************************************************************
SUBROUTINE ILIM(IT,IMAX,HC,R,DPTB,IR,IB,IE,IRO,IBO,IEO)
  INTEGER IT,IMAX,IR,IB,IE,IRO,IBO,IEO,I
  DOUBLE PRECISION DIMENSION (IMAX)  HC
  DOUBLE PRECISION R,DPTB
  DO I=1,IMAX
        IF(HC(I)+R.LE.0.0.AND.HC(I+1)+R.GT.0.0)IR=I !RUNUP LIMIT
        IF(HC(I).LE.0.0.AND.HC(I+1).GT.0.0)IB=I+1   !SHORELINE POSITION
        IF(HC(I).LE.DPTB.AND.HC(I+1).GT.DPTB)IE=I+1 !BREAKING POINT
  END DO
  IF(IT.EQ.1)THEN
        IRO=IR
        IBO=IB
        IEO=IE
  END IF

  RETURN
  END

!*****************************************************************************
!**      DETERMINE THE COEFFICIENTS OF GOVERNING EQUATIONS                  **
!*****************************************************************************
SUBROUTINE COEFF1(A,B,C,D,AS,BS,CS,DS,DPTH,QO,NNN,WAVH,DISP,AROLL, &
   DSTAR,PERIOD,IHC,IEC)
  IMPLICIT NONE
  DOUBLE PRECISION,PARAMETER   POW=2.0
  INTEGER   NNN,IRC,IHC,IEC,I
  DOUBLE PRECISION,DIMENSION (NNN):: A,B,C,D,AS,BS CS,DS,DPTH,QO WAVH, &
        DISP,AROLL
  DOUBLE PRECISION   RHO,GRAV,BKAPPA,DT,KQ1,DY,APROF PERIOD,BSL
  DOUBLE PRECISION   DSTAR,B1,B2,B3,ALPHA,C1 C2  C5
  COMMON /COM1/ RHO,GRAV BKAPPA,DT,KQ1,DY,APROF,BSL

  !----------COEFFICIENTS FOR TRANSPORT RATE EQUATION
   ---------DALLY AND BROWN'S BOLLER MODEL
  BETAD=0.1
  ALPHA=DSTAR/BSL
  C1=RHO*GRAV**1.5/(8.0*DY);       C2=RHO*GRAV/(2.0*PERIOD*DY)
```

```
  DO I=IBC,IEC
          IF(DPTH(I-1),LT.0.0)THEN
                  AS(I)=0.0
                  CS(I)=0.0
                  DS(I)=0.0
          ELSE
                  B1=DISP(I)-DSTAR+ALPHA*(DPTH(I)-DPTH(I-1))/DY
                  C5=DPTH(I)+DPTH(I-1)
                  B2=2.0*KH*0*GRAV*BETAB*AROLL(I)/PERIOD/CS**2.0
                  B3=B2
                  AS(I)=POW*KQ(I*(B2+ALPHA/DY)*ABS(B1)**(POW-1.0)
                  CS(I)=POW*KQ(I*(B3-ALPHA/DY)*ABS(B1)**(POW-1.0)
                  DS(I)=KQ(I*B1*ABS(B1)**(POW-1.0)
          END IF
          BS(I)=1.0
  END DO
------COEFFICENTS FOR CONTINUITY EQUATION
  DO I=IBC,IEC
          A(I)=DT/DY*0.5
          B(I)=1.0
          C(I)=-A(I)
          D(I)=(QQ(I+1)-QQ(I))*DT/DY*0.5
  END DO
RETURN
END

!**********************************************************************
!**                                SUBROUTINE FSWEEP                 **
!**********************************************************************
SUBROUTINE FSWEEP(A,B C,D E,F,AS,BS,CS,DS ES FS,Q,NNN IBC IEC)
IMPLICIT NONE
INTEGER   NNN ILAST,I,IC,ICM,IBC IEC
DOUBLE PRECISION,DIMENSION (NNN)... A,B C,D,E,F,AS,BS,CS,DS,ES,FS,Q
DOUBLE PRECISION   DEN1 DEN2

FS(IEC+1)=Q(IEC+1)
ES(IEC+1)=0.0
ILAST=IEC
DO I=IBC,ILAST
          IC=ILAST I+(IBC+1
          ICM=IC 1
          )F(I NE IBC)THEN
                  DEN1=BS(IC)+CS(IC)*E(IC)
                  ES(IC)=-AS(IC)/DEN1
                  FS(IC)=(DS(IC)-CS(IC)*F(IC))/DEN1
                  IF(I EQ.ILAST)THEN
                          ES(ICM)=0.0
                          FS(ICM)=Q(ICM)
                  END IF
          END IF
          DEN2=B(ICM)+C(ICM)*ES(IC)
          E(ICM)=-A(ICM)/DEN2
          F(ICM)=(D(ICM)-C(ICM)*FS(IC))/DEN2
END DO
RETURN
END

!**********************************************************************
!**                                SUBROUTINE SSWEEP                 **
!**********************************************************************
SUBROUTINE SSWEEP(E,F ES FS H DH,Q,IBC IEC,NNN)
IMPLICIT NONE
```

```
INTEGER   IBC IEC,I IM,NNN
DOUBLE PRECISION,DIMENSION (NNN)~ E,F,ES,FS,Q,DH,H
DO I=IBC IEC
          IM=I-1
          Q(I)=DH(IM)*ES(I)+FS(I)
          DH(I)=E(I)*Q(I)+F(I)
          H(I)=H(I)+DH(I)
END DO
RETURN
END
!**********************************************************************
!** SUBTOUTINE SMOOTH  THIS SUB SMOOTHS PROFILE TO A LIMITING SLOPE   *
!**********************************************************************
SUBROUTINE SMOOTH(Y,H II I2,SLOPE,NNN)
  IMPLICIT NONE
  INTEGER   II,I2,NMAX,I,N,NNN
  DOUBLE PRECISION,DIMENSION (NNN)  Y H
  DOUBLE PRECISION .. DY DH DHE SLOPE,DDH
  NMAX=50
  DO N=1 NMAX
          DO I=II I2
                    DY=Y(I)-Y(I~1)
                    DH=H(I)-H(I-1)
                    DHE=DH DY*SLOPE
                    IF(DHE GE.0 0)THEN
                              DDH=1 1*DHE
                              H(I)=H(I)-DDH/2.0
                              H(I 1)=H(I 1)+DDH/2.0
                    END IF
          END DO
  END DO
RETURN
END

!**********************************************************************
!**                SUBROUTINE FOR RANDOM NUMBER GENERATION           **
!**                ADOPTED FROM NUMERICAL RECIPE OF FORTRAN          **
!**********************************************************************
FUNCTION ran0(idum)
IMPLICIT NONE
INTEGER idum,IA,IM IQ,IR,MASK
INTEGER k
DOUBLE PRECISION ran0,AM
PARAMETER (IA=16807 IM=2147483647,AM=1 /IM IQ=127773,IR=2836 MASK=1234559876)

idum=ieor(idum,MASK)
k=idum/IQ
idum=IA*(idum-k*IQ)-IR*k
if (idum.lt 0) idum=idum+IM
ran0=AM*idum
idum=ieor(idum,MASK)
RETURN
END
```

APPENDIX B
SIMULATION RESULTS FOR OCEAN CITY, MARYLAND

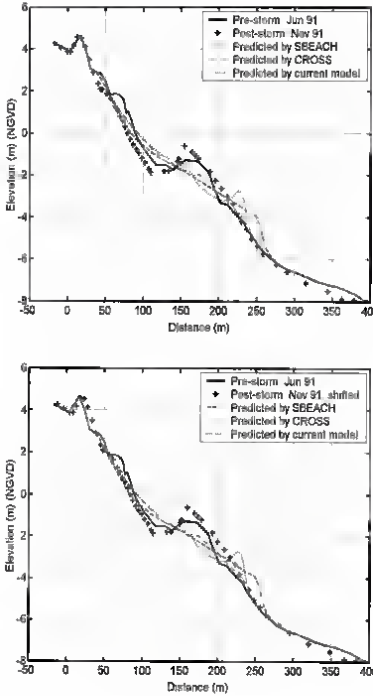

Figure B-1 Results of simulation of the Halloween storm for profile at 37th street

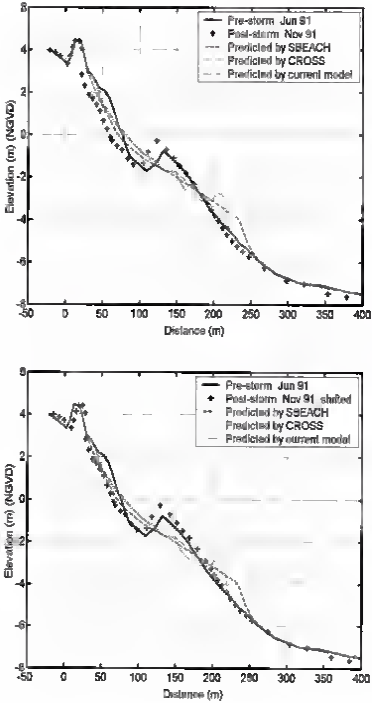

Figure B-2. Results of simulation of the Halloween storm for profile at 45th street

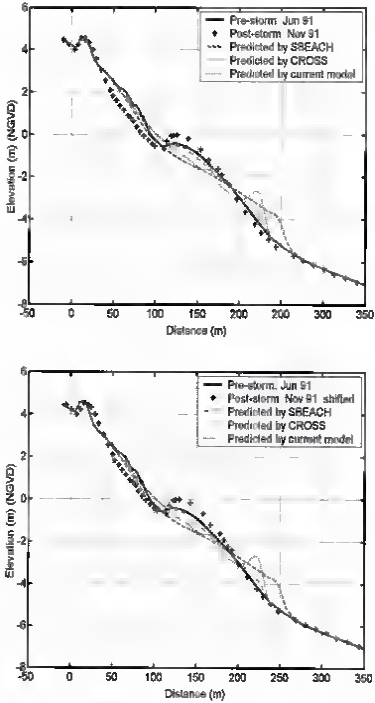

Figure B-3 Results of simulation of the Halloween storm for profile at 56th street.

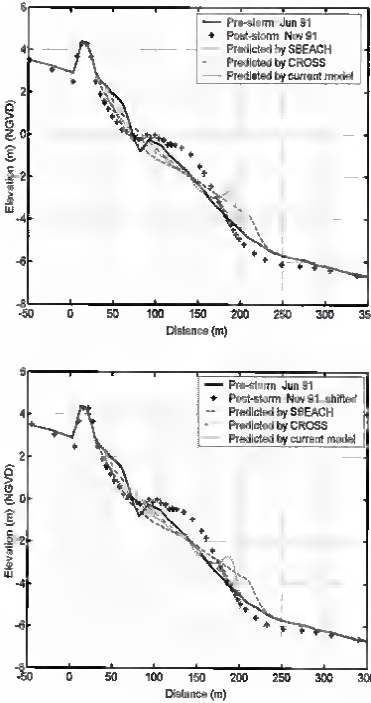

Figure B-4 Results of simulation of the Halloween storm for profile at 63rd street.

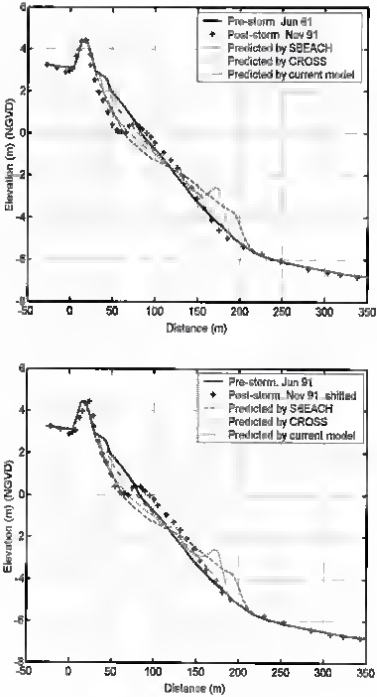

Figure B 5 Results of simulation of the Halloween storm for profile at 74th street.

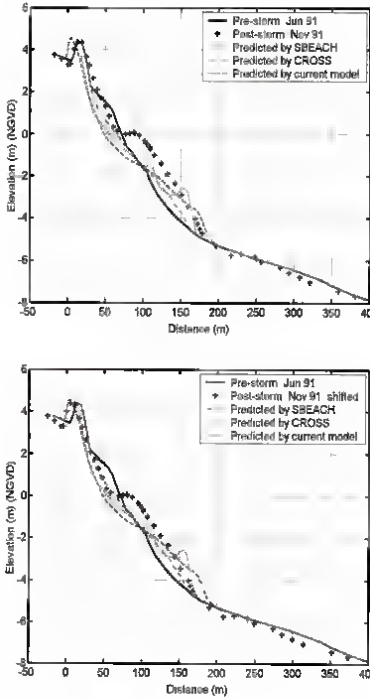

Figure B-6 Results of simulation of the Halloween storm for profile at 103rd street.

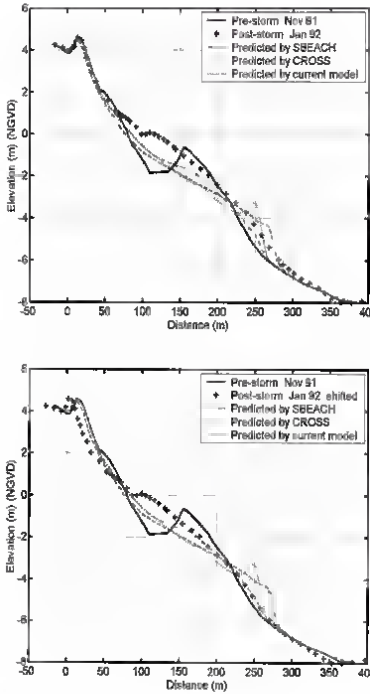

Figure B-7. Results of simulation of the Nov-Jan storm for profile at 37th street.

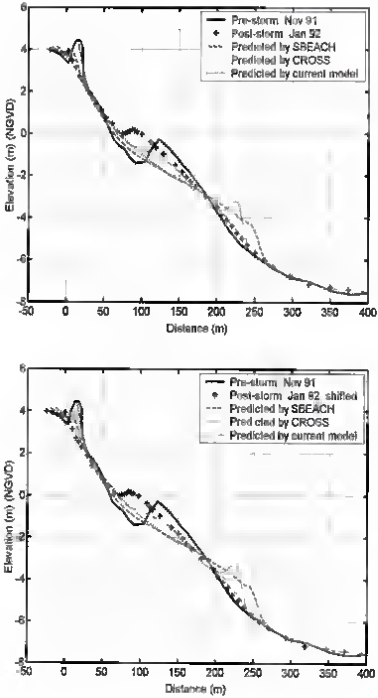

Figure B-8 Results of simulation of the Nov-Jan storm for profile at 45th street.

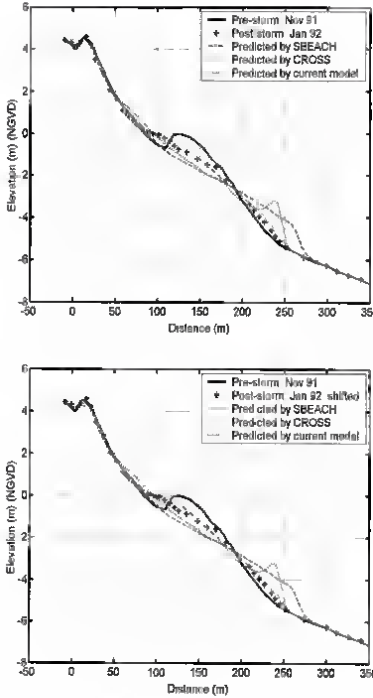

Figure B-9 Results of simulation of the Nov-Jan storm for profile at 56th street

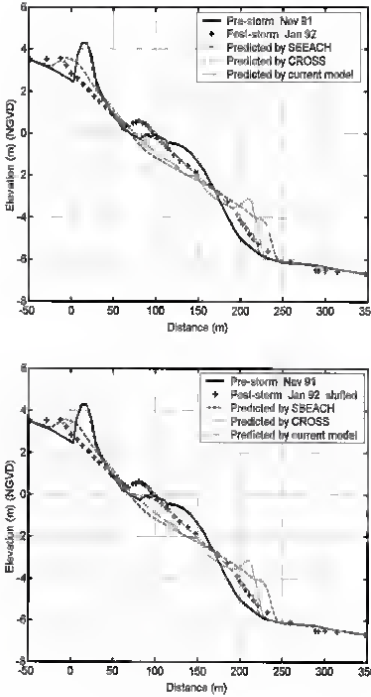

Figure B-10 Results of simulation of the Nov Jan storm for profile at 63rd street

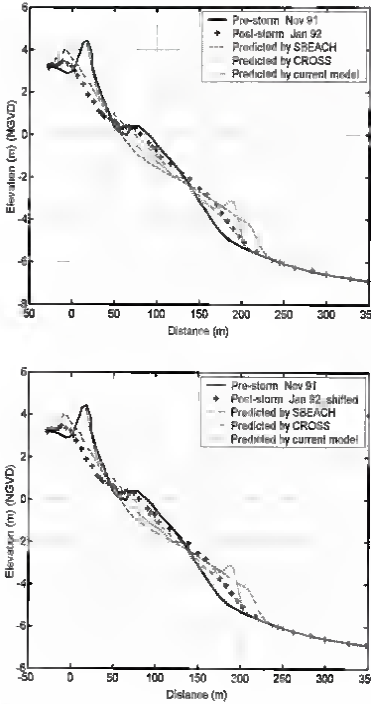

Figure B-11 Results of simulation of the Nov-Jan storm for profile at 74th street.

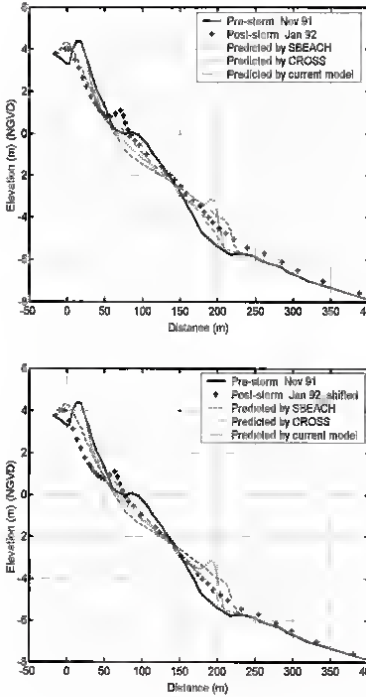

Figure B-12 Results of simulation of the Nov Jan storm for profile at 103rd street

REFERENCES

Arcilla, A S , Roelvink, J A., O'Connor, B.A., Reniers, A., Jimenez, 1994 The Delta Flume 93 experiment. Coastal Dynamics 94, pp 488-502

Bailard, J A., 1981 An energetic total load sediment transport model for a plane sloping beach Journal of Geophysical Research, American Geophysical Union, Vol 86 (C11) pp 10938-10954

Bailard, J A., 1982 Modeling on-offshore sediment transport in the surf zone. Proceeding of the 18th International Conference on Coastal Engineering, ASCE, pp 1419-1438

Bailard, J.A., Inman, D.L., 1981 An energetic bedload model for a plane sloping beach. Local transport. Journal of Geophysical Research, American Geophysical Union, Vol.86 (C3), pp 2035-2043

Baldock, T.E., Holmes, P., Bunker, S , Van Weert, P , 1998 Cross-shore hydrodynamics within an unsaturated surf zone. Coastal Engineering, Elsevier, Vol 34 pp173-196

Battjes, J.A., 1974 Surf similarity Proceedings of the 14th International Conference on Coastal Engineering ASCE, pp 466-479

Battjes, J A , Janssen, J P F.M., 1978. Energy loss and set-up due to breaking of random waves Proceeding of the 16th International Conference on Coastal Engineering, ASCE, pp 569-587.

Bodge, K R , 1992 Representing equilibrium profiles with an exponential expression. Journal of Coastal Research, Vol 8 (1), pp 47-55.

Bowen, A J , 1980 Simple models of nearshore sedimentation beach profiles and longshore bars In The coastline of Canada Littoral Processes and Shore Morphology, edited by McCann, S B , pp 1-11, Geological Survey of Canada, Ottawa, Ontario

Broker Hedegaard, I., Roelvink, J A., Southgate, H N , Pechon, P , Nicholson, J , Hamm, L., 1992 Intercomparison of coastal profile models Proceeding of the 23rd International Conference on Coastal Engineering ASCE pp 2108-2121

Bruun, P., 1954 Coast erosion and development of beach profiles. Beach Erosion Board, Technical Memorandum No 44, Washington, DC

Camenen B., Larroude, P., 2003 Comparison of sediment transport formulae for the coastal environment Coastal Engineering, Elsevier, Vol 48, pp 111-132

Chiu, T Y , 1977 Beach and dune response to Hurricane Eloise of September 1975 Coastal Sediments 77, pp 116-134

Chiu, T Y , Dean, R.G., 1984 Methodology of coastal construction control line establishment Department of Natural Resources, Beaches and Shores Technical and Design Memorandum No 84-6

Chiu T Y , Dean, R G , 1986 Additional comparison between computed and measured erosion by hurricanes Beaches and Shores Resource Center, Institute of Science and Public Affairs, Florida State University, Tallahassee, Florida.

Church, J C Thornton, E B , 1993 Effects of breaking wave induced turbulence within a longshore current model Coastal Engineering, Elsevier, Vol 20, pp 1-28

Creed, C G , Dalrymple, R A , Kriebel, D L., Kaihatu, J M , 1992 Equilibrium beach profiles with random seas Proceedings of the 23rd International Conference on Coastal Engineering, ASCE, pp 1973-1986

Dally W R , 1980 A numerical model for beach profile evolution Masters Thesis, University of Delaware, Newark, DE

Dally, W R , 1987 Wave transformation in the surf zone. Doctoral Dissertation, Department of Coastal and Oceanographic Engineering, University of Florida, Gainesville, FL.

Dally, W R., 1990 Random breaking waves a closed-form solution for planar beaches Coastal Engineering 1990, Elsevier, Vol 14 (3) pp 233-263

Dally, W R., 1992 Random breaking waves' field verification of a wave-by-wave algorithm for engineering application Coastal Engineering 1992, Elsevier, Vol.16 (4), pp 369-397

Dally, W R., Brown, C A., 1995 A modeling investigation of the breaking wave roller with application to cross-shore currents Journal of Geophysical Research, American Geophysical Union, Vol 100, No C12, pp 24873-24883

Dally, W R , Dean, R G , 1984 Suspended sediment transport and beach profile evolution Journal of Waterway, Port, Coastal, and Ocean Engineering ASCE, Vol 110 (1), pp 15-33

Dally, W.R., Dean, R G., 1986 Transformation of random breaking waves on surf beat Proceedings of the 20th International Conference on Coastal Engineering, ASCE, pp 109-123

Dally, W.R , Dean, R.G , Dalrymple, R.A , 1984 A model for breaker decay on beaches Proceeding of the 19th International Conference on Coastal Engineering, ASCE, pp 82-98

Dally, W.R., Dean, R.G Dalrymple, R.A , 1985 Wave height variation across beaches of arbitrary profile. Journal of Geophysical Research, American Geophysical Union, Vol.90 (C6) pp 11917-11927

Dalrymple, R.A, 1992 Prediction of storm/normal beach profiles. Journal of Waterway, Port, Coastal, and Ocean Engineering, Vol.118 (2), pp 193-200

Dean, R.G , 1973 Heuristic models of sand transport in the surf zone. Proceeding of Conference on Engineering Dynamics in the surf zone, Sydney, Australia.

Dean R G , 1977 Equilibrium Beach Profiles US Atlantic and Gulf Coasts Ocean Engineering Report No 12, University of Delaware, Newark

Dean, R.G , 1987 Additional sediment input into the nearshore region Shore and Beach, Vol 55 (3-4), pp 76-78.

Dean, R.G , 1991 Equilibrium beach profiles characteristics and applications. Journal of Coastal Research, Vol 7 (1), pp 53-84

Dean, R G , 1995 Cross-shore sediment transport processes In Advances in Coastal and Ocean Engineering, Vol 1, pp 159-220 edited by Liu, P L-F , Cornell University.

Dean, R.G , 1999 Phase 1 development of a "next generation ' beach and dune erosion model for CCCL and other beach management applications Department of Coastal and Oceanographic Engineering University of Florida, Gainesville, FL.

Dean, R.G , Dalrymple, R.A., 2002 Coastal processes with engineering application Cambridge University Press.

Deigaard, R., Justesen, P , Fredsoe, J , 1991 Modeling of undertow by a one-equation turbulence model Coastal Engineering, Elsevier, Vol.15, pp 431-458.

Dette H H , Larson, M , Murphy, J , Newe, J , Peters, K. Reniers, A., Steetzel, H , 2002 Application of prototype flume tests for beach nourishment assessment Coastal Engineering, Elsevier, Vol 47, pp 137-177

Dette, H.H , Peters, K , Newe, J , 1998 Large wave flume experiments 96/97, equilibrium profiles with different beach slopes. Leichtweiss-Institute , Technical University Braunschweig, Report No 825, January 1998.

Dette, H H., Uliczka, K., 1987 Prototype investigation on time-dependent dune recession and beach erosion. Coastal Sediments 87, pp 1430-1443

Galvin, C.J , 1968 Breaker type classification on three laboratory beaches Journal of Geophysical Research American Geophysical Union, Vol 73, pp 3651 3659

Inman, D L., Elwany M H S , Jenkins S A , 1993 Shorerise and bar-berm profiles on ocean beaches Journal of Geophysical Research, American Geophysical Union Vol 98 No C10, pp 18181-18199

Kajima, R., Shimizu T , Maruyama, K , Saito, S , 1982 Experiments on beach profile change with a large wave flume. Proceeding of the 18th Coastal Engineering Conference, ASCE, pp 1385-1404

Kobayashi, N., 1987 Analytical solution for dune erosion by storms Journal of Waterway, Port, Coastal, and Ocean Engineering, Vol 113 (4), pp 401-418

Komar, P.D., McDougal, W G , 1994 The analysis of exponential beach profiles Journal of Coastal Research, Vol.10 (1) pp 59-69

Kraus, N G., Larson, M., 1988 Beach profile change measured in the tank for large waves, 1956-1957 and 1962 Technical Report CERC-88-6, Coastal Engineering Research Center, U S Army Engineer Waterways Experiment Station, Vicksburg MS

Kraus, N C , Larson, M , Kriebel, D.L., 1991 Evaluation of beach erosion and accretion predictors. Coastal Sediments'91, pp 572-587

Kraus, N G , Smith, J M , 1994 SUPERTANK laboratory data collection project, volume 1: Main Text. Technical Report CERC-94-3, Coastal Engineering Research Center, U S Army Engineer Waterways Experiment Station, Vicksburg, MS

Kriebel, D L , 1982 Beach and dune response to hurricanes. Master of Science Thesis, Civil Engineering Department, University of Delaware

Kriebel, D.L , 1986 Verification study of a dune erosion model. Shore and Beach Vol 54, No 3, pp 13-21

Kriebel, D.L , 1990 Advances in numerical modeling of dune erosion. Proceeding of the 22nd International Conference on Coastal Engineering, ASCE, Vol.3, pp 2304-2317.

Kriebel, D.L , Dean, R.G., 1985 Numerical simulation of time-dependent beach and dune erosion Coastal Engineering, Elsevier, Vol 9 pp 221-245

Kriebel, D L., Dean, R G , 1993 Convolution method for time dependent beach profile response Journal of Waterway, Port, Coastal, and Ocean Engineering, Vol 119 (2), pp 204-226

Kriebel, D L., Kraus, N C., Larson, M , 1991 Engineering methods for predicting beach profile response. Coastal Sediments 91, Vol 1, pp 557-571

Kuriyama, Y., Nakatsukasa, T., 2000. A one-dimensional model for undertow and longshore current on a barred beach. Coastal Engineering, Elsevier, Vol 40, pp 39-58.

Larson, M., 1988. Quantification of beach profile change. Report No 1008, Department of Water Resource Engineering, Lund University, Lund, Sweden.

Larson, M., 1991. Equilibrium profile of a beach with varying grain size. Coastal Sediments'91, pp 905-919.

Larson, M., 1995. Model for decay of random waves in surf zone. Journal of Waterway, Port, Coastal, and Ocean Engineering, Vol 121 (1), pp 1-12.

Larson, M., 1996. Model of beach profile change under random waves. Journal of Waterway, Port, Coastal, and Ocean Engineering, Vol 122 (4), pp 72-181.

Larson, M., Capobianco, M., Wise, R.A., 1999. Modeling cross-shore sediment transport at different scales using equilibrium beach profile theory. Coastal Sediments'99, pp 1371-1386.

Larson, M., Kraus, N.C., 1989. SBEACH: Numerical model for simulating storm-induced beach change. Report 1: Empirical foundation and model development. Technical Report CERC-89-9, Coastal Engineering Research Center, U.S. Army Engineer Waterways Experiment Station, Vicksburg, MS.

Larson, M., Kraus, N.C., 1992. Numerical model of longshore current for bar and trough beaches. Journal of Waterways, Port, Coastal, and Ocean Engineering, ASCE, Vol 117 (4), pp 326-347.

Larson, M., Kraus, N.C., 1998. SBEACH: Numerical model for simulating storm-induced beach change. Report 5: Representation of nonerodible (hard) bottoms. Technical Report CERC-89-9, Coastal Engineering Research Center, U.S. Army Engineer Waterways Experiment Station, Vicksburg, MS.

Larson, M., Kraus, N.C., Byrnes, M.R., 1990. SBEACH: Numerical model for simulating storm-induced beach change. Report 2: Numerical formation and model tests. Technical Report CERC 89-9, Coastal Engineering Research Center, U.S. Army Engineer Waterways Experiment Station, Vicksburg, MS.

Larson, M., Kraus, N.C., Wise, R.A., 1999. Equilibrium beach profiles under breaking and non-breaking waves. Coastal Engineering, Elsevier, Vol 36, pp 59-85.

Leadon, M.E., Nguyen, N.T., Clark, R.R., 1998. Hurricane Opal: beach and dune erosion and structural damage along the Panhandle Coastal of Florida. Report No BCS-98-01, Bureau of Beaches and Coastal Systems, Department of Environmental Protection, State of Florida.

Lee, C B , Kim, M H , Edge, B L., 1996 Numerical model for on-offshore sediment transport with moving boundaries Journal of Waterway, Port, Coastal and Ocean Engineering, Vol 122 (2), pp 84-92

Lee, C.E., Kim, M H , Edge, B L., 1999 Generation of nearshore bars by multi-domain hybrid numerical model Journal of Coastal Research, Vol 15 (4), pp 892-901

Leont'ev, I.O , 1985 Sediment transport and beach equilibrium profile. Coastal Engineering, Elsevier, Vol 9, pp 277-291

Lippmann, T C , Brookins, A.H., Thornton, E.B , 1996 Wave energy transformation on natural profiles Coastal Engineering, Elsevier, Vol.27, pp 1-20

Longuet-Higgins, M.S., 1983 On the joint distribution of wave periods and amplitudes in a random wave field Proceedings of the Royal Society of London, Series A, Vol 389, pp 241-258

MacMahan, J , Thieke, R.J , 2000 Cross-shore sediment transport indices. Proceeding of the 27th International Conference on Coastal Engineering, ASCE, pp 3193-3204

Mase, H , Iwagaki, Y., 1982 Wave height distribution and wave grouping in surf zone Proceedings of the 18th International Conference on Coastal Engineering, ASCE, pp 58-76

Medina, R., Vidal, B C , Gonzalez, M., 2000 Relationship between beach morphodynamics and equilibrium profiles Coastal Engineering 2000, pp 2589-2601

Moore, B D , 1982 Beach profile evolution in response to changes in water waves and wave height. Master Thesis, University of Delaware.

Nairn, R.B , Roelvink, J.A., Southgate, H.N , 1990 Transition zone width and implications for modeling surf zone hydrodynamics Proceeding of the 22nd International Conference on Coastal Engineering, ASCE, pp 68-81

Nairn, R.B , Southgate, H N , 1993 Deterministic profile modeling of nearshore processes-Part 2 sediment transport and beach profile development. Coastal Engineering, Elsevier, Vol 19, pp 57-96

Newe, J., Peters, K, Dette, H H , 1999 Profile development under storm conditions as a function of the beach slope. Coastal Sediments'99, pp 2582-2596

Okuyasu, A., Shibayama, T , Mimura, N , 1988 Vertical variation of undertow in the surf zone Proceeding of 21st International Conference on Coastal Engineering, ASCE, pp 478-491

Okazaki, S , Sunamura, T., 1991 Re-examination of breaker-type classification on uniformly inclined laboratory beaches Journal of Coastal Research, Vol 7, pp 559 564

Plant, N.G , Ruessink, B G , Wijnberg, K M , 2001 Morphologic properties derived from a simple cross-shore sediment transport model American Geophysical Union,, Vol 106 (C1), pp 945-958

Rakha, K.A., Deigaard, R., Broker, I., 1997 A phase-resolving cross shore sediment transport model for beach profile evolution Coastal Engineering, Elsevier, Vol.31, pp 231 261

Raman, H , Barattupuzha, J J , 1972 Equilibrium conditions in beach wave interaction. Proceeding of the 13th International Conference on Coastal Engineering, ASCE, pp 1237-1256

Rattanapitikon, W., Shibayama, T , 2000 Verification and modification of breaker height formulas Coastal Engineering Journal, Vol 42 (4), pp 389-406

Rector, R.L., 1954 Laboratory study of equilibrium profiles of beaches Beach Erosion Board, Tech Memo , No 41

Reniers, A.J H M , Battjes, J.A , 1997 A laboratory study of longshore currents over barred and non-barred beaches. Coastal Engineering, Elsevier, Vol.30, pp 1-22.

Roelvink, J A., Reniers, A J H M , 1995 LIP 11D Delta Flume experiments a dataset for profile validation. Delft Hydraulics H 2130, January 1995

Sanchez-Arcilla, A., Roelvink, J A , O'Connor, B A , Reniers A , Jimenez, J A , 1994 The Delta Flume'93 experiment Coastal Dynamics'94, ASCE pp 488 502

Schoonees, J S and Theron, A.K , 1995 Evaluation of 10 cross-shore sediment transport morphological models Coastal Engineering, Elsevier,Vol.25, pp 1-41

Smith, E R , Kraus, N C , 1991 Laboratory study of wave-breaking over bars and artificial reefs Journal of Waterway, Port, Coastal, and Ocean Engineering, Vol 117, pp 307 325

Smith, E R., Kraus, N C , 1995 SUPERTANK laboratory data collection project, volume II Appendices A-I Technical Report CERC-94-3, Coastal Engineering Research Center U S Army Engineer Waterways Experiment Station, Vicksburg, MS

Son, C B , Noda, H., 1999 Cross-shore beach profile response to storm surge Coastal Sediments'99 pp 354-366

Southgate, H N , Nairn, R.B.. 1993.. Deterministic profile modeling of nearshore processes, Part I. waves and currents. Coastal Engineering, Elsevier, Vol 19, pp 27-36.

Stanble, D.K., Garcia, A.W., Kraus, N C., Grosskopf, W G , Bass, G.P , 1993. Beach nourishment project response and design evaluation. Ocean City, Maryland, Report 1. 1988-1992. Technical Report CERC-93-13, Coastal Engineering Research Center, U S. Army Engineer Waterways Experiment Station, Vicksburg, MS

Steetzel, H.J.. 1993. Cross-shore transport during storm surges. Ph.D. Dissertation, Delft Hydraulics

Stive, M.J F., 1986. A model for cross-shore sediment transport. Proceeding of the 20th International Conference on Coastal Engineering, ASCE, pp 1550 1564.

Sunamura, T , Horikawa, K., 1974. Two-dimensional beach transformation due to waves. Proceeding of the 14th international Conference on Coastal Engineering, ASCE, pp 920-938

Sunamura, T , Maruyama, K., 1987. Wave-induced geomorphic response of eroding beaches-with special reference to seaward migrating bars. Coastal Sediments'87, pp 788-801

Svendsen, I A , 1984. Mass flux and undertow in a surf zone. Coastal Engineering, Elsevier, Vol 8, pp 347-365

Thornton, E B., Guza, R.T., 1983. Transformation of wave height distribution. Journal of Geophysical Research, American Geophysical Union, Vol 88. (C10), pp 5925 5938

Ting, F C.K , Kirby, J T , 1994. Observation of undertow and turbulence in a laboratory surf zone. Coastal Engineering, Elsevier. Vol 24, pp 51-80

Ting, F C K , Kirby J T , 1995. Dynamics of Surf zone turbulence in a strong plunging breaker. Coastal Engineering, Elsevier, Vol 24, pp 177-204

Ting, F C.K., Kirby, J T., 1996. Dynamics of Surf zone turbulence in a spilling breaker. Coastal Engineering, Elsevier, Vol27, pp 131-160

Van Rijn, L.C , Walstra, D.J.R., Grasmeger, B , Sutherland, J , Pan, S , Sierra, J P , 2003. The predictability of cross-shore bed evolution of sandy beaches at the time scale of storms and seasons using process-based profile models. Coastal Engineering, Elsevier, Vol.47, pp 295-327

Wang, P , Davis, R.A , Jr , 1998. A beach profile model for barred coast — with a case study from Sand Key, West-Central Florida. Journal of Coastal Research, Vol 14 (3), pp 981-991

Wang, S.Y., Chiu, T.Y., 1993. Application of the EDUNE model to the CCCL establishment. Beaches and Shores Resource Center, Institute of Science and Public Affairs, Florida State University, Tallahassee, Florida.

Watanabe, A., 1988. Numerical predictive model of evolution of beach topography. In: Nearshore dynamics and coastal processes, Part III, edited by Horikawa, K., University of Tokyo.

Watanabe, A., Riho, Y., Horikawa, K., 1980. Beach profiles and on-offshore sediment transport. Proceeding of the 17th International Conference on Coastal Engineering, ASCE, pp 1106-1121.

Watts, G.M., 1954. Laboratory study of effect of varying wave periods on beach profiles. Beach Erosion Board, Tech. Memo., No. 53.

Wise, R.A., Smith, S.J., Larson, M., 1996. SBEACH: Numerical model for simulating storm induced beach change. Report 4. Cross-shore transport under random waves and model validation with SUPERTANK and field data. Technical Report CERC-89-9, Coastal Engineering Research Center, U.S. Army Engineer Waterways Experiment Station, Vicksburg, MS.

Work, P.A., Dean, R.G., 1991. Effect of varying sediment size on equilibrium beach profiles. Coastal Sediments'91, pp 891-904.

Zheng, J., 1996. Improved cross-shore sediment transport relationships and models, Ph.D. Dissertation. UFL/COEL-TR/112, Department of Coastal and Oceanographic Engineering, University of Florida, Gainesville, FL.

Zheng, J., Dean, R.G., 1997. Numerical models and intercomparisons of beach profile evolution. Coastal Engineering, Elsevier, Vol 30, pp 169-201.

BIOGRAPHICAL SKETCH

Zhanxian Wang was born in 1973 in a small town in Gaoqing, Shandong Province, China. Due to his interest in electrical equipment and one swimming accident in his childhood, he planned to study electrical engineering and avoid any major related to water after graduating from high school. However, ironically, he was placed in the Department of Ocean Engineering in Tianjin University. Realizing the amount of fun and challenge in that field, he began loving his major after 1 year of study. After he obtained both his bachelor's and master's degree in ocean engineering from Tianjin University, he found that there was still a limitation in his knowledge base. In 1999, he fortunately received an assistantship from the University of Florida to support his doctoral study in coastal engineering. Following his dream, he left his family and friends in China and came to Gainesville. Now, after nearly four and a half years studying and doing research under Professor Robert G. Dean, Mr. Wang plans to graduate and pursue a professional career in the field of coastal/ocean engineering.

I certify that I have read this study and that in my opinion it conforms to acceptable standards of scholarly presentation and is fully adequate in scope and quality as a dissertation for the degree of Doctor of Philosophy

Robert G Dean, Chairman
Graduate Research Professor of Civil and Coastal Engineering

I certify that I have read this study and that in my opinion it conforms to acceptable standards of scholarly presentation and is fully adequate, in scope and quality as a dissertation for the degree of Doctor of Philosophy

Daniel M Hanes
Professor of Civil and Coastal Engineering

I certify that I have read this study and that in my opinion it conforms to acceptable standards of scholarly presentation and is fully adequate, in scope and quality as a dissertation for the degree of Doctor of Philosophy

Ashish J Mehta
Professor of Civil and Coastal Engineering

I certify that I have read this study and that in my opinion it conforms to acceptable standards of scholarly presentation and is fully adequate in scope and quality, as a dissertation for the degree of Doctor of Philosophy

Robert J Thieke
Assistant Professor of Civil and Coastal Engineering

I certify that I have read this study and that in my opinion it conforms to acceptable standards of scholarly presentation and is fully adequate, in scope and quality as a dissertation for the degree of Doctor of Philosophy

Ulrich H Kurzweg
Professor of Mechanical and Aerospace Engineering

This dissertation was submitted to the Graduate Faculty of the College of Engineering and to the Graduate School and was accepted as partial fulfillment of the requirements for the degree of Doctor of Philosophy

May 2004

Pramod P Khargonekar
Dean, College of Engineering

Winfred M Phillips
Dean, Graduate School